11-2021

IMMOBILIZATION OF LIPASE ON METAL ORGANIC FRAMEWORKS FOR BIODIESEL PRODUCTION

Reem I Safwan Shoma

United Arab Emirates University

College of Engineering

Department of Chemical and Petroleum Engineering

IMMOBILIZATION OF LIPASE ON METAL ORGANIC FRAMEWORKS FOR BIODIESEL PRODUCTION

Reem Safwan Shomal

This thesis is submitted in partial fulfilment of the requirements for the degree of Master of Science in Chemical Engineering

Under the Supervision of Professor Sulaiman Al Zuhair

November 2021

Declaration of Original Work

Reem Safwan Shomal, the undersigned, a graduate student at the United Arab Emirates University (UAEU), and the author of this thesis entitled "*Immobilization of Lipase on Metal Organic Frameworks for Biodiesel Production*", hereby, solemnly declare that this thesis is my own original research work that has been done and prepared by me under the supervision of Professor Sulaiman AlZuhair, in the College of Chemical and Petroleum Engineering at UAEU. This work has not previously formed the basis for the award of any academic degree, diploma or a similar title at this or any other university. Any materials borrowed from other sources (whether published or unpublished) and relied upon or included in my thesis have been properly cited and acknowledged in accordance with appropriate academic conventions. I further declare that there is no potential conflict of interest with respect to the research, data collection, authorship, presentation and/or publication of this thesis.

Student's Signature:  Date: 20/10/2021

Approval of the Master Thesis

This Master Thesis is approved by the following Examining Committee Members:

1) Advisor (Committee Chair): Prof. Sulaiman Al Zuhair
   Title: Professor
   Department of Chemical and Petroleum Engineering
   College of Engineering
   Signature S.Al-Zuhair Date 08/12/2021

2) Member: Dr. Mohammednoor Altarawneh
   Title: Professor
   Department of Chemical and Petroleum Engineering
   College of Engineering
   Signature  Date 09/12/2021

3) Member (External Examiner): Prof. Sankar Bhattacharya
   Title: Professor
   Department of Chemical and Biological Engineering
   Institution: Monash University, Australia
   Signature  On behalf of Date 08/12/2021

This Master Thesis is accepted by:

Acting Dean of the College of Engineering Professor Mohamed Al-Marzouqi

Signature Mohamed AlMarzouqi Date 16/02/2022

Dean of the College of Graduate Studies: Professor Ali Al-Marzouqi

Signature Ali Hassan Date 16/02/2022

Copy ____ of ____

Abstract

For economical application of enzymatic processed in biodiesel production, lipase enzyme has to be used in immobilized form to allow easy retention and reuse. The main challenges facing industrialization of enzymatic process are the high mass transfer resistance, tendency to adsorb the by-product glycerol onto the support matrix and poor operational stability. These problems can be solved by good selection of supports of favorable surface characteristics and pore sizes. In that regard, increasing interest has recently been on Metal-Organic Frameworks (MOFs) as a new kind of porous supports for enzyme immobilization. Physical adsorption, which is a fast and easy method of enzyme immobilization ensures limited enzyme denaturation and does not affect the enzyme activity, native structure and active sites. However, the physically adsorbed enzyme is prone to leaching resulting in low stability, owing to the weak interaction between the enzyme and the support. As an alternative, chemisorption in which the nucleophiles of the enzymes are covalently bonded to the organic linkers of MOFs to form peptide bonds. However, physically immobilized lipase is generally more active reached than chemically immobilized ones, owing to the negative effect of the chemical bonds on the structure of the enzyme. However, enzyme attachment into the internal pores of MOFs may not be efficient, as part of the enzymatic activity may be lost due to conformational changes during diffusion into small cavities. In this process, the enzyme is caged inside the pores of the MOFs during the crystallization process. In addition, enzymes immobilized by this approach exhibit mass transfer limitations and their diffusion are restricted as the substrate may not be able to access the entire active sites. Kinetics and thermodynamics studies of the adsorption process, which is scarce in literature, could provide invaluable information to explain the different performance of surface adsorption on pre-synthesized MOFs and encapsulation during crystallizations can provide valuable in terms of (i) chemical affinity between external surface area of the MOF and the enzyme, (ii) accessibility of enzymes to pores, (iii) enzyme leaching, and (iv) catalytic activities. Therefore, in this work, the mechanism, kinetics, and thermodynamics of lipase adsorption on the surface of different MOFs, namely ZIF-67, ZIF-8 and HKUST-1, have been thoroughly investigated and tested for biodiesel production. The three supports have different structures, pore sizes, chemical properties, and surface areas. The influence

of temperature, initial protein loading, and contact time on the adsorption and catalytic properties of the resultant biocatalysts were investigated. The catalytic properties were assessed on biodiesel production from olive oil transesterification. The highest lipase adsorption capacity of 26.9 mg/g was achieved using ZIF-67 at 45^{o}C and initial protein concentration of 0.6 mg/mL. The maximum capacities of ZIF-8 and HKUST-1 were 18.95 mg/g and 0.50 mg/mL at 35^{o}C and 17.53 mg/mL at 45^{o}C and 0.60 mg/mL, respectively. The equilibrium adsorption data suggested that the lipase adsorbed physically on ZIF-67 and ZIF-8 and chemically of HKUST-1. The data were best fitted with Langmuir isotherm model for the three supports. Whereas, of the adsorption kinetics data were best fitted using Elovish's model for ZIF-67 and ZIF-8, and pseudo second model for HKUST-1. It was also found that the process was influenced by intraparticle and film diffusion. The prepared bio-catalyst was successfully used to catalyze the transesterification of olive oil to produce biodiesel in a solvent-free medium. The ZIF-8 and ZIF-67 showed better catalytic activity achieving 88% and 90% conversion, whereas HKUST-1 showed better operational stability owing to the stronger chemical adoption. In addition, diffusion-reaction kinetics of biodiesel production using adsorbed lipase on ZIF-8 has been analyzed. The investigation provided an insight into adsorption pathways and probable mechanism involved and a better understanding of their application in biodiesel production.

Keywords: Lipase, Adsorption, Thermodynamic, Zeolitic Imidazolate Frameworks, Metal Organic Frameworks, Biodiesel.

Title and Abstract (in Arabic)

استخدام الأطر المعدنية العضوية لدعم وحفظ انزيم الليباز لانتاج الوقود الحيوي

الملخص

يتم إنتاج معظم وقود الديزل الحيوي حاليًا في جميع أنحاء العالم من خلال تحلل المحفز القلوي والمحفز الانزيمي الحيوي. جذب الإنتاج المحفز الانزيمي بالليباز اهتمامًا متزايدًا، حيث يمكن استخدامه بشكل فعال في الزيت غير المكرر، بالإضافة إلى مزاياه الأخرى، بما في ذلك التشغيل في ظروف معتدلة، ومتطلبات الطاقة المنخفضة، وسهولة فصل المنتج. من أجل التطبيق الاقتصادي للأنزيمات المعالجة في إنتاج الديزل الحيوي يجب استخدام إنزيم الليباز في شكل ثابت للسماح بالاحتفاظ وإعادة الاستخدام بسهولة. تتمثل التحديات الرئيسية التي تواجه تصنيع الوقود الحيوي من الانزيمات المدعمة في مقاومة نقل الكتلة العالية والميل إلى امتصاص الجلسرين المنتج الثانوي على مصفوفة الدعم وضعف الاستقرار التشغيلي. يمكن حل هذه المشكلات عن طريق الاختيار الجيد للدعامات ذات خصائص السطح الملائمة وأحجام المسام. تُفضل الدعامات المسامية بشكل عام نظرًا لارتفاع مساحة سطحها، مما يسمح بتحميل أعلى وحماية أفضل للإنزيم. لذلك، يلعب حجم المسام دورًا مهمًا في النشاط التحفيزي والاستقرار. في هذا الصدد، كان الاهتمام المتزايد مؤخرًا بالأطر المعدنية العضوية (MOF's) كنوع جديد من الدعامات المسامية لتثبيت الإنزيم. ينتج عن ذلك دعامية حيوية لحفظ الانزيم ذات ثبات عالٍ، وانخفاض ترشيح الإنزيم، وأكثر صلابة يعمل على استقرار بنية الإنزيم. في هذا العمل، تم فحص الآلية والحركية والديناميكا الحرارية لتدعيم الليباز بالامتصاص الكيميائي على سطح الأطر العضوية المعدنية المختلفة، وهي ZIF-67 و ZIF-8 و -HKUST، بدقة واختبارها لإنتاج وقود الديزل الحيوي. تحتوي الدعامات الثلاثة على هياكل وأحجام مسام وخواص كيميائية ومساحات سطحية مختلفة. تم دراسة تأثير درجة الحرارة، التحميل الأولي للبروتين، ووقت التلامس على خصائص الدعامات الحيوية الناتجة. تم تقييم الخصائص التحفيزية على إنتاج الديزل الحيوي من استرة زيت الزيتون. تم تحقيق أعلى قدرة لامتصاص الكيميائي الليباز 26.9 مجم / جم باستخدام ZIF-67، عند 45 درجة مئوية وتركيز البروتين الأولي 0.6 مجم / مل. كانت السعات القصوى لـ ZIF-8 وHKUST-1 أقل، حيث وصلت إلى 18.95 مجم / جم و 0.50 مجم / مل عند 35 درجة مئوية وتركيز البروتين الأولي 17.5 مجم / مل و 45 درجة مئوية و 0.60 مجم / مل على التوالي. اقترحت بيانات امتصاص التوازن أن الليباز يمتص فيزيئياً على ZIF-67 و ZIF-8 وكيميائيًا لـ HKUST-1.

تمثل بيانات الحرارة نموذج Langmuir للدعامات الثلاثة. بينما، من الأفضل ملاءمة لبيانات الحركية باستخدام نموذج Elovish لـ ZIF-67 و ZIF-8، والنموذج الثاني لـ HKUST-1. وجد أيضًا أن العملية تأثرت بالانتشار داخل الجسيمات. تم استخدام المحفز الحيوي المحضر بنجاح لتحفيز الاسترة التبادلية لزيت الزيتون لإنتاج وقود الديزل الحيوي في وسط خالٍ من المذيبات. أظهر ZIF-8 و ZIF-67 نشاطًا تحفيزيًا أفضل حيث حقق تحويلًا بنسبة 82٪ و 90٪ ، بينما أظهر HKUST-1 استقرارًا تشغيليًا أفضل نظرًا لاعتماد المواد الكيميائية بشكل أقوى.

مفاهيم البحث الرئيسية: انزيم الليباز، الامتزاز، الديناميكا الحرارية، الاطر المعدنية العضوية، الاطر زوليتيك إيميدازولات، الوقود الحيوي.

Acknowledgements

First of all, this work was accomplished by the grace of God the Entirely Merciful, who gave me the strength to complete this research work.

My sincere thanks, deepest gratitude and appreciation go to my supervisor Prof. Sulaiman ALZuhair, I am extremely grateful for his guidance, time, and effort not only during this study but throughout my journey in the master and bachelor studies, who was always a great source of knowledge and experience to me. I believe that this novel thesis would not be accomplished without his continuous support and his assistance throughout my preparation of this thesis. I will always remember him in my prayer wishing him more success. His dynamism, vision, sincerity, and motivation have deeply inspired me. My words cannot be expressed for thanking him. I would also like to acknowledge all members of the Chemical and Petroleum Engineering Department at the UAE University for their kind assistance during my studies.

My special thanks and extreme appreciations are extended to Prof. Mohammad Ali Abdalkreem from University of Sharjah, for his collaboration during covid-19 pandemic, who helped and supported me to complete the research work of providing me a friendly research environment in Research Institute of Science & Engineering (RISE). Nonetheless, he welcomed me into his team and laboratory with kindness and modesty. The respect and sincere bond between the team made me appreciate this experience immensely. I look at my time with the team and working in his laboratory not just as an opportunity, but also a blessing to meet such inspiring and genuine people with great sagacity. I will always remember him in my prayers owing his collaboration. I have been honored to Meet. Dr. Pragati Shinde she helped to sustain a positive atmosphere and gave me a continuous encouragement. Dr. Najrul Hussain, Eng.

Muhammed Irshad, Eng Mohammed Shamir, Eng Fahad Hassan, Ms. Fatima Abla and Dr. Hussain Awad, who helped me with instrumentation and characterization.

I would like also to give many thanks to Ms. Mona Mahfood and Ms. Naimat Dak-E-Bab for their kind assistance in the experimental work. My beloved friends, Shaima, Basma, Dima, Raghad, Doha, Yasmin.

Last but not the least I would like to express my special gratitude and appreciation to my Husband Eng. Mahmoud Kmaleh and my mother-in-law, Aminah Qabesh who supported me spiritually, take care of my son and for their continuous encouragement throughout my studies. Special deepest thanks go to beloved parents, Samira Hadad and Safwan Shomal and sisters, Eman , Rasha and Noor who helped me along the way from birth. I am sure they suspected it was endless. I hope that they will be proud of me.

Dedication

To my beloved parents Samira and Safwan and my husband Mahmoud, and especially my son Saif, who is my everything

Table of Contents

List of Tables

List of Figures

List of Abbreviations

MOF	Metal Organic Framework
ZIF	Zeolitic Imidazolate Frameworks
XRD	X-ray Diffraction Analysis
FTIR	Fourier-Transform Infrared Spectroscopy
FeSEM	Field Emission Scanning Electron Microscope
FFAs	Free Fatty Acids
KOH	Potassium Hydroxide
IL’s	Ionic Liquids
CuBTC	Copper- Benzene-1,3,5-Tricarboxylic Acid
pH	Potential of Hydrogen
HMeIM	2-Methylimidazol
TEA	Triethyl Amine
DIW	Deionized Water
EIE	Enzyme Immobilization Efficiency
PBS	Phosphate Buffer Saline
FAME’s	Fatty Acid Methyl Esters
FID	Flame Ionization Detector
GC	Gas Chromatography
N_2	Nitrogen
UV	Ultraviolet–Visible Spectroscopy
BET	Brunauer-Emmett-Teller

Chapter 1: Introduction

1.1 Statement of the Problem

Biodiesel is a promising candidate for sustainable and renewable energy and extensive research is being conducted worldwide to optimize its production process. The employed catalyst is an important parameter in biodiesel production. Metal–Organic Frameworks (MOFs), which are a set of highly porous materials comprising coordinated bonds between metals and organic ligands, have recently been proposed as catalysts. MOFs exhibit high tunability, possess high crystallinity and surface area, and their order can vary from the atomic to the microscale level. However, their catalytic sites are confined inside their porous structure, limiting their accessibility for biodiesel production. Modification of MOF structure in this work by immobilizing enzymes could be a solution to this challenge and can lead to better performance and provide catalytic systems with higher activities [1]. Kinetics and thermodynamics studies of the adoption process, which is scarce in literature, could provide invaluable information on the surface chemical affinity, enzyme accessibility and leaching [2]. Therefore, in this work, the mechanism, kinetics and thermodynamics of lipase adsorption on the surface of different MOFs, namely ZIF-67, ZIF-8 and HKUST-1, have been thoroughly investigated and tested for biodiesel production. The three supports have different structures, pore sizes, chemical properties, and surface areas. Figure 1 represents the process of biodiesel production from MOF.

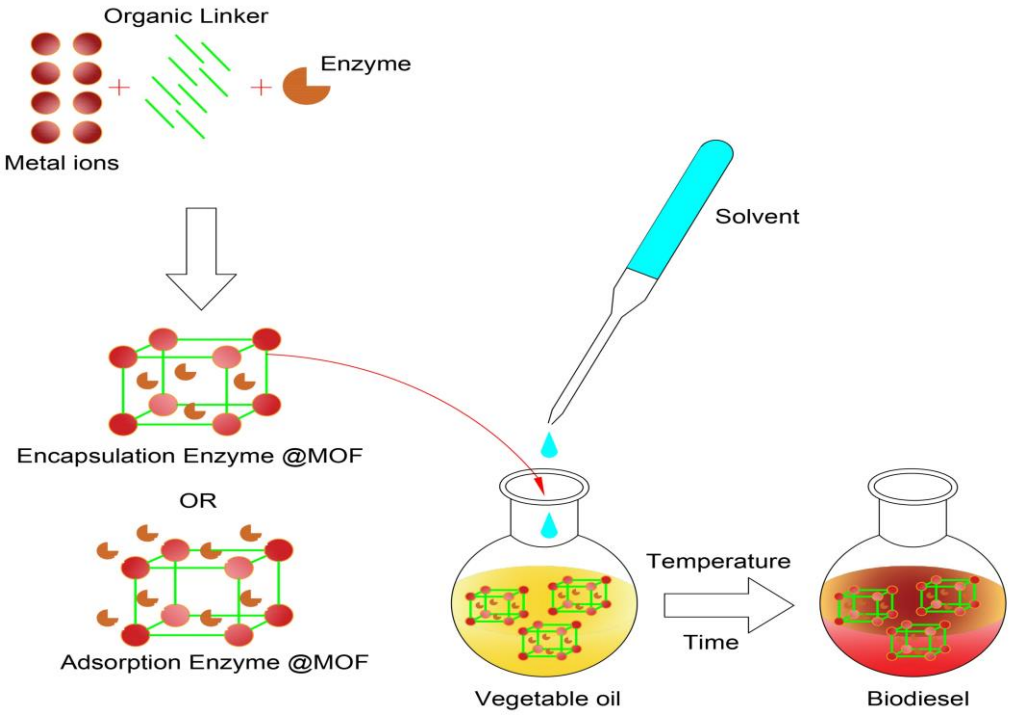

Figure 1: Biodiesel production from immobilized MOF

1.2 Research Objectives

The aim of this study is to investigate the feasibility Immobilized enzyme onto Metal Organic Frameworks as a green and potentially energy saving system for the production of biodiesel. In order to achieve it, the following objectives have been set:

- Synthesis of three MOFs of different pore sizes and surface properties.
- Characterize the synthesized MOFs in terms of their surface properties, pore sizes, morphology and crystallinity.
- Determine the optimum condition of lipase immobilization into synthesized MOFs (time, temperature, and concentration of enzyme loading).
- Determine the thermodynamics and kinetics of lipase adsorption on the prepared MOFs.

- Test the effectiveness of the prepared immobilized lipase on MOFs in biodiesel production.
- Develop and test a mathematical model to describe the diffusion reaction system.
- Assess the reusability of the prepared immobilized lipase on MOFs.

1.3 Organization of Thesis

The first chapter provides an overview of the research work and a statement of problems which explains immobilized enzyme into Metal Organic Frame Works (MOF's) and biodiesel production. The chapter further continues with the research objectives of the experimental works and ends up with the challenges faced during the experimental works. includes recent literature reviewed about biodiesel production, enzymatic reaction and immobilization of enzyme into different support and lastly the implementation The second chapter of MOF in biodiesel production. Chapter three consists of the experimental procedures carried out for synthesizing MOFs and characterizing MOFs by different methods like nitrogen adsorption, XRD, Fe-SEM, Raman spectroscopy and FT-IR. Secondly, the adsorption and encapsulation reactions carried out at different conditions (temperature, time and Concertation's of enzyme), and lastly the biodiesel production using of immobilized enzyme from vegetable oil. Furthermore, in chapter four, the experimental outcomes are discussed. Finally, chapter five summarizes with derived conclusions.

Chapter 2: Literature Review

2.1 Biodiesel production

The need to protect the environment from fossil fuel emissions together with the continuously growing energy needs has led to focus on renewable energy sources [1-9]. Apart from their expected depletion in the future, fossil fuels have unstable prices, intensifying the search for more sustainable and reliable energy sources [10]. Ideal fuel substitutes should possess better properties than conventional fuels, such as renewability, nontoxicity, biodegradability, and less-than-zero release of harmful gases into the environment [11-13]. Possible alternative energy sources include sunlight, wind, and biofuels [14].

Biodiesel is gaining increasing recognition worldwide due to the abundance of various possible feedstocks [15-20] and its superior properties compared to petroleum diesel, including better cetane number, higher flash point, and zero sulfur content [21]. These benefits along with its almost direct use in the diesel engine have encouraged the replacement of petroleum diesel with biodiesel [7-26]. Biodiesel is mainly produced by the transesterification of triglycerides and the esterification of Free Fatty Acids (FFA) found in vegetable oils and animal fats [27]. However, in biodiesel production, the feedstocks should be carefully selected and the production process should be optimized for economic competitiveness with petroleum diesel production. For instance, use of waste oil instead of pure vegetable oil can effectively reduce production costs. However, such feedstocks suffer from inconsistent availability and collection complexity [14, 28-33]. Microalgae appear to be the most promising feedstock for biodiesel production, as they can generate high lipid amounts, their cultivation does not require arable land, and many strains can grow in saline water. In

this chapter, I will explore the recent advances in catalytic biodiesel production with particular emphasis on enzymatic reactions and innovative ways of immobilizing enzymes on MOFs.

2.2 Conventional Catalysts

In addition to the appropriate feedstock selection, the catalyst used to convert oils into biodiesel plays an important role in the economic feasibility and high yield of the overall process [14, 34-35]. Homogeneous chemical catalysts, especially alkaline catalysts, are commonly used in biodiesel production due to their fast reaction rates and high yield. However, these catalysts are corrosive, cannot be easily recycled, and should be washed out from the product, generating large wastewater amounts [36-39]. Moreover, in the case of alkaline catalysts, the feedstock should be pretreated if its FFA content exceeds 1% to prevent saponification reactions, which consume the catalyst, reduce the yield, and complicate the downstream separation of the product [37]. In contrast, acid catalysts are not sensitive to FFA and can therefore be used to convert low quality feedstock into biodiesel without pretreatment. For instance, tin tetrachloride ($SnCl_4$) can catalyze the esterification of *Zanthoxylum bungeanum* seed oil with >96% yield under optimum reaction conditions. However, compared to alkaline catalysts, acid catalysts have lower reaction rates and require higher alcohol/oil molar ratios to promote the reaction [40]. For example, sunflower oil transesterification was achieved in 91.7% yield upon treatment with sodium hydroxide for 1 h [41], whereas *Z. bungeanum* seed oil transesterification afforded 94% yield upon treatment with sulfuric acid for 12 h. Therefore, a two-step process has been developed to optimize the reaction yield. In particular, the feedstock was first esterified using an acid catalyst to reduce the FFA content in the oil, and then, the triglycerides

were transesterified using an alkaline catalyst. Transesterification of *Spirogyra sp.* microalgae oil after 180 min at 40°C using a mixture of potassium hydroxide, sodium hydroxide, and sulfuric acid as the catalysts at an oil/methanol ratio of 1:3 and a catalyst loading of 1.5% resulted in a biodiesel yield of 96.9%. In contrast, the application of KOH alone under the same reaction conditions afforded a biodiesel yield of 94.9% [42].

To overcome the drawbacks of homogeneous catalysts, heterogeneous solid catalysts have been used in many organic reactions [43], as they can reduce the soap formation and can be easily separated and reused. Moreover, heterogeneous catalysts can be directly employed in continuous flow reactors [34, 44]. However, their application is restricted by their mass transfer limitations and low thermal stability [14].

Recently, biocatalysts and ionic liquids (ILs) have attracted increasing attention as alternatives to conventional chemical catalysts [45-47]. Pristine and functionalized metal–organic frameworks (MOFs) have also been shown to improve the performance of heterogeneous catalysis due to their high-order structure, high porosity with high specific surface area, and tunable acidity [48].

2.3 Enzymatic Biodiesel Production

Lipases are used as alternatives to chemical catalysts in biodiesel production. Since the lipases catalyze the esterification of FFA, the reaction conditions are mild and the saponification reaction is prevented [49]. However, the enzymatic reactions are relatively slower when using lipases than alkaline catalysts. Furthermore, the enzymes may be inhibited by methanol, the most commonly used reactant in enzymatic biodiesel production. Using the enzymes in soluble form hinders their

separation and reuse [50]. Therefore, enzymes are immobilized on porous supports with high surface area to enhance their stability and facilitate their separation and reuse. Nevertheless, immobilized enzymes suffer from mass transfer limitations and glycerol deposition as a byproduct in the pores of the support, preventing the substrate from reaching the enzyme active cites.

2.3.1 Factors Affecting Enzymatic Biodiesel Production

2.3.1.1 Lipid Source

Biodiesel can be produced from crop oils [51-53], waste cooking oils [54-59], animal fat [60-66], and microalgae oils. Hence, earlier studies have focused on determining the chemical composition of several lipids in these raw materials [67]. The lipids used in biodiesel production differ in their agronomic characteristics, and the content of FFA, water, and phospholipids have the greatest effect on biodiesel quality. Compared to alkali-catalyzed transesterification, the FFA content in the biodiesel feedstock does not affect the enzymatic reaction, as lipases can directly esterify FFA to produce biodiesel. However, phospholipid concentrations of >1% in raw oils can stop the generation of biodiesel, as reported for the transesterification catalyzed by *Candida antarctica* lipase [68].

In the case of heterogeneous catalysts, chemical catalysts or immobilized enzymes, the effects of water and FFA content on transesterification are less significant. However, water inhibits the acid-catalyzed transesterification of raw oils. It has been shown that the conversion of soybean oil to methyl esters decreased from 90.5% to 58.8% when the FFA content increased from 5% to 33%. In contrast, when H_2SO_4 was used as the catalyst, a yield of 90% was only afforded upon reaction with

3.0 wt% H_2SO_4 and a methanol/oil molar ratio of 6:1 at 60°C for 96 h only when the water content in soybean oil was below 0.5 wt%.

Interestingly, water also affects the stability and catalytic activity of lipase-catalyzed transesterification in nonaqueous media. Lipases distinctly act at interfaces of organic and aqueous phases, and their activity depends on the interfacial area. A small amount of water is therefore required to maintain the enzymatic activity in organic solvents as it increases the available interfacial area. However, excess water promotes the hydrolysis of the oil. Thus, the optimum water content should be carefully identified to maximize the enzymatic activity [69].

Lipases exhibit interfacial activation, which is an increase in activity when the substrate (lipid) forms a distinct phase near the adsorbed enzyme. X-ray analyses have shown that lipases contain an amphiphilic amino acidic chain, known as the lid, which is mobile and protects the enzyme active sites, and thus, it is responsible for the enzyme activation [70]. When the lid is closed, the active sites are protected from the environment and the lipase remains inactive. Lipase activity is observed only in the open conformation.

2.3.1.2 Alcohols

Methanol is the most commonly used alcohol in enzymatic biodiesel production and is added in excess to improve the reaction rate and yield. However, high alcohol concentrations cause unfavorable unfolding of the enzyme to a more helical state by stripping essential water molecules, thus impairing its activity [71]. In addition, high alcohol/triglyceride ratios increase glycerol solubility and affect its separation.

Several measures have been proposed to overcome the inhibition of lipases by methanol, including the stepwise addition of methanol, the use of another acyl acceptor, and the introduction of a suitable solvent that dissolves methanol. For immobilized *Candida antarctica* lipase, the stepwise addition of methanol resulted in 98.4% conversion of vegetable oil in 48 h [72]. Similar results were observed for lipases from other sources, such as *Pseudomonas fluorescens* [73], *Rhizopus orzyae* (74), and *Candida* 99–125 [75]. Moreover, over 87% of the initial enzyme activity was maintained at the end of the process with the stepwise addition of methanol. However, this method is complex and cannot be applied to large-scale industrial sectors [76].

Methanol inhibition occurs when its amount in the reaction medium exceeds its solubility. Due to its low solubility in oils, methanol and oil separate at concentrations just above their stoichiometric ratio. Subsequently, the alcohol molecules strip off the essential water microlayer surrounding the lipase, which is required to maintain the conformation and catalytic activity of the enzyme [77]. Therefore, an organic solvent is commonly added to increase the solubility of the substrates and reduce the inhibitory effect of methanol [78]. The addition of an organic solvent can also reduce the viscosity of the reaction medium and enhance the stability and recovery of the immobilized enzyme [79]. Among the possible organic solvents, *n*-hexane is most commonly used in enzymatic transesterification reactions, as it can enhance lipase activity and biodiesel productivity. For example, the biodiesel yield using *Mucor miehei* lipase at a 3:1 methanol/oil ratio increased from only 19% in the solvent-free system to 95% using *n*-hexane within the same reaction time of 5 h [80]. However, most of the suitable organic solvents are toxic and volatile, leading to hazardous effects. Furthermore, an additional purification step is required to remove the second organic solvent from the final product, increasing the cost and energy

demand of the process. In addition, the use of organic solvents with immobilized lipases causes the deposition and adsorption of glycerol due to its low solubility in hydrophobic solvents. Thus, an outer glycerol film is formed, which reduces the mass transfer of the hydrophobic substrates to the enzyme active sites, leading to lower reaction rates [71].

Replacing methanol with ethanol as the acyl acceptor can also reduce the inhibitory effect of methanol. A biodiesel yield of 91% was achieved in 90 min with a methanol/oil molar ratio of 10.44:1 using KOH as the catalyst at 66.8°C. In contrast, the yield was reduced to 77.4% using an ethanol/oil molar ratio of 8.42:1 and KOH as the catalyst for 120 min at 61.3°C. These results also indicated that the temperature plays a more significant role in methanolysis compared to ethanolysis. Moreover, the separation of ethyl esters from glycerol was more difficult compared to that of methyl esters [80].

2.4 Immobilized Enzymes in Biodiesel Production

Immobilization is defined as the attachment of an enzyme onto an insoluble solid support material. In addition to the easy reuse in continuous reactors, immobilization endows lipases with shear and thermal stability as well as easy downstream processing [81]. Furthermore, their confinement in the porous structure of the support protects them from harsh media. Reusability is essential for the feasible application of high-cost enzymes and is the most practical approach for their industrial application. Enzyme immobilization methods can be classified as adsorption, covalent bonding, entrapment, and cross-linking, which together with the appropriate support material play a significant role in the development of an efficient lipase [82].

Moreover, enzyme immobilization greatly relies on the amine functional group of the amino acids in the enzyme, which contribute to the binding to the support.

Despite the advantages of immobilized enzymes, several drawbacks still exist that limit their use in biodiesel production, including the (1) loss of enzymatic activity during immobilization, (2) high cost of carriers, (3) low stability in oil–water systems, (4) large mass transfer limitation, and (5) glycerol adsorption [9]. To improve the properties of immobilized enzymes, coordinated matrices with mesoporous structure and average surface area, such as MOFs, should be used to facilitate substrate diffusion through the pores while reducing enzyme leaching [81].

2.5 MOFs

2.5.1 MOF Structure and Properties

As already discussed, heterogeneous catalysts suffer from mass transfer limitations and catalytic instability. Therefore, MOFs have been employed as support to improve the performance of heterogeneous catalysts [14, 49, 50, 83] due to their high crystallinity, high porosity, and strong interactions in their metal–ligand network [84]. MOFs can be easily prepared with high surface area (5900 m^2/g) and specific volume (2 cm^3/g) [36, 84-98]. Here, we review the recent advances in biodiesel production using modified catalysts. We focus on enzyme and IL immobilization on MOFs, the balance between increased stability and reusability of the immobilized enzyme and mass transfer limitations, pore size and porosity control, manipulation of the hydrophobicity/hydrophilicity in the reaction medium, and optimization of the biodiesel production process.

2.5.2 MOF Preparation

MOFs are porous polymers comprising metal-containing nodes and organic ligands linked through coordination bonds [82]. They possess unique characteristics, such as tunable ultrahigh porosity (up to 90% free volume), large surface area (>6000 m^2/g), diverse functionality, high thermal and mechanical stability, and good electronic properties [99]. Owing to these properties and the wide variety of organic and inorganic components in their structures, MOFs have been widely studied in the fields of storage, separation, catalysis, biomedical applications, and sensor materials [90]. For example, MOFs have been effectively used for gas storage (e.g., H_2, CH_4, CO_2, and NO) without the need for high pressure and/or compression as well as for the separation of toxic organic compounds [100]. Various cost-effective, green, and rapid synthetic methods have also been developed, which can be classified as solvothermal, slow evaporation/direct precipitation, microwave-assisted, electrochemical, mechanochemical, and sonochemical [101] (Table 1). These classifications are selected based on the type of metal, organic linker, and targeted application [99].

Table 1: Examples of MOFs used in biodiesel production

MOF	Oil Source/Alcohol	Synthesis	Pore Size	Temperature/ Energy (°C)	Yield (%)	Ref
CuBTC-MOF	Palm oil/methanol (1:5)	Solvothermal	1.68 cm^3/g	60	91	[100]
ZrSiW/Fe-BTC	Oleic acid/methanol (20:1)	Hydrothermal	0.135 m^3/g	160	85	[102]
ZrSiW/UiO-66	Oleic acid/methanol (20:1)	Hydrothermal	0.243 m^3/g	150	98	[102]
$Mg_3(bdc)_3(H_2O)_2$	Oleic acid/methanol (15:1)	Microwave irradiation	-	150 Watt	97	[103]
MIL-53 (Fe)	Oleic acid/ethanol (1:16)	Ultrasonic irradiation	239 cm^3/g	150 Watt	96	[104]
MIL-53 (Fe)	Oleic acid/*n*-butanol (1:16)	Ultrasonic irradiation	239 cm^3/g	150 Watt	98	[104]
HKUST-1	Palm oil/ethanol (1:1)	Electrolysis	0.19 cm^3/g	room temperature, 15 V	54	[105]

2.5.2.1 Conventional Methods

In conventional solvothermal synthesis, a mixture of metal ions and organic linkers in an appropriate organic solvent is heated in a glass vial for low temperature processes or in a Teflon-lined autoclave or bomb reactor for temperatures >400 K. If water is used as the solvent, the method is referred to as hydrothermal. The desired MOF structure can be prepared by controlling the reaction parameters, including pressure, temperature, solvent composition, and reagent concentration. When the reaction temperature is higher than the boiling point of the solvent, the reaction is referred to as solvothermal, while at reaction temperatures below the boiling point of solvent, the reaction is called non isothermal. Moreover, some MOFs, such as MOF-5, MOF-74, MOF-177, HKUST-1, and ZIF-8, have been synthesized under ambient conditions [102]. For example, rod-like CuBTC-MOF particles were prepared via the solvothermal method using benzene-1,3,5-tricarboxylic acid (BTC) and divalent

copper in 50 v/v% ethanol/water. CuBTC-MOF had a unit cell length of 37.12 nm, surface area of 1085.72 m^2/g, and total pore volume of 1.68 cm^3/g. Utilization of 0.04 g CuBTC-MOF as the sole catalyst for biodiesel production from palm oil afforded a maximum yield of 91% after 4 h in a methanol/oil volume ratio of 5:1 at 60°C [100].

2.5.2.1 Microwave Synthesis

To improve the produced MOF's crystallinity, a microwave-assisted method based on chemically inert metal ions has been developed to provide the energy required for the reaction and to homogeneously increase the temperature in a localized zone. Microwave synthesis is an environmentally friendly alternative to conventional heating, offering fast crystallization, narrow particle size distribution, and better morphological control of the target MOFs [101]. Cr-MIL-100 was the first MOF synthesized via the microwave-assisted method, achieving conversion yields of up to 97% [103].

2.5.2.2 Sonochemical Synthesis

Sonochemical synthesis is a rapid and environmentally friendly method for the synthesis of MOFs using 10–20 MHz ultrasonic radiation in a homogeneous liquid. The cavitation created by the ultrasonic waves sharply increases the temperature and pressure, creating hot spots that facilitate the rapid formation of homogeneous MOF crystals [104]. Consequently, the crystallization time and particle size are significantly reduced compared to those of the conventional solvothermal synthesis. The first MOF synthesized by the sonochemical method was $[Zn_3(BTC)_2]$ [105].

2.5.2.3 Electrochemical Synthesis

For the electrochemical synthesis of MOFs, metal ions are continuously supplied through anodic dissolution instead of metals salts; they react with the linker molecules and a conducting salt dissolved in the reaction medium [105]. The method was first used for the preparation of HKUST-1 [$Cu_3(BTC)_2$], which afforded promising results in renewable fuel production [106].

2.5.3 Properties of MOF-Immobilized Enzymes

2.5.3.1 Enzyme Stability

In general, enzymes are denatured at moderate temperatures and in the presence of chemical denaturants, but remain stable at very high pressures. Therefore, enzymes can be immobilized on a MOF structure to protect it from denaturation and to increase its stability. MOF–enzyme bioconjugates possess higher catalytic stability and thermal tolerance than free enzymes. For example, the half-life of a lipase encapsulated in zeolite imidazolate framework-8 (ZIF-8) at 55–75°C was increased by 3.2 times and its deactivation rate decreased compared to that of the free enzyme [109]. The enhanced thermal stability of the ZIF-8-immobilized enzyme was attributed to the confinement of the enzyme inside the biocompatible microenvironment, which prevented protein unfolding. Additional studies have shown that the activity of enzymes immobilized on MOFs is not affected by exposure to denaturing organic solvents, such as methanol, ethanol, dimethylformamide, and dimethyl sulfoxide. The enzymes immobilized on MOFs retain 100% of their initial activity, in contrast to free enzymes, which retain only up to 20% of their initial activity under the same denaturation conditions [48].

2.5.3.2 Enzyme Recovery and Reusability

An important advantage of enzyme immobilization is the efficient recovery and reuse of catalysts, which is particularly important for reducing the overall cost of enzyme-based procedures. For example, the residual activity of lipase@ZIF-8 after repeated use for seven cycles was 54% of that in the first cycle, while that after storage for 25 days was 90% of the initial activity [109]. A similar result was observed for laccase adsorbed on Zr-MOF, a bimodal micro-mesoporous MOF, where the residual activity was 50% of that in the first cycle after being used for 10 cycles. Furthermore, enzyme immobilization in MOFs reduces product contamination, thus affording lower impurities than free enzymes. However, the nano-size of the enzyme–MOF conjugates hinders their reusability on an industrial scale.

Recent studies have suggested the use of a new 3D matrix as a support for MOFs [110]. For example, a commercially available melamine sponge was tested as a 3D matrix for embedding α-amylase entrapped in ZIF-67 [111]. The melamine sponge was selected due to its low cost, low weight, and high nitrogen content, which provides enormous binding sites for enzyme–MOF bioconjugation [112,113]. The α-amylase embedded MOF–sponge matrix was synthesized by dip coating the melamine sponge in a solution of the pre-synthesized α-amylase entrapped in ZIF-67 at room temperature for 1 h. The α-amylase/ZIF-67 layers on the sponge skeletons were formed because of electrostatic and π–π stacking interactions [112].

2.5.3.3 Allosteric Effect

Allostery involves the binding of a ligand, known as the effector, to the allosteric site of an enzyme, leading to conformational changes in the enzyme active site [114]. Effectors that enhance the enzymatic activity, such as oxygen and metal

ions including Fe^{3+}, Ca^{2+}, and Zn^{2+}, are also known as allosteric activators. For example, a $CaHPO_4$ – α - amylase hybrid biocatalytic nanosystem has been designed based on the allosteric effect using Ca^{2+} as the effector [115]. The immobilized α-amylase showed improved enzymatic activity in the hydrolysis of 2-chloro-4-nitrophenylmaltotrioside. Thus, the allosteric effect is very promising for improving biodiesel production using lipases immobilized on MOFs.

2.6 Lipase Immobilization on MOF's

An immobilized lipase can be defined as a lipase localized in a well-defined region without losing its activity, thus showing high reusability [116]. The main methods used to form immobilized lipase are physical (surface) adsorption, covalent binding, encapsulation, cross-linking, and in situ synthesis shown in Figure 2. The appropriate method for the preparation of each conjugate should be carefully selected, as it can significantly affect the enzymatic activity in the reaction.

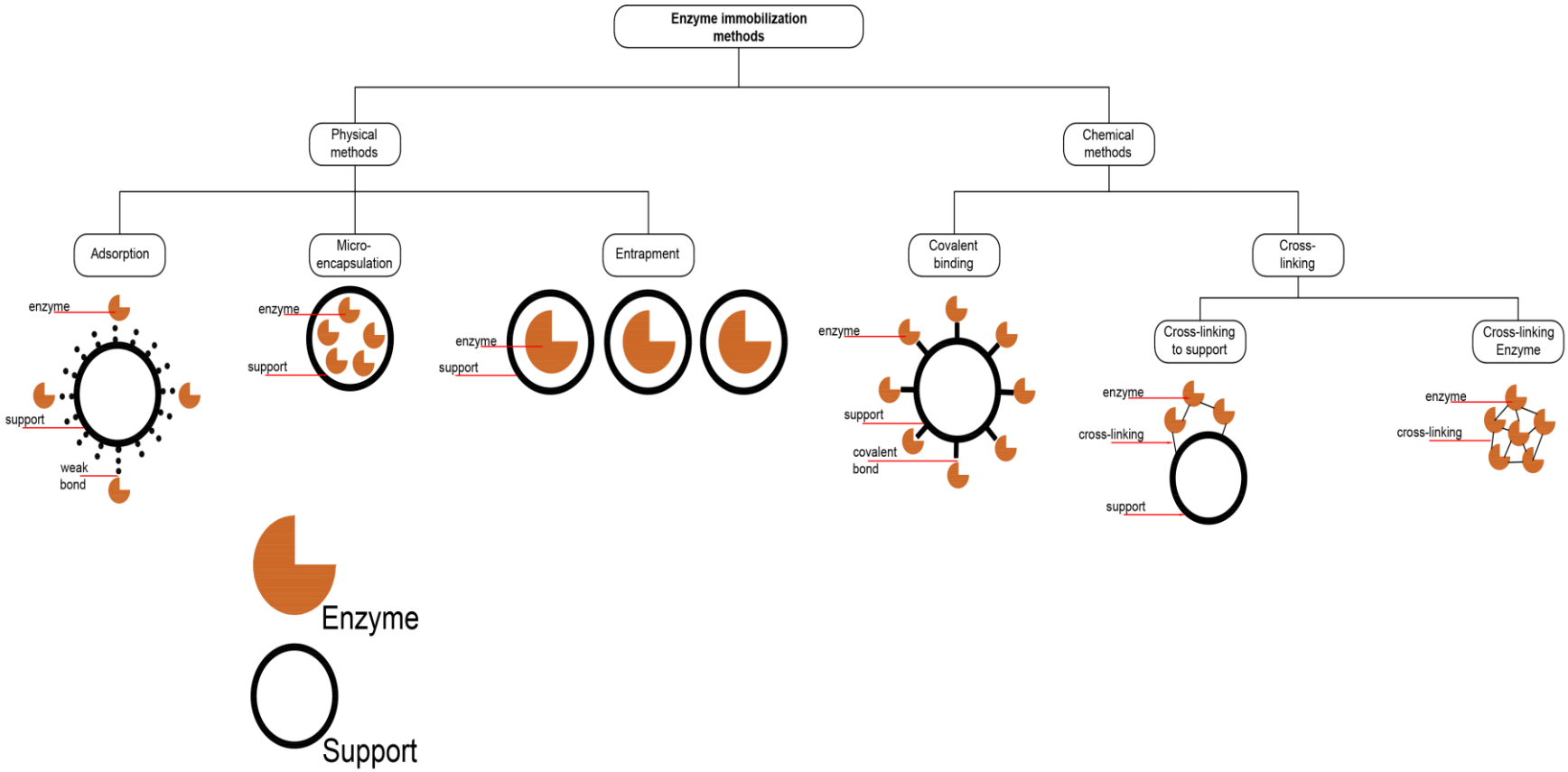

Figure 2: Enzyme immobilization methods

2.6.1 Physical Adsorption

In physical adsorption, enzymes are immobilized on a support matrix by weak interactions, Van der Waals forces, hydrogen bonding, and electrostatic interactions. The main advantage of physical adsorption is that it does not affect the enzyme activity as the weak attraction forces do not alter its native structure and active sites [81]. MOFs can be used as an adsorption support matrix as they offer a large enzyme loading capacity due to their high surface area. In addition, the attachment of the enzymes on the surface of an already prepared MOF protects them from the harsh conditions applied to synthesize MOFs. Moreover, no functional groups are required in physical immobilization.

In a recent study, *Burkholderia cepacia* lipase that was physically immobilized on hierarchical zeolite imidazolate framework (BCL-ZIF-8) was tested for biodiesel production [81]. The immobilization efficiency depended on the adsorption time, immobilization temperature, pH, and morphology of ZIF-8. The biodiesel yield was 93.4% at a lipase loading of 700 mg and the activity recovery reached 98.8%. Interestingly, unlike other MOFs, ZIFs can be prepared at room temperature, but their pore size is very small (~1.5 nm). Therefore, CetylTrimethylammonium Cromide (CTAB) and histidine were used as templating and assisting templating agents, respectively, to interact with the ZIF precursors, forming specific building units. Consequently, the pore size of ZIF-8 was increased to 23.1 nm and its enzyme loading efficiency was improved [87]. Similar results were also obtained using CTAB and 1,3,5-trimethylbenzene [117]. Furthermore, the nature of metal nodes and organic linkers in MOFs can affect the physical loading of the enzyme [118]. Therefore, nodes

or linkers with strong affinity for the enzyme should be used to increase the enzyme uptake.

2.6.2 Covalent Binding

Although immobilization by physical adsorption offers high enzymatic activity for the transesterification process, the enzymes are subject to leaching due to the weak enzyme–MOF interactions [119]. To improve enzyme stability, the weak interactions can be replaced by covalent interactions between the nucleophiles of the enzymes (free amino acids) and the organic linkers (mainly carboxylate groups) of MOFs to form peptide bonds [102]. Among the strong chemical bonds developed during enzyme immobilization, multipoint covalent attachment between the MOF and functional groups of the enzyme, such as amino, glyoxyl, and epoxy [104], leads to the formation of a rigid backbone that stabilizes the enzyme structure, enhances its resistance to unfolding and denaturation, and reduces enzyme leaching (a common feature of chemisorption) [105]. For example, *Candida antartica* lipase-B was immobilized by covalent bonding on activated is reticular MOF-3 by dicyclohexylcarbodiimide with an enzyme loading of 0.18 mg/g, improving the enzymatic activity by up to 103 times compared to that of the free enzyme [120]. Nevertheless, in addition to the large internal surface of MOFs, other features such as low steric hindrance and high reactive group density are needed for effective multipoint covalent attachment. Moreover, the enzyme should retain its activity under the immobilization conditions [106].

2.6.4 Entrapment/Encapsulation

The entrapment of enzymes within the MOF pores requires the diffusion of the enzyme molecules through gaps that are generally smaller than the MOF cavity. Due

to their high porosity, MOFs allow the adsorption of enzymes into their mesoporous structure, instead of only on their surface, thus increasing enzyme loading. Moreover, the entrapment of enzyme molecules into the MOF pores protects them from harsh denaturing conditions as the enzyme is not attached to the support and does not chemically interact with it, thus improving stability. However, enzymes immobilized by this approach exhibit mass transfer limitations and their diffusion is restricted as the substrate may not be able to access the entire active site [102]. In addition, enzyme entrapment into nano- or microporous MOFs may not be efficient, while part of the enzymatic activity may be lost due to conformational changes during diffusion into small cavities [102]. To avoid these challenges, MOFs with macroporous structure are gaining increasing attention for enzyme immobilization.

When the MOF pore sizes are smaller than the enzyme, the enzyme can only be immobilized through encapsulation into MOF crystals, a process known as co-precipitation. During this approach, enzyme immobilization simultaneously occurs with the nucleation and MOF crystal growth. Recently, mesoporous MOFs, such as MIL-100(Fe) and HKUST-1, have been tested as supports for lipase immobilization through co-precipitation [99,122]. However, low enzyme loadings were achieved due to the long-range ordering and nonuniformity of MOFs. In contrast, highly ordered MOFs with large specific areas and uniform and adjustable nano sizes could be loaded with high enzyme amounts and were effectively used for in situ enzyme encapsulation [99,109]. This technique is relatively new, and the first protein molecules directly embedded into ZIF-8 by the co-precipitation method have been reported in 2014 for cytochrome c (Cyt c) [122]. In this process, the enzymes were incubated with the precursors, i.e., zinc nitrate and 2-methylimidazole, in methanol and in the presence of PolyVinylPyrrolidone (PVP) to prevent protein agglomeration in the organic solvent.

Cyt c immobilized on ZIF-8 exhibited 10 times higher activity than the free enzyme due to the metal ion activation effect. Other enzymes immobilized on MOFs by the co-precipitation method are horseradish peroxidase in ZIF-8, Cyt c in ZIF-10, and lipase in ZIF-8. Enzyme encapsulation into ZIF-8 has also been achieved in an aqueous solution instead of an organic solution [123], thus eliminating the need for PVP and extending the scope of the co-precipitation method to enzymes that are significantly inactive in organic solutions. *Aspergillus niger* lipase has also been encapsulated into ZIF-8 [109], as confirmed by an amide I band observed at 1658.7 cm^{-1} in the Fourier-transform infrared spectrum, which is typical for enzymes and corresponds to the N–H bending mode. Furthermore, a biomimetic mineralization method has recently been reported as an alternative enzyme encapsulation strategy in MOFs. For instance, the encapsulation of urease using this technique affords improved thermal stability [124].

The biological functions of enzymes could be altered when they are encapsulated in MOFs, due to the interactions between them. This was investigated using catalase encapsulated in solid and hollow ZIF-8 microcrystals [125]. At a constant catalase loading, characterization of the immobilized enzyme after H_2O_2 degradation reaction showed no change in the structure, and kinetic study indicated no significant mass transport limitation. Nevertheless, the interfacial interactions between the enzymes and MOFs impacted their activities. To overcome this, the solid MOF microcrystals was proposed to be hollowed before enzymes encapsulation. Before the hollowing process, the enzymes were confined in the solid MOF crystals, whereas they were sealed inside of the central cavities of the hollow MOF crystals in a freestanding form, with minimum interaction. The permeable MOF shell allowed reactants to penetrate the shell and reach the enzyme, preventing the enzymes from leaching [125].

Another method that has been recently developed to overcome the interaction problem of the enzyme with the MOF the de novo approach. In this system, enzyme molecules are embedded in a MOF crystal with small pores in water at mild conditions. Similar to other encapsulation techniques, the de novo approach allows MOFs with pore sizes smaller than the size of the enzymes to be used. This not only prevents leaching but also greatly expands the selection of enzymes and MOFs, making the method generally applicable for various functional applications. This concept has been used with ZIF-90 of 1 nm pore size to coat catalase molecules of 10 nm size [126]. The small pore size of ZIF-90 prevented the leaching and provided size-selective sheltering to increase tolerance against protease. The interactions between the enzyme and the MOF have marginal influence in the de novo system, which has a positive effect on enzyme activity. After being embedded in the MOF microcrystals via a de novo approach, the enzyme maintained its biological function under a wide range of conditions. By exposure to a denature reagent, urea, and high temperature of 80°C, embedded catalase in ZIF-90 maintained its activity in the decomposition of hydrogen peroxide even, whereas free catalase was completely deactivated [127].

The immobilization of porcine pancreatic lipase (PPL) by encapsulation was explored using three different MOFs: HKUST-1, which is prepared using copper as metal nodes and BTC as the organic linker; mesoporous MIL-100(Fe); and MIL-100(Fe) containing Keggin phosphotungstic acid [122]. In particular, 5 mg of each MOF was introduced into a buffered PPL solution, followed by mild shaking at room temperature for 2 h. The encapsulation of PPL in the MOF pores was spectroscopically confirmed; the characteristic bands of MOFs in PPL@MOF were shifted relative to those of free MOFs.

Mechanochemical processes is another encapsulation method, which has been recently proposed for enhanced enzyme activity and stability. In this process, the traditional solution-based processes are replaced with a more environment-friendly mechanical alternative, such as ball milling. The process minimizes the use of organic solvents and strong acids during the MOF synthesis, allowing the encapsulation of enzymes into robust MOFs, while maintaining enzymatic biological activity. In addition, the mechanical processes are rapid and can be easily scaled-up to industrial levels. However, the advantages of this process were only demonstrated on enzyme encapsulation in ZIF-type of MOFs. The synthetic conditions required for other types, such as UiO-66-NH_2 and Zn-MOF-74, were too harsh for the encapsulated enzymes to retain their activity [128].

2.6.3 Cross-Linking

Enzymes can also develop intermolecular interactions with the support through covalent bonds in the presence of a multifunctional reagent that serves as a linker. There are two methods of enzyme immobilization by cross-linking: Cross-Linking Enzyme Crystal (CLEC) shown in Figure 3 and cross-linking enzyme aggregate (CLEA) shown in Figure 4 [121]. In CLEC, glutaraldehyde is used as the linker between the free amino groups of the enzyme and the reactive sites of a neighboring molecule. However, the addition of glutaraldehyde could seriously alter the enzyme structure, thus affecting its activity. To address this issue, inert proteins, such as gelatin or bovine serum albumin, can be added. In the case of CLEA, which is an im-proved version of CLEC, the introduction of a salt, nonionic polymer, or organic solvent promotes the formation of enzyme aggregates without distorting the enzyme properties. However, CLEA cannot be combined with MOFs as it does not require an

external support. Taken together, immobilization by cross-linking is a simple method with a very low possibility of enzyme leaching due to the strong chemical bonds between the enzyme molecules. Furthermore, enzymes can be modified using adequate stabilizing agents to adapt to any microenvironment.

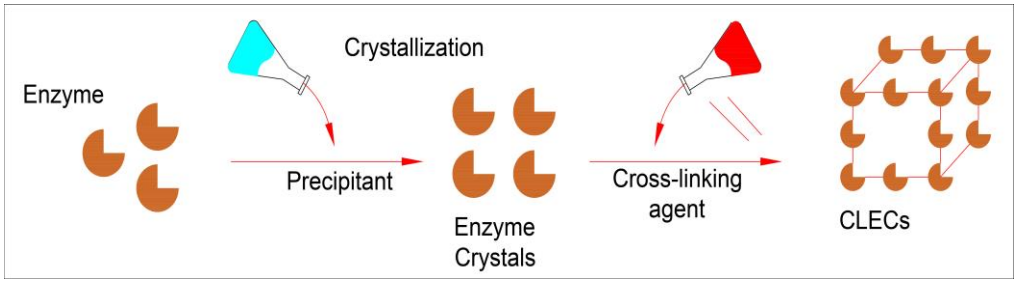

Figure 3: Cross-linking enzyme crystal

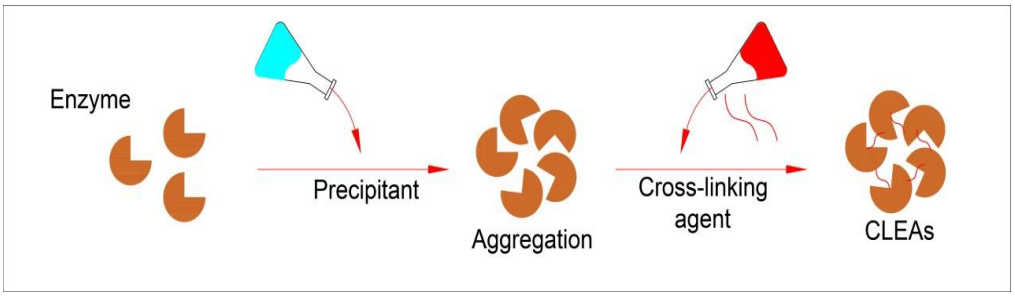

Figure 4: Cross-linking enzyme aggregate

2.7 Use of Immobilized Enzyme in Biodiesel Production

Lipase is attached in commercially available Novozym@435 by cross-linking divinylbenzene and methacrylic acid on polyacrylic resin. These cross-liking agents have high protein affinity, which reduce enzyme leaching, while minimizing the negative effect of chemisorption on enzyme activity. Functional groups carried by the monomers of a cross-linking polymer can be selected according to the immobilized enzymes. These functional groups can facilitate the binding of the enzyme to the

support or increase the affinity of the substrate and the immobilized enzyme, thereby increasing the enzyme activity [129]. Therefore, Novozym@435 was shown to exhibit high efficiency for biodiesel production [130]. It was successfully used with waste cooking oil achieving a conversion up to 93%, with high stability [131].

The replacement of conventional organic solvents with greener ILs has opened up new opportunities for Novozyme@435 in biodiesel production. The use of ILs containing long alkyl chains on the cation has the important advantage of producing homogeneous systems at the start of the reaction but, when the reaction is complete, a three-phase system is created that allows selective extraction of the products using straightforward separation techniques, while the IL and the enzyme can be reused [132]. Biodiesel yield from soybean oil using Novozym@435 in [Emim][TfO] IL was 80% after 6 h, which was eight times higher than that archived in solvent-free system and 15% higher than the that using tert-butanol as an additive [133] at the same conditions. Other ILs that showed promising results with Novozyme@435 are [C_{16}MIM] [NTf_2] and [BMIm][PF_6], achieving 98% and 86% biodiesel yields from Triolein and microalgae oil, respectively [132,134].

As mentioned earlier, MOFs have been used as promising carriers for the enzyme immobilization. The MOF-enzymes biocomposites exhibited excellent biocatalytic properties, improved stability, and reusability. By using lipase of the same genus, *Candida* sp., of that used in Novozym@435, encapsulated inside ZIF-67, 78% biodiesel yield was achieved [135]. By using *Rhizomucor miehei* lipase encapsulated in X-shaped ZIF-8, a biodiesel production conversion of soybean oil reached 92.3% after 24 h reaction time. The enzyme retained 84.7% of its initial activity after 10 repeated cycles [15]. By using hierarchical mesoporous (ZIF-8) to

immobilize *Burkholderia cepacia* lipase (BCL) into surface adsorption the conversion of transesterification reaction 93.4% yield, when the optimum conditions for biodiesel production were transesterification time 12 h with three-step addition of alcohol at 4 h intervals and reaction temperature 40°C. There was no significant drop in conversion yield relative to original activity for BCL-ZIF-8 when continuously reused for eight cycles [136].

On the other hand, when Novozym 435 used in esterification of free fatty acids from palm oil fatty acid distillate (PFAD), 93% conversion was obtained after 2.5 h using ethanol with 1.0 wt % of Novozym 435 at 60°C. Novozym 435 was reused 10 times with conversion reaching 88% and 65% after the 11th reaction with ethanol and methanol, respectively [137].

When Novozym 435 was used in esterification reaction in the presence IL [BMIM][PF_6] and Methyl acetate as the acyl acceptor, a biodiesel yield of 80% was achieved at the optimum conditions of 14:1 oil:acyl acceptor molar ratio; 20% (*w* immobilized lipase/*w* of oil) and a temperature in the range of 48–55°C. After nine repeated runs, a decline in in lipase activity was observed after the sixth run [138].

By immobilizing lipase from *Candida rugosa* in magnetic Fe_3O_4@MIL-100(Fe) MOF, prepared by coating Fe_3O_4 magnetite with porous MIL-100(Fe) MOF using amide linkages, a maximum biodiesel conversion of 92.3% was obtained at a methanol/oil molar ratio of 4:1, with a three-step methanol addition manner, and a reaction temperature of 40°C. The biocatalyst was recycled easily by magnetic separation without significant mass loss, and displayed 83.6% of its initial activity after five runs, thus allowing its potential application for the cleaner production of biodiesel [139].

A covalent immobilized *Candida antarctica* lipase (CALB) onto the bio-based MOF with adenine as the organic ligand based on the concept of biomimetic assembly was used in the esterification of oleic acid with methanol for biodiesel production. The highest yield of 98.9% was obtained under the optimized conditions: methanol/oil ratio of 3.65:1, a reaction temperature of 46.3°C, a CALB@MOF loading of 117.77 mg and a reaction time of 11.55 h [140]. Table 2 shows a summary of comparison between the performance of lipase immobilized on different supports in biodiesel production.

Table 2: Performance of lipase immobilized on different supports in biodiesel production

Enzyme	**Support**	**Immobilization Support**	**Solvent**	**Temperaure (ºC)**	**Time (hr)**	**Biodiesel yield %**
Novozym@ 435	-	Cross linking	ethanol	60	2.5	93
Novozym@ 435	[BMIM][PF_6]	Cross linking	Methyl acetate	55	6	80
Candida Rugosa	Fe_3O_4@MIL-100(Fe)	Covalent attached	Methanol	40	60	92.3
Candida antarctica	CALB@MOF Bio-based	Encapsulated	Methanol	46.3	11.55	98.8
Novozym@435	[Emim][TfO]	Cross linking	Free solvent	50	12	80
Novozyme@435	[C_{16}MIM] [NTf_2]	Cross linking	Free-Solvent	60	6	98
Novozyme@435	[BMIm][PF_6]	Cross linking	Methanol	40	48	86
Candida sp	Zif_67	Encapsulation	Methanol	45	60	78
Rhizomucor miehei	X-shaped ZIF-8	Encapsulation	ethanol	45	24	92.3
Burkholderia cepacia	Mesoporous ZIF-8	Adsorption	ethanol	40	12	93.4

2.8 Cost Analysis and Viability of Immobilized Enzymes

As mentioned earlier, the advantages of enzymatic approach over conventional alkali-based processes have been clearly demonstrated in biodiesel production from non-refined feedstock. The enzymatic approach is less energy intensive, more environment friendly, simplifies the separation of the byproduct glycerol, and eliminates the need for water-washing step that consequently reduce wastewater treatment cost [141, 142]. Most importantly however, enzymes are insensitive towards free fatty acids (FFA) content in the feed, allowing it to be used with low quality feedstock. They even catalyze the FFA together with the transesterification of the triglycerides, which increases the overall biodiesel yield. Nevertheless, the high cost of enzymes remains the main challenge facing the commercialization of enzymatic biodiesel production processes [142, 143]. In an economic study on the production of 1000 tons of biodiesel from palm oil, alkali process was found to be more feasible that enzymatic process, when the enzyme was used in a soluble form [144]. It is obvious therefore that enzymatic process can only be feasible if the enzymes are repeatedly used with maintained activity. As mentioned before, this is achieved by enzyme immobilization on a suitable support. By using immobilized enzyme in the economic [144], the feasibility of the process increased. Although the alkali catalyzed process was found to be still more feasible, the study limited the number of reuses to only five. If reusability is increased, the lipase process becomes more feasible. Allowing the use of low-quality feedstock also favors the use of enzymes over alkaline processes. In 2006, a biodiesel production line of 20,000 t/y capacity was built in China using waste cooking oil as feedstock, in which a combination of different immobilized lipases has been used as a catalyst [123, 145].

The successful immobilization of the enzyme on the support for maintained activity and stability, with minimization of mass transfer limitation, play major role in shifting the economic balance towards the enzymatic process. Although many technologies have been developed for lipase immobilization at lab scale, only a few are industrialized. The main challenges are the high cost of the carrier support, low enzyme capacity and enzymatic activity and stability retaining challenges. The most widely used immobilized enzyme in biodiesel production is Novozym@435, which is sold at a price of about US$1000/kg [142]. In addition, the advancement in biotechnology promises to offer new enzymes of lower production costs and higher catalytic activity and stability, which would further improve the feasibility of enzymatic process. It has been recently reported that immobilized lipase products, specifically designed for biodiesel production, have been developed with a reduced price of about $150/kg [116]. This will pave the way for commercial use of enzymatic processes.

Another aspect that needs to be considered is the environmental factor, which may not be readily transferred into cost. Enzymes are more environment friendly process, which reduces the wastewater production. In that regard, the use of green solvents, instead of conventional organic solvents that require additional separation and purification units are therefore essential. Among the most promising alternative solvents are ILs, which as mentioned earlier can further enhance enzyme reusability with enhanced mass transfer [123]. However, ILs are generally more expensive than organic solvents. The cost of the most commonly used ILs in enzymatic biodiesel production, namely 1-*n*-butyl-3-methylimidazolium tetrafluoroborate ([BMI][BF_4]) and 1-*n*-butyl-3-methylimidazolium hexafluorophosphate ([BMI][PF_6]), are about 25 times more than organic solvent. Therefore, feasible use of enzyme-IL systems

requires repeated reuse with maintained activity and stability and efficient separation of the products is another important factor [145]. Additionally, deep eutectic solvents (DESs), is a potential replacement to ILs, which are more cost-effective and environmentally friendly. The properties of DESs can be finely tuned, similar to those of ILs, by selecting different cation and anion combinations. They have characteristics similar to those of ILs, such as high purity, ease of preparation, non-toxicity, biodegradability, requirement of mild reaction conditions, and insensitivity to water [146]. In addition, BASF has recently commercialized four MOF materials, including BASOLITE-A100 (MIL-53), BASOLITE-C300 (HKUST-1), and BASOLITE-Z1200 (ZIF-8) with prices ranging between 10 to 15 US$/g, making these MOFS only affordable for research purpose at this time. However, with advance in raw materials selection and synthesis technology, lower prices that are comparable to that of synthetic zeolites may be achieved for large scale synthesis of some MOFs in the future [147].

2.9 Hypothesis

In this Thesis, using enzymatic process for biodiesel production (Lipase) (Hypothesis: This will help the reaction to not suffer from saponification, and Lipase active sites will contact effectively with MOF), Immobilize lipase into different type of MOFs (Hypothesis: This will improve the catalytic performance and operational stability of lipase immobilized on porous MOFs for biodiesel production)

Study the kinetics and isotherm of the immobilization reaction (Hypothesis: This will provide an insight into adsorption pathways and probable mechanism involved in the reaction for better understanding), Study the diffusion-reaction model (Hypothesis: This will provide a better understanding of their application in biodiesel

production and for future enhancement), High biodiesel production (Hypothesis: Due to high surface area of MOF to immobilize the enzyme, a much lower mass transfer can be achieved compared to conventional immobilized lipase and allows its repeated reuse).

Chapter 3: Methods

3.1 Method and Theory

Most produced biodiesel worldwide is currently achieved through alkaline-catalyzed methanolysis. However, in this process, the oils feedstock needs to be refined to remove free fatty acids, which not only increase the processing cost but also lead to loss of part of the feedstock [148, 149]. Lipase-catalyzed production on the other hand, has drawn increasing attention, since it can be effectively used unrefined oil, in addition to its other advantages, including the operation at mild conditions, low energy requirements and easy product separation [150].

For economical application of enzymatic processed in biodiesel production, lipase enzyme has to be used in immobilized form to allow easy retention and reuse. In addition, immobilization has been reported to result in enhanced enzyme thermal and shear stability [148, 153]. The main challenges facing industrialization of enzymatic process are the high mass transfer resistance, tendency to adsorb the by-product glycerol onto the support matrix and poor operational stability [150]. These problems can be solved by good selection of supports of favorable surface characteristics and pore sizes [154, 155].Porous supports are generally preferred due to their high surface area, which allows a higher loading and better protection of the enzyme [154]. Therefore the pore size plays an important role on the catalytic activity and stability [156, 157, 158].

In that regard, increasing interest has recently been on Metal-Organic Frameworks (MOFs) as a new kind of porous supports for enzyme immobilization [159, 160]. In addition, it was shown that by immobilizing peroxidase and trypsin on

MOF composites higher stability and catalytic performance was attained [159]. Physical adsorption, which is a fast and easy method of enzyme immobilization ensures limited enzyme denaturation and does not affect the enzyme activity, native structure and active sites [160]. However, owing to the weak interaction between the enzyme and the support, with this method enzymes are prone to leaching, which results in low stability [161]. Hierarchical mesoporous (ZIF-8) was also used to immobilize *Burkholderia cepacia* lipase (BCL) by surface adsorption, and in biodiesel production [162]. A biodiesel yield of 93.4% was achieved after 12 h with three-step addition of alcohol at 40°C showed the immobilization efficiency was shown to depend on the adsorption time, immobilization temperature, pH, and morphology of ZIF-8. As an alternative, chemisorption in which the nucleophiles of the enzymes (free amino acids) are covalently bonded to the organic linkers (mainly carboxylate groups) of MOFs to form peptide bonds has been used [163]. This result in more stable biocatalysts, with less enzyme leaching and more rigid backbone [150, 164, 165]. However, the negative effect of the chemical bonds on the structure of the enzyme renders physically immobilized lipase generally more active,, despite the higher operational stability of chemically immobilized lipase [161]. Having said that, it should be noted that with both adsorption approaches, enzyme attachment into the internal pores of MOFs may not be efficient, as part of the enzymatic activity may be lost due to conformational changes during diffusion into small cavities [150, 158].

To reduce the leaching problem encountered by physical adsorption, while avoiding the chemical adsorption which could negatively affect the activity of the enzyme, mesoporous MOFs, such as MIL-100(Fe) and HKUST-1, have been used as supports for lipase immobilization through co-precipitation [154, 166]. In this case, the enzyme is caged inside the pores of the MOFs during the crystallization process.

As the immobilization is presumably non-covalent, so minor activity loss against that of the free enzyme could be reached Lipase encapsulated inside MOFs was successfully used in transesterification reaction and showed higher thermal stability than free lipase [158]. However, owing to the long-range ordering and nonuniformity of MOFs, low enzyme loadings were achieved. Lipase was firstly in situ encapsulated inside ZIF-8 and ZIF-10 for biosensing of explosive organic-peroxides [158], *Candida antarctica* lipase B was also encapsulated inside UiO-66 and ZIF-8 and used for the transesterification of vinyl acetate and vinyl laurate [168]. By using encapsulated lipase inside ZIF-67, 78% biodiesel yield was achieved after 60h at 45^{o}C [176]. A higher biodiesel yield of 92.3% was achieved within 24 h using *Rhizomucor miehei* lipase encapsulated in X-shaped ZIF-8 at 40^{o}C. In addition, the enzyme retained 84.7% of its initial activity after 10 repeated cycles [169]. In addition, enzymes immobilized by this approach exhibit mass transfer limitations and their diffusion is restricted as the substrate may not be able to access the entire active sites [170]. Kinetics and thermodynamics studies of the adoption process, which is scarce in literature, could provide invaluable information on the surface chemical affinity, , enzyme accessibility and leaching [149]. Therefore, in this work, the mechanism, kinetics and thermodynamics of lipase adsorption on the surface of different MOFs, namely ZIF-67, ZIF-8 and HKUST-1, have been thoroughly investigated and tested for biodiesel production. The three supports have different structures, pore sizes, chemical properties, and surface areas.

Adsorption is a process that results in the removal of a solute from a solution and concentrating it at the surface of the adsorbent, until the amount of the solute remaining in the solution is in equilibrium with that at the surface. In this work, the assumption based that after 24 hr of batch reaction will reach an equilibrium[174].

In this work, the mechanism, kinetics and thermodynamics of lipase adsorption on the surface of different MOFs, namely ZIF-67, ZIF-8 and HKUST-1, have been thoroughly investigated and tested for biodiesel production. The three supports have different structures, pore sizes, chemical properties, and surface areas.

Many theoretical and empirical models have been developed to represent the various types of adsorption isotherms. At present, there is no single model that satisfactory describes all mechanisms and shapes. Langmuir and Freundlich models, described by Equations (1) and (2) have been widely used to describe adsorption isotherms [174, 175, 172]:

$$q_e = \frac{q_m b C_e}{1 + b C_e} \quad (1)$$

$$q_e = a_F C_e^{1/b} \quad (2)$$

Where, q_e is the equilibrium amount of solute adsorbed (mg/g of solid), C_e is the equilibrium concentration of solute in solution (mg/L), q_m (mg/g) and b (mg/L^{-1}) are constants, representing the maximum adsorption capacity for the solid phase loading and the energy constant related to the heat of adsorption, respectively, and a_F ($mg^{(1-1/b)}$ $l^{1/b}/g$) and b are constants.

The Langmuir isotherm assumes uniform and constant binding of the sorbate on the surface of the adsorbent. The Freundlich model does not have thermodynamic basis and does not offer physical interpretation of the adsorption data.

The value for the Langmuir isotherm constant (b) determined at different temperatures can be used to calculate the enthalpy change of adsorption

thermodynamic parameters, such as Gibbs free energy (ΔG), change in enthalpy (ΔH), and entropy (ΔS), as given by Equation (3) [172]:

$$lnb = -\frac{\Delta G}{RT} = \frac{-\Delta H}{RT} + \frac{\Delta S}{R} \quad (3)$$

Where T is the temperature (K), R is the gas constant (8.314 J/mol K), and b is the Langmuir constant. Adsorption kinetics on the other hand, describes the reaction pathways and the time needed to reach the equilibrium. In order to examine the controlling mechanism, kinetics models that have been commonly used are the Lagergren pseudo-first order, Elovich's model and Pseudo-Second order and intraparticle diffusion models. The linearized form of those models is given in Equations (4-7), and in Table 3 respectively [172]:

$$ln(q_e - q) = ln(q_e) - \frac{kt}{2.303} \quad (4)$$

$$q = \frac{1}{b} ln(ab) + \frac{1}{b} ln\,(t) \quad (5)$$

$$\frac{t}{q} = \frac{1}{k_2 q_t^2} + \frac{1}{q_e} t \quad (6)$$

$$q_t = C + k_{id} t^{0.5} \quad (7)$$

Where, k is the kinetics constant of pseudo-first order adsorption (min^{-1}), q_e and q (mg/g) are the amounts adsorbed at equilibrium and at time t (min), respectively, a is the initial adsorption rate (mg/g/min), and 1/b (mg/g) is a parameter related to the number of sites available for adsorption, k_2 (g/mg/min) is the pseudo-second order rate constant of adsorption, k_{id} is the rate constant of the intraparticle transport

(mg/g/min$^{0.5}$) and C (mg/g) is a constant related to the thickness of the boundary layer. The higher the value of C, the greater boundary layer effect.

Table 3: Rearranging of linear kinetic models' parameter's

Type	Linear Form	Plot	Parameter
Pseudo Second order model	$\frac{t}{q_t} = \frac{1}{kq_e^2} + \frac{1}{q_e}t$	t/q_t vs. t	q_e= 1/slope k=slope^2/Intercept
Pseudo First order model	$ln(q_e - q) = ln(q_e) - \frac{kt}{2.303}$	ln(q_e-q) vs t	qe=e$^{(Intercept)}$ k= -Slope x 2.303
Elovich's model	$q = \frac{1}{b}ln(ab) + \frac{1}{b}ln\,(t)$	Q vs. ln(t)	b=1/slope Intercept = slope x ln(1/slope x a)

The rate limiting step in the Pseudo-Second order is the surface adsorption that involves chemisorption, where the adsorbate removal from a solution is due to physicochemical interactions between the two phases [174]. Wherein, Pseudo first order model assumes intraparticle transport (pore diffusion) rate-limiting step [175].

In the intraparticle diffusion model assumed the process to be diffusion-controlled, and the rate of adsorption depends on the speed at which adsorbate diffuses towards adsorbent [174].The intraparticle diffusion coefficients can be determined using Equations (8)[152]:

$$D_p = 0.03 \times r_p^2 / t_e^{0.5} \quad (8)$$

Where, D_P is the intraparticle diffusion (cm^2/s), r_P is the average radius obtained from BET (nm) and t_e is the contact time required to reach the equilibrium (min)

3.2 Materials

Eversa ® Transform 2.0 were donated from Novozymes, Denmark. Bradford reagent ,2-methylimidazole (HMeIM) (99%), zinc nitrate hexahydrate (99%) and 1,3,5-benzenetricarboxylic acid (95%) (BTC) were obtained from Merck, USA. Cobalt (II) nitrate hexahydrate (≥ 99%) and triethylamine (TEA) (≥ 99%) were obtained from Fisher chemicals, USA. Copper (II) nitrate trihydrate (≥ 99.5 %) was obtained from EMSURE® analytical reagent, India. Phosphate Buffer Saline, pH 7.4, was obtained from HIMEDIA, USA. Methanol of 99.5%purity, n-hexane of 99% purity and ethanol of 99.9% purity were of analytical grade and obtained from S D Fine Chem Limited (SDFCL), India. Hydrogen, zero air (ultra-pure), helium, were supplied by Sharjah Oxygen Company, UAE. A standard solution of high purity FAMEs mix consisting of 4% myristic acid (C14:0), 10% palmitic acid (C16:0), 6% stearic acid (C18:0), 25% oleic acid (C18:1n9c), 10% Elaidic acid (C18:1n9t), 34% linoleic acid (C18:2n6c), 2% linolelaidic acid (C18:2n6t), 5% linolenic acid (C18:3), 2% arachidonic acid (C20:0), and 2% of behenic acid (C22:0) was purchased from Merck, USA. Olive oil, with nearly 99% purity, was purchased from local markets. The Deionized Water (DIW) used in all experiments was purified in a water purification system (UltraPure, ThermoFisher, USA), the water was not analyzed after the analysis.

3.3 MOFs Synthesis

3.3.1 Synthesis of ZIF-67

A method similar to the one reported in [189], with slight modifications, has been used to prepare ZIF-67. Briefly. A solution (B), consisting of 5.5 g HMeIM in 80 mL of DIW was gradually added to another solution (A), consisting of 0.45 g cobalt nitrate hexahydrate in 12 mL of DIW. The mixture was left on a magnetic stirrer (DAIHAN MaXtirTM 500S, Korea) at 200 rpm for 60 min at room temperature. After that, the mixing was stopped, and the mixture was left overnight. The next day, the resulting purple precipitates were collected by centrifugation (Hettich ROTANTA 460 R, Germany) at 8600 rpm for 10 min, and washed with 40 mL of (50:50) DIW-methanol solution for 3 times on a vacuum filter. The collected crystals were then vacuum dried at 80°C for 24 h. shown in Figure 5.

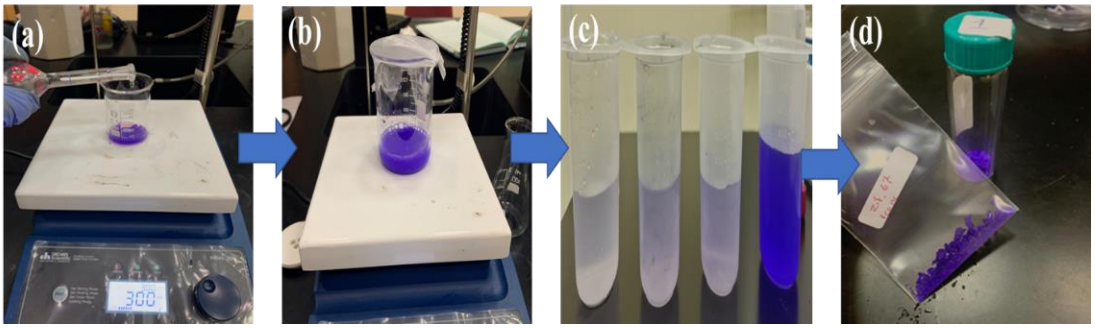

Figure 5: ZIF-67 preparation method: (a) organic solution was gradually mixed with metal solution at 300 rpm (b) after complete mixing, the mixture was stirred for 1 hour, (c) after day, the solution was centrifuged and washed until the supernatant shift into transparence color to remove all the unreacted precursors (d) ZIF-67 powder

In the preparation of lipase encapsulated in ZIF-67, similar method to the one used in the preparation of the empty ZIF-67 was adopted shown in Figure 6, but the

amounts were reduced to four, in the presence of the enzyme. Briefly, 5 mL of lipase stock solution were added to modified solution B, prepared by dissolving 1.375 g HMeIM in 15 mL DW to keep the concentration of HMeIM similar to that used with the preparation of empty ZIF-67. The 20 mL of enzyme-enriched solution (B) was then added gradually to solution A of 0.1125 g of cobalt nitrate hexahydrate in 3 mL of DIW, to keep the ratio of precursors consistent. The crystallization steps were similar to the free ZIF-67 preparation procedure, in that the solution was stirred kept on a magnetic stirrer at 200 rpm at room temperature for 60 min, left overnight without mixing, and then the precipitate was collected by centrifugation at 8600 rpm and -4^{o}C for 10 min. However, in this case the washing was done in three times with 20 mL of phosphate buffer solution (PBS) (0.25 M), to avoid exposing the enzyme to methanol. Ina addition, the drying of the lipase encapsulated ZIF-67 was done in freeze dryer (Labconco FreeZone, USA) operated at -84.4^{o}C and 0.059 mbar and then stored at 4^{o}C for later use.

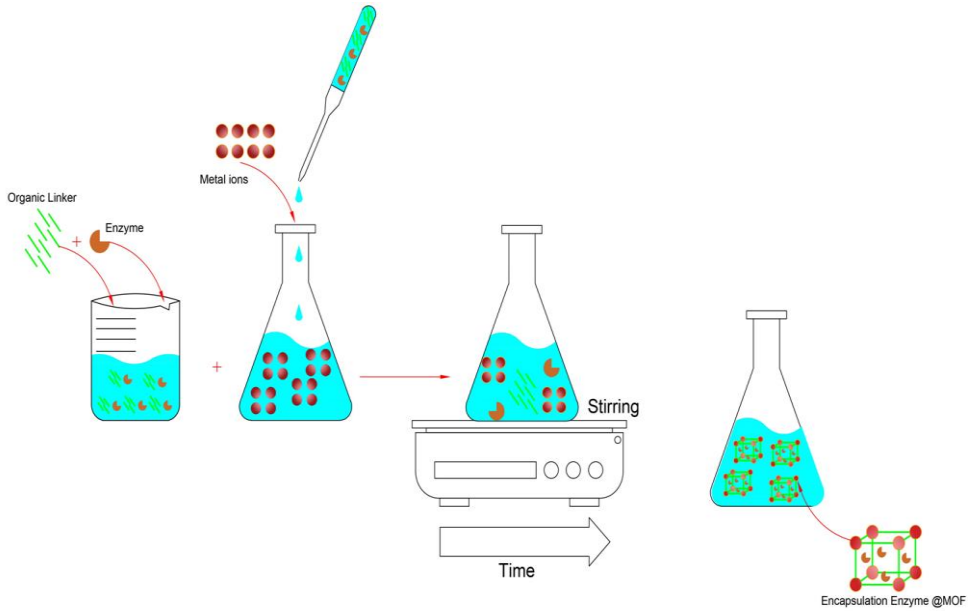

Figure 6: Scheme of encapsulation and preparation MOF@Enzyme

3.3.2 Synthesis of HKUST-1

For the synthesis of mesoporous HKUST-1, 0.716 g of copper dinitrate trihydrate and 0.421 g benzene tricarboxylic acid were dissolved in 12 mL of ethanol-water (50:50) solution under continuous mixing using a magnetic stirrer (DAIHAN MaXtirTM 500S, Korea) at 150 rpm for 30 mins [185] in Figure 8. Throughout this time, the reaction cell was covered with paraffin tape to avoid ethanol evaporation. The solution was then transferred into a Teflon container and placed in a hydrothermal synthesize reactor. After tightly securing the reactor lid, the reactor was placed in a pre-heated thermostatic oven (Witeg WOV, Germany), and kept at 109^{o}C for 24 h. After that, the reactor was allowed to cool down to room temperature. The solution, which has a turquoise blue color, was sonicated (Ultrasonic Cleaner MH-031X, UK) at an amplitude of 20 for about 8-10 minutes to break the aggregates of micron-sized colloidal particles in the solution. After that, the solution was vacuum filtered to collect the precipitated crystals, which were then washed with 40 mL ethanol and dried at room temperature in Figure 9. The crystals were stored under vacuum for later use. Owing to the high temperature used in the preparation of this MOF, encapsulation of lipase was not possible, as the exposure to the high temperature would deactivate the enzyme all process in Figure 7.

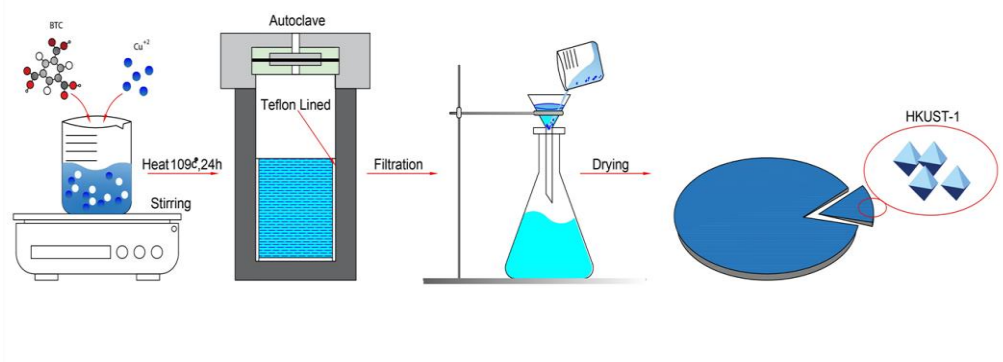

Figure 7: Scheme of synthesis method of HKUST-1

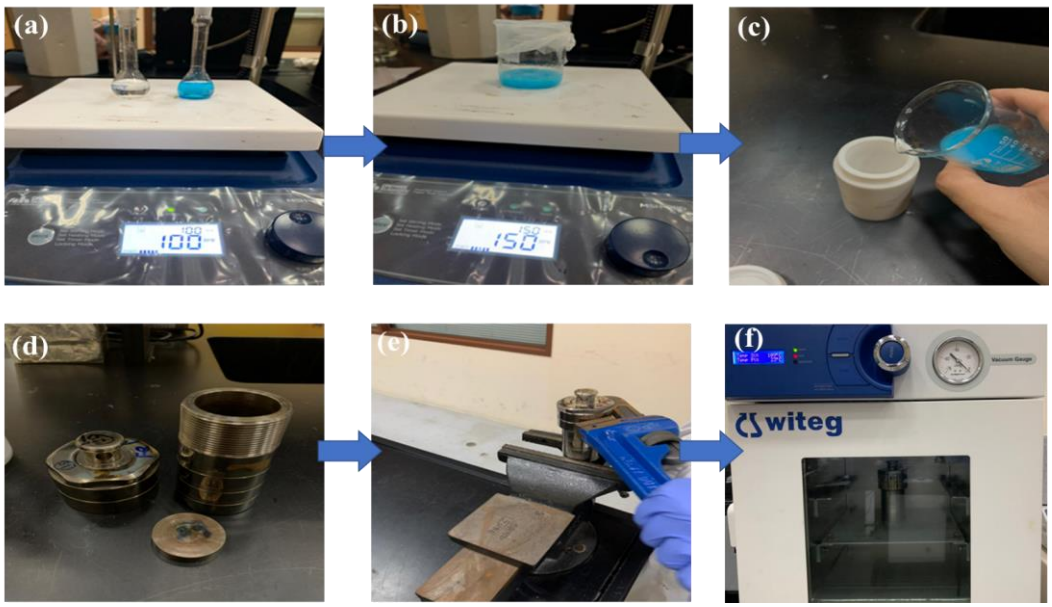

Figure 8: HKUST-1 preparation method: (a) metal and organic linear solutions were stirred until complete dissolving (b)after mixing the solution stirred for 30 min teflon container at 150 rpm, and covered to avoid ethanol evaporation (c-d) The mixture shifted into Teflon container placed in the hydrothermal reactor (e) the reactor lid closed tightly and shifted into heating oven (f) for 24 hr at 109ºC

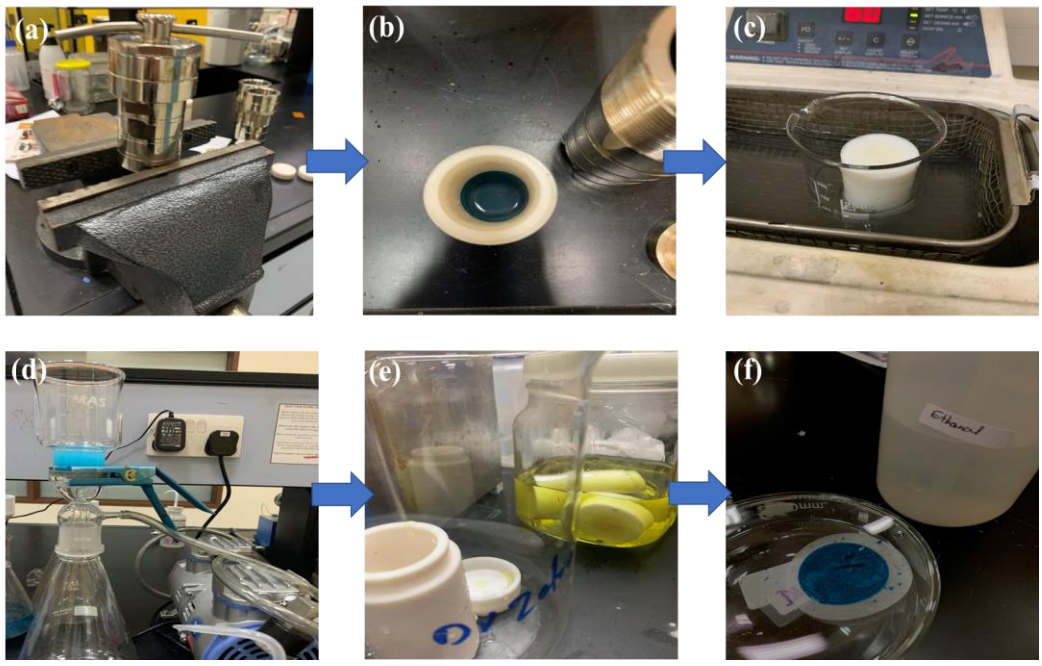

Figure 9: After synthesis steps of HKUST-1: (a) after 24 hr of reaction, the reactor cooled down until reach room temperature (c) the solution changed it color into turquoise blue (c) the solution sonicated for about 10 min (d) the solution washed and filtered for 1 day (e) teflon transferred into pre-prepared cleaning solution for later use (f) HKUST-1 powder

3.3.3 Synthesis of hexahedral mesoporous ZIF-8

Mesoporous hexahedral ZIF-8 was synthesized according to the method described in [162]. Solution A prepared by dissolving 0.845 g of $Zn(NO_3)_2.6H_2O$ in 50 mL DIW and stirred (DAIHAN MaXtirTM 500S, Korea) until complete dissolving. Solution B prepared by dissolving of 1.85 g HMeIM and 2.5 g TEA in 50 mL DIW and stirred until completely dissolved. TEA was added to deprotonate the HMeIM, which accelerates the formation of ZIF-8. Solution B was then gradually added to solution under continuous stirring at 200 rpm and room temperature until the mixture turned white and kept under mixing for 60 min. After that, the mixture was left without mixing overnight. The precipitated ZIF-8 nanoparticles were collected by centrifugation and washed with DIW three times. After that, the crystals were dried at 80^{o}C under vacuum before use in Figure 10.

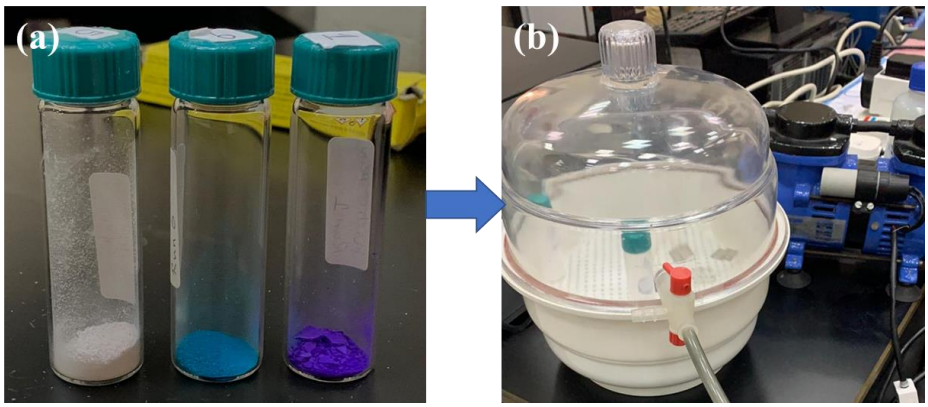

Figure 10: Storage of MOF powder: (a) ZIF-8,HKUST-1 and ZIF-67 powder (b) stored under in vacuum desiccator

For lipase encapsulation in ZIF-8, 5 mL of stock lipase solution were added to modified solution B, prepared by dissolving 0.37 g HMeIM and 0.5 g TEA in 10 mL DIW to keep the concentration of HMeIM the same as in the case of empty ZIF-8. The enzyme enriched solution B was then added gradually 10 mL of solution A, to keep the ratio of the precursors consistent. The solution was stirred on a magnetic stirrer at 200 rpm and room temperature for 60 min. The mixture was left at room temperature overnight without mixing, and then the precipitated crystals were collected by centrifugation at 8600 rpm and -4^{o}C for 10 min and washed three times with 40 mL of phosphate buffer solution (PBS) (0.25 M), before being freeze-dried at -84.4^{o}C and 0.059 mbar. The lipase encapsulated ZIF-8 was stored at 4^{o}C for later use, shown in Figure 11.

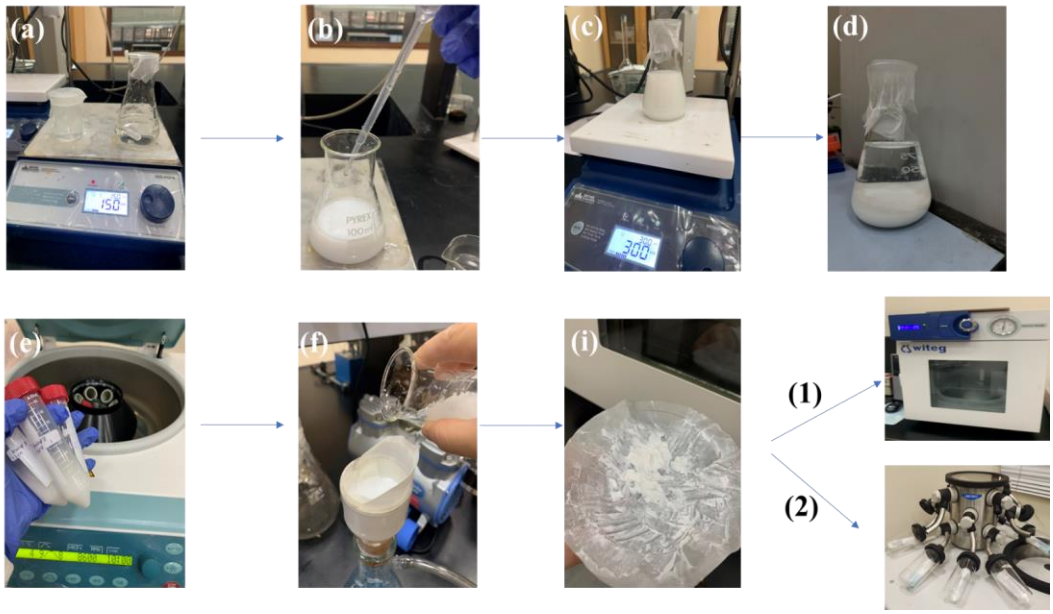

Figure 11: ZIF-8 preparation: (a) solution A and b stirred until dissolved (b) solution b gradually added to solution A and stirred for 1 hr (d) after 24 hr of reaction at room temperature and white precipitate collected (e-f) the samples were centrifuge and washed using vacuum filtration (i) the washed ZIF-8 sent for drying if (1) empty crystal dried in vacuum oven or (2) if encapsulated with enzyme dried using freeze dryer

3.4 Batch adsorption of lipase on activated MOFs

All synthesized MOFs were vacuum dried and activated prior to immobilization. HKUST-1 was activated at 120°C, whereas ZIF 67 and ZIF-8 were activated at 100°C for 6 hours. After activation the color of the HKUST-1 crystals changed from light turquoise to dark blue color shown in Figure 12.

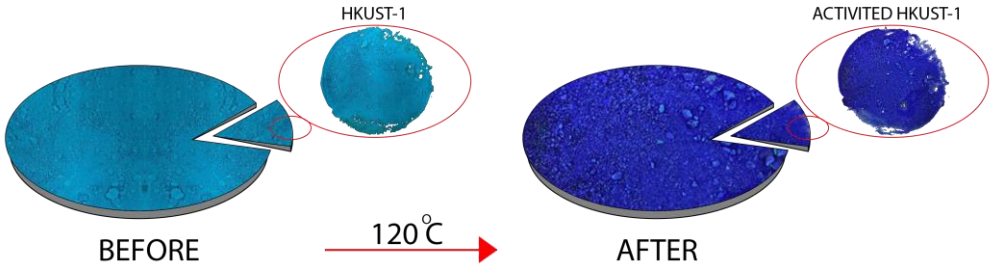

Figure 12: Activated HKUST-1: before and after vacuum activation. at 120°C for 6 h

Before the adsorption batch, experiment stated 0.1 g of activated MOF to 5 mL of phosphate buffer solution (pH 7.4) in sealed glass bottles. Before adding the enzyme, the MOF particles were dispersed by sonication at an amplitude of 30 HZ for about 10 minutes, shown in Figure 13.

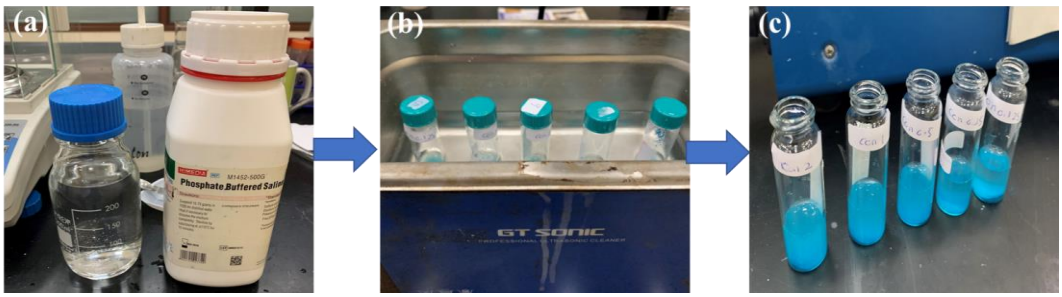

Figure 13: Sonication of activated HKUST-1: (a) prepared Phosphate buffer (b) the samples were sonicated with buffer for 10 min (c) the enzyme solution of different concentrations was added

After that, 5 mL of enzyme solutions of different concentrations, were added to the sealed bottles were placed in a shaking water bath set at 200 rpm and different temperatures ranging from 35–45^{o}C. The initial enzyme concentrations in the mixtures ranged between 2.75 and 0.6875 mg/mL, the process shown in the below Figure 14.

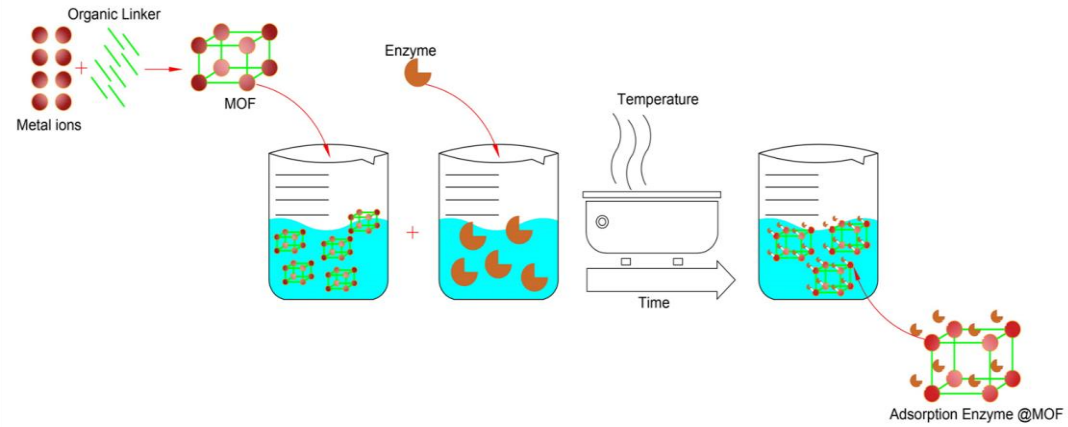

Figure 14: Scheme of adsorption preparation of Enzyme@MOF

At regular intervals, 20 µL samples were withdrawn and filtered. After that, 180 µL of Bradford reagent were added and the optical density was measured at 595 nm using microplate UV spectrophotometer (Multiskan GO, UK). The enzyme concentration in the withdrawn samples was determined by comparing the optical density against a calibration curve prepared using serial dilutions of standard protein, albumin, and solution of known concentration. After 24 h, the MOFs with the immobilized lipase were collected by centrifugation at 8600 rpm and -4^{o}C for 8 min and washing twice with buffer solution. The remaining enzyme concentration in the supernatant after 24 h was assumed to be the equilibrium concentration shown in Figure 16. [37]. The MOF with the adsorbed enzyme was then freeze dried for further use. A similar procedure was followed for measuring the encapsulated enzyme. The

initial protein concentration was measured, and at the end of the crystallization, the remaining concentration of enzyme in the solution was measured shown in Figure 15. In this experiment, the background was the initial precursors solution without the enzyme at initial time after mixing and after 24 h at the end. A calibration curve using the same background was also used, shown in Figures 16 and 17, the process of measuring.

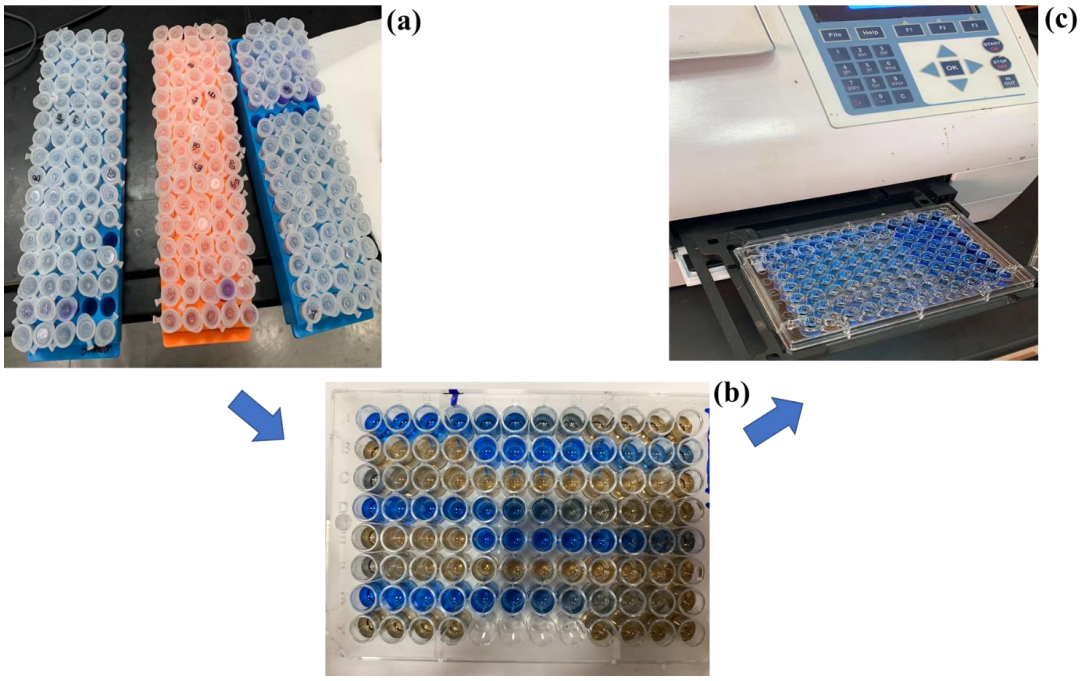

Figure 15: Analyzing the samples of adsorption studies: (a) Collected samples at different time from adsorption experiment to meausre the protein concentration drop (b) Micro-plate UV spectrophotmeter flat surface with mixing bradford reagent and collected samples (c) Micro-UV spectrophotometer instrument

All experiments were carried out in duplicates and the average values were reported and the standard deviation was shown as error bars in the figures. The

enzyme immobilization efficiency (EIE) and immobilization capacity (q_m) were determined using Equations (9) and (10), respectively.

$$EIR = \frac{(C_i - C_f)}{C_i} \times 100\% \quad (9)$$

$$q_m = \frac{(C_i - C_f)V}{m} \quad (10)$$

Where, C_i and C_f (mg/mL) are the initial and final enzyme concentrations, respectively, q_m (mg/g) is the MOF capacity, m (g) is the weight of the MOF and V (mL) is the solution volume.

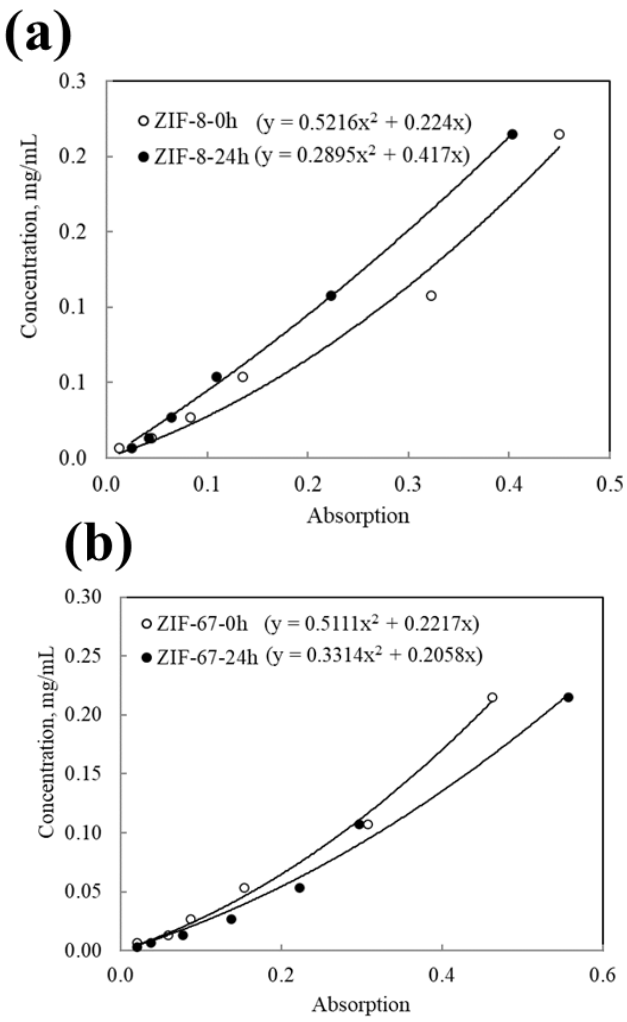

Figure 16: Calibration curve of concentration of protein vs the absorption: at 0 hr and 24 hr encapsulation of enzyme on (a) ZIF-8 and (b) ZIF-67

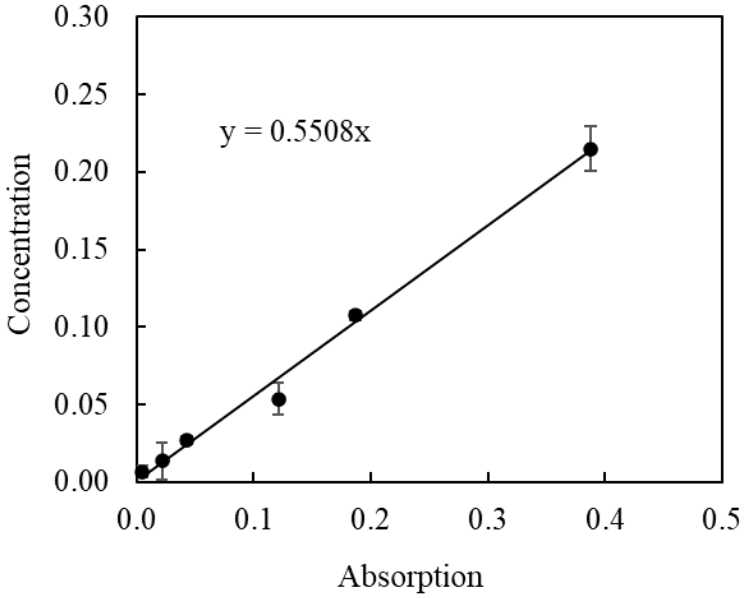

Figure 17: Calibration curve for adsorption experiment

3.5 Biodiesel production

For biodiesel production experiment, the immobilized enzyme in MOFs (both encapsulated and adsorbed) were used at the optimum condition as found in Section 2.3. The reaction mixture consisted of 1 g of olive oil and 0.57 mL methanol (equivalent to 1:12 molar ratio), and 1 mL of n-hexane based or preliminary test. When immobilized enzyme was tested, 0.2 g of the enzyme was added to initiate the reaction. When soluble free enzyme was tested, 2 mL of enzyme solution was used instead. The reaction mixture was placed in a shaking water bath set at 40℃ and 110 rpm. After 4 h of reaction, 5 mL of *n*-hexane were added to extract the produced biodiesel. After mixing thoroughly with hexane, the solution was centrifuged at 8600 rpm for 5 min to separate the two layers shown in Figure 18. A sample of 1 mL from the upper hexane layer was withdrawn and sent for Gas Chromatography (GC) (Shimadzu, GC-2010, Japan) for fatty acids methyl esters (FAMEs) analysis. The GC was facilitated with a

flame ionization detector (FID) and a SP-2560 capillary column. The carrier gas used was helium at a flow rate of 40 mL/min. The temperature of the GC oven was set at 195℃ for 4 min and then heated to 240℃ at a rate of 5℃ per min and maintain for 12 min. A sample of 1 µm was injected into the column through 0.45 µm filter and compared to a calibration determined using standard FAMEs mixture. The FAME production yield was determined using Equation (11).

$$FAME\ yield = \frac{m_{FAME}}{m_{Oil}}\% \tag{11}$$

Where, m_{FAME} and m_{oil} are the weights of produced FAME and used oil, respectively. The experiments were carried out in duplicate, and the presented results are the average values, with the standard deviation shown as error bars in the figures. The reusability of Immobilized lipase on the MOF composites was investigated. At the end of the reaction described above, the immobilized enzyme was separated by centrifugation 8600 rpm and reused in another run with fresh oil, methanol and hexane. This procedure was repeated 4 runs and the FAMEs produced was determined for each run.

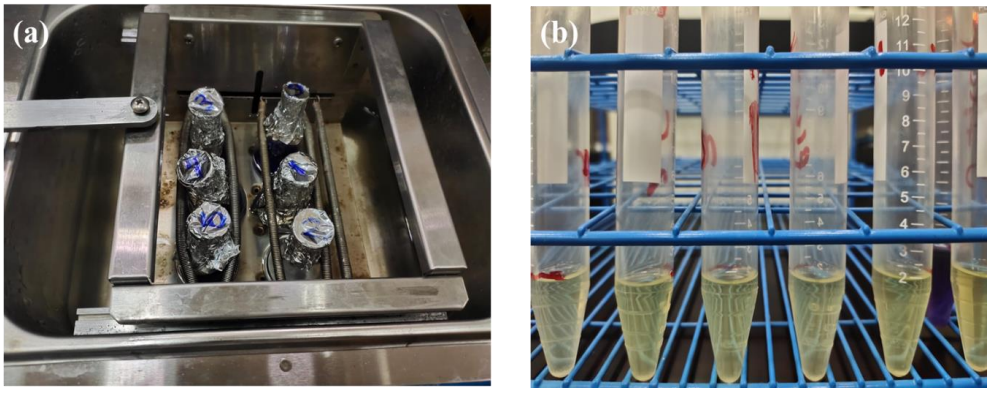

Figure 18: Biodiesel production: (a) Water shaking path at 40^{o}C (c) the collected upper layer separated from glycerol and enzyme@MOF for GC analysis.

To model the diffusion-reaction system used adsorbed lipase on ZIF-8, experiment was carried out using different initial concentrations of oil, while keeping the methanol and enzyme concentration consistent, by adjusting the volume of n-hexane to bring the overall volume to 10 mL. The methanol concentration and enzyme loading were kept constant at 0.057 mol/mL and 0.02 mg/mL, and the oil concentration was changed in the range of 0.5-0.3 mg/mL. Assuming the production rate to be linear in the first 4 h of reaction, the initial rate of reaction at each condition was calculated by dividing the concentration of FAMEs after 4 h of reaction by 4 h.

3.6 MOF characterization

X-ray diffraction study was done using D8 Advance, Bruker, X-ray diffractometer (XRD) with a Cu Kα having wavelength λ = 1.54056 Å as an X-ray source at a generator voltage of 40 kV and a generator current of 40 mA. The analysis of the immobilization functional groups present in all materials was obtained using Fourier-transform infrared spectrometer (FT/IR-6300, JASCO) (FT-IR). Raman spectra of composite materials were recorded using Renishaw InVia Raman Microscope with Wire 4.0 software and excitation wavelength of 514 nm for ZIF-67 and HKUST-1, 633 nm for ZIF-8. The surface morphology of the materials was observed using FE-SEM (Fei Apreo C, Czech Republic). The elemental composition of all the samples was attained from Energy Dispersive Spectroscopy (EDS) (Oxford Instruments, UK). The surface area, average pore size, and total pore volume of all the synthesized composite materials were obtained using Brunauer-Emmett-Teller (BET) and Barrett-Joyner-Halenda (BJH) analysis using Quantachrome TouchWin™ version 1.22, All characterization were repeated three times, Figures 19 and 20 shows the instruments used.

The hydrophobicity of ZIF-8, ZIF-67and HKUST-1 was tested using contact angle measurements using Rame-hart Instrument co at 110-240VAC. The image of the water drop on the surface was captured, and the contact angles were determined by drawing a tangent close to the edge of the droplet. The reported contact angle values were the average of three separate measurements carried out at three different locations on the surface.

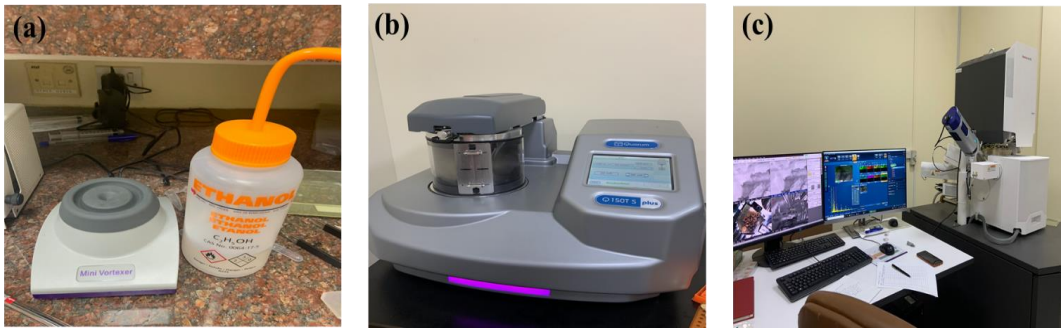

Figure 19: Fe-SEM machine steps: (a) washing the samples with Ethanol to remove the agglomeration (b) gold coating machine (c) FE-SEM instrument

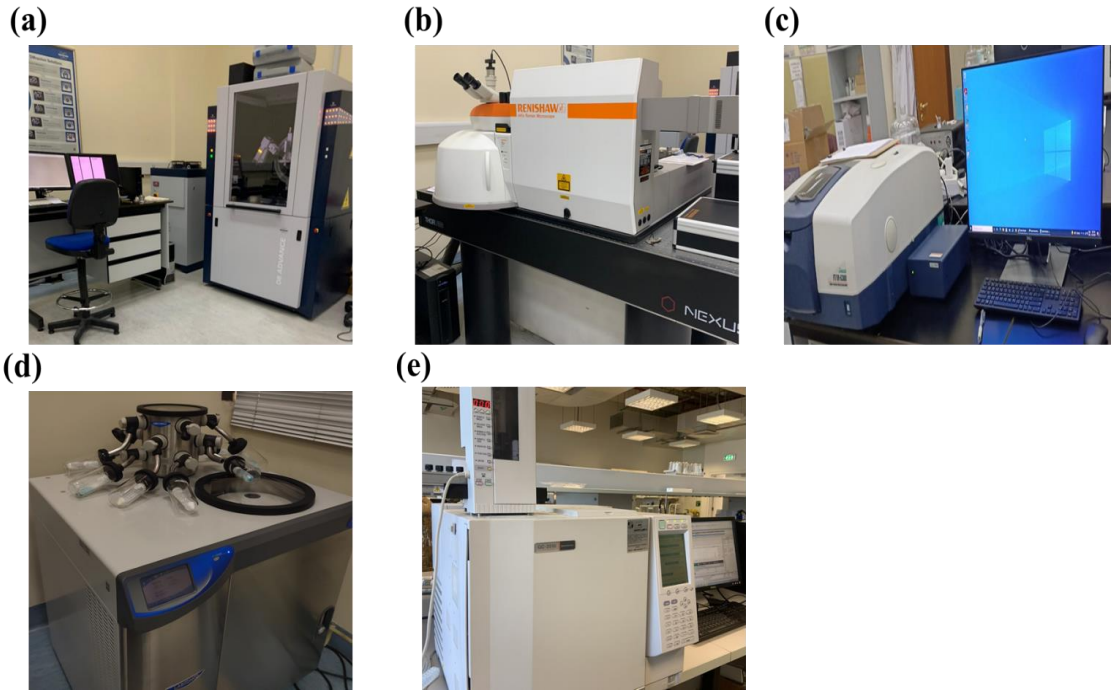

Figure 20: Instruments in this work: (a) XRD (b) Raman Spectroscopy (c) FT-IR (d) Freeze dryer (e) Gas chromatography (GC)

Chapter 4: Results

4.1 MOFs Characterization

4.1.1 FTIR

FT-IR spectra of free lipase, empty MOF and MOF with immobilized lipase are shown in Figure 21 for all three tested MOFs. Figure 21A, shows the spectrums of (a) empty HKUST-1 (b) HKUST-1 with adsorbed lipase at 40^{o}C and 0.6 mg/mL initial lipase concentration and (c) free lipase. The FT-IR spectra of HKUST-1 matches well with that reported in the literature [177]. The characteristic peak at 1380 cm^{-1} in Figure 21A(a) is assigned to the C–O of BTC, and the bands at 1451 cm^{-1} and 1560 cm^{-1} were attributed to the C=O of BTC. The characteristic peak at 1650 cm^{-1} resulted from aromatic C=C of BTC indicate a stretching vibration from the carboxylate group). The –OH group above 3000 cm^{-1} increased significantly with lipase immobilization, as shown in Fig21A(b), which is a good indication of the successful adsorption of the enzyme on HKUST-1 crystals. Figure 21A(c) shows that the free lipase spectrum exhibits two characteristics absorption bands at 1650 and 3304 cm^{-1}, corresponding to CO stretching vibration mode in amide I bonds and NH stretching vibration, respectively [176].

The FT-IR spectra of ZIF-67 (a) empty, (b) with adsorbed Lipase at 40^{o}C and 0.6 mg/mL initial enzyme concentration and (c) with encapsulated lipase are shown in Figure 21B. The vibrational bands in the range of 600-1500 cm^{-1} shown in Figure 21B(a) correspond to the characteristic stretching and bending modes of the imidazole ring. Also, the band at 1570 cm^{-1} is attributed to the stretching mode of C═N in HMeIM, whereas the bands at 2921 and can be ascribed to the stretching mode of C-

H from the aromatic ring and the aliphatic chain of HMeIM, respectively. All of the above bands are well presented in spectra of the crystals with adsorbed and encapsulated Lipase. The absorption bands at 1664 and 3304 cm^{-1} in Figures 21B(b) and 21B(c) are corresponding to the bands in the free enzyme mentioned earlier, which confirm the presence of the lipase [176].

Figure 21C shows the spectra of hexahedral ZIF-8 (a) empty, (b) with adsorbed lipase at 40°C and 0.6 mg/mL initial enzyme concentration and (c) encapsulated lipase. Bands at 425 cm^{-1} in Figure 21C(a) are ascribed to Zn–N. The acute band vibrations at 760 cm^{-1} and 1450 cm^{-1} are attributed to the HMeIM ring and the weak peaks at 2790–2950 cm^{-1} are due to the aromatic and aliphatic stretching C–H of HMeIM [162]. The above-mentioned bands were in the spectra of ZIF-8, with adsorbed and encapsulated lipase, shown in Figures 21C(b) and 21C(c). The two characteristic absorptions at 1670 cm^{-1} and 3425 cm^{-1}, which are related to amide (–CO–NH–) I and II bands for lipase. Following the immobilization of lipase in hexahedral ZIF-8, the same characteristic bands of lipase were maintained.

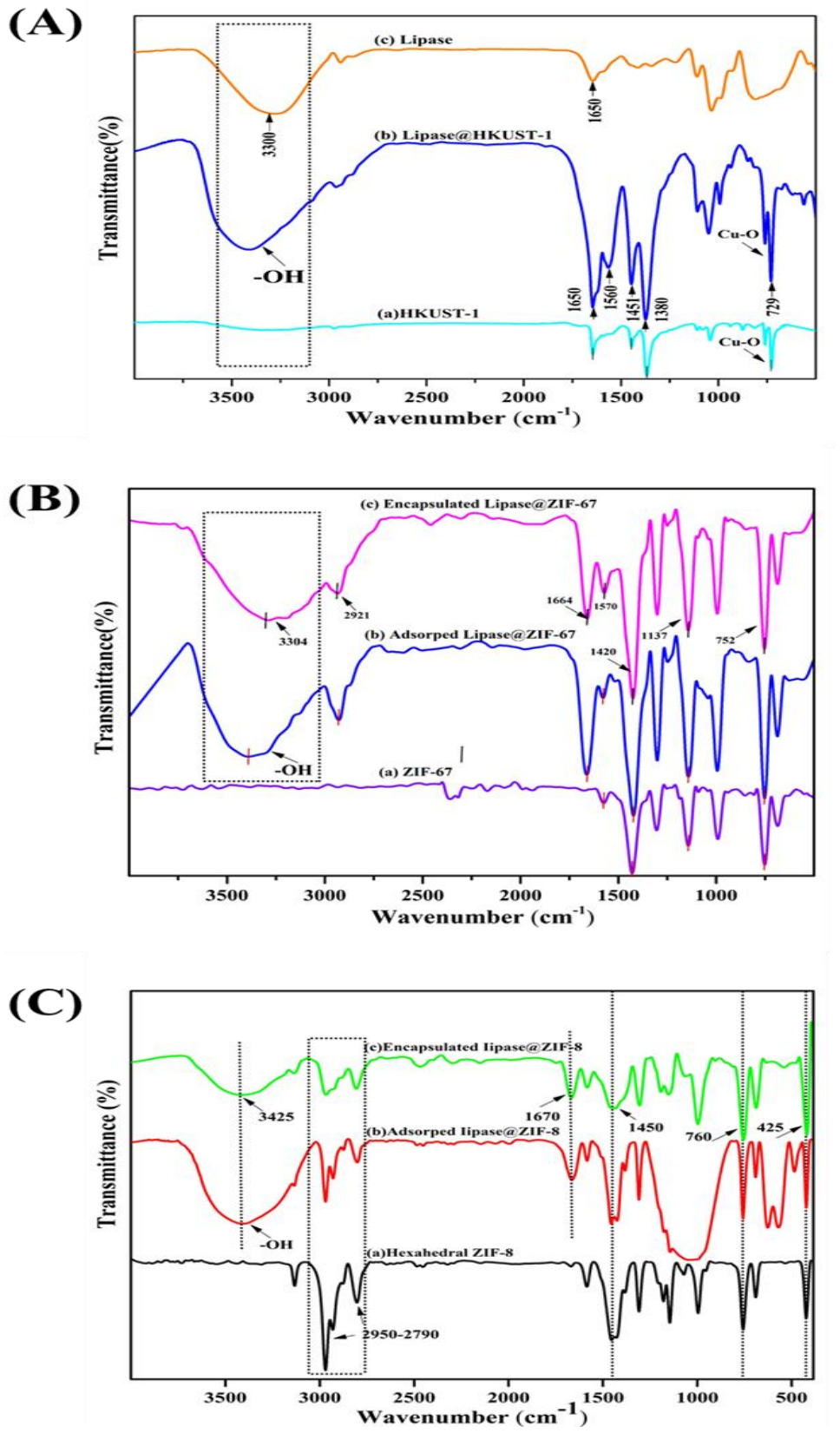

Figure 21: FTIR spectra: of (A) HKUST-1: (a) empty (b) with adsorbed lipase and (c) free lipase. (B) ZIF-67: (a) empty (b) with adsorbed lipase (c) with encapsulated lipase, (C) ZIF-8: (a) empty (b) with adsorbed lipase (c) with encapsulated lipase

4.1.2 XRD

XRD was used to characterize the crystalline structures of the three MOF's, empty and with immobilized lipase. Figure 22A shows the XRD results of HKUST-1. It can be seen from Figure 22A(a) that the pattern of the empty HKUST-1 shows typically standard diffraction peaks similar to those of the simulated pattern (PD : 00-062-1183) [178] shown Figure 22A(b), which indicate the successful synthesis of HKUST-1 crystals. The diffraction peaks at 6.6°, 9.4°, 11.5°, 13.3°, 18.9° and 25.6° are assigned to (200), (220), (222), (400), (440) and (731) crystal planes, respectively. After adsorption of lipase to post-synthesized HKUST-1, the positions of main diffraction peaks remain consistent with that of the empty HKUST-1, as shown in Figure 22A(c). This result indicates that the immobilization process did not damage the HKUST-1 crystals. However, intensity of the peaks reduced with the immobilization of lipase, which is mainly due to the low spacing between the atomic layers in the crystal material due the occupation of enzyme molecules on the surface [162], which resulted in a decrease in HKUST-1 crystallinity after lipase immobilization.

The XRD patterns of empty ZIF-67 and with encapsulated and adsorbed lipase are shown in Figure. 22B. The pattern of the empty ZIF-67 in Figure 22B(b) are similar to those reported in literature [179] and of the simulated crystal shown in Figure 22B(a), which confirms the successful synthesis of ZIF-67 (CIF: 7222297). The diffraction peaks at 7.2°, 10.2°, 12.6°, 14.5°, 16.3°, 17.9°, 22.0°, 24.3°, 26.5° appearing for the empty ZIF-67 are assigned to the (001), (002), (112), (002), (013), (222), (114), (233) and (134) crystal planes, respectively. The diffractogram of pure ZIF-67 has a lower intensities of diffraction peaks to that of the simulated ZIF-8

pattern reported in the literature [180]. This may be due to the concentration of cobalt ions and HMeIM, which could play a key role in XRD patterns. The XRD patterns in Figures 22B(c) and 22B(d) clearly show that the immobilization of lipase did not affect the crystal structure of ZIF-67, and the main reflections perfectly match those of pure ZIF-67. The intensity of the peaks with adsorbed lipase slightly dropped as compared to the empty crystals, which indicates that lipase adsorption did not affect the crystallinity. With encapsulated lipase however, the intensity of most prominent peak, corresponding to the plane (011) of Co^{2+}, decreased, dropped, which indicates that the crystallinity reduced. This is mainly due to the diminished distance between the atomic layers in the crystalline material.

The XRD patterns of empty hexahedral ZIF-8, and with encapsulated and adsorbed lipase are shown in Figure 22C. The pattern of the empty ZIF-8 shown in Figure 22C(b) matches well with the simulated powder pattern (CIF NO: 4118891) shown in Figure 22C(a). The principal diffraction peaks signify the intensification for ZIF-8 position at 2θ of 7.22◦, 10.3◦, 12.6◦, 14.7◦, 16.5◦ and 18.17◦ which were related to 011, 002, 112, 022, 013, and 222 crystals planes, respectively [181]. No obvious changes in the peaks were detected in the XRD patterns with lipase adsorption or encapsulation Lipase, shown in Figures 22C(c) and 22C(d), respectively, suggesting that lipase immobilization does not affect the ZIF-8 crystals. However, the small shift observed in the XRD spectra after immobilization of lipase indicates that the lipase successfully immobilized onto ZIF-8.

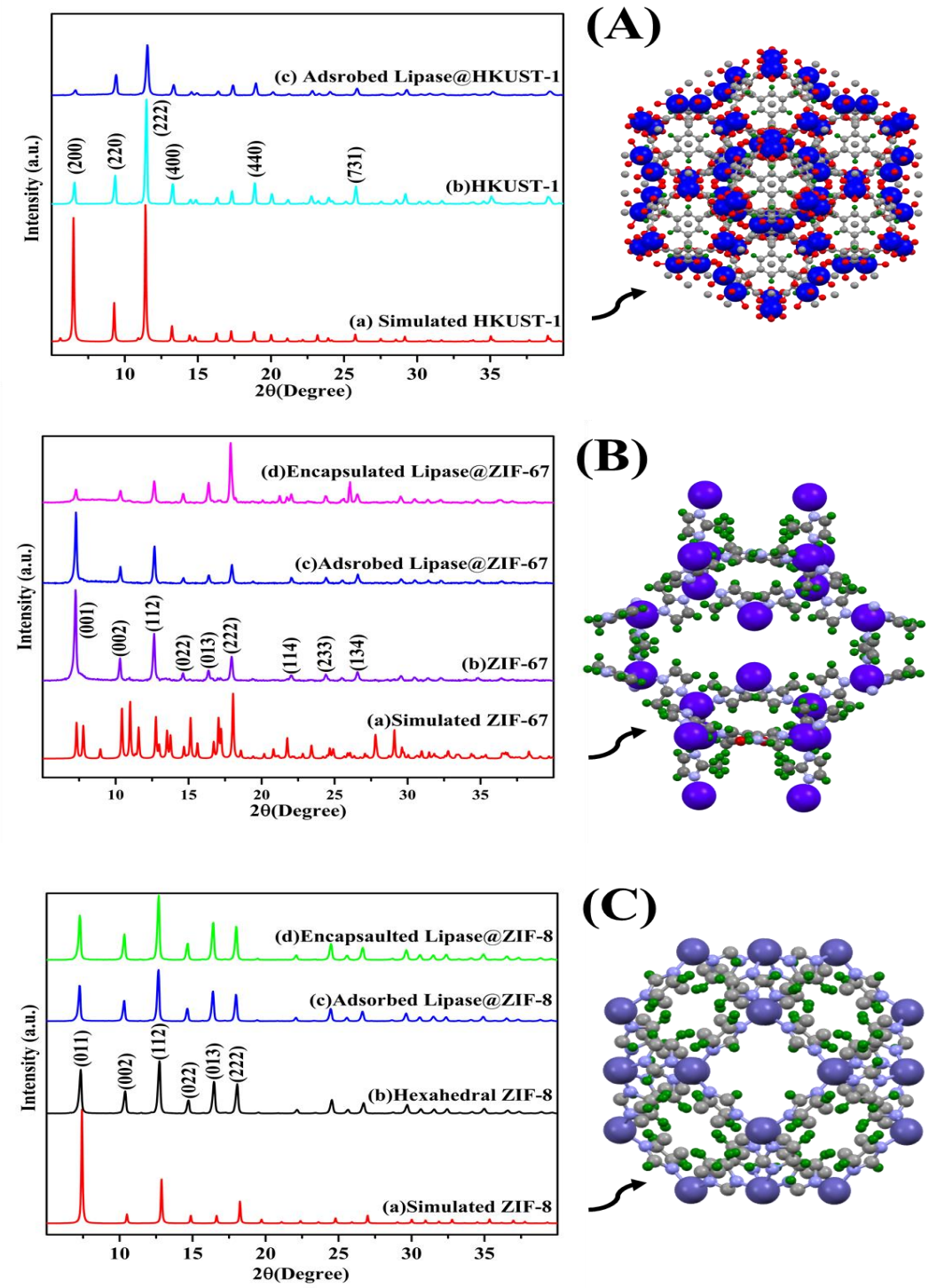

Figure 22: Results of XRD: (A) HKUST-1: (a) simulated (b) empty (c) with adsorbed, (B) ZIF-67: (a) simulated (b) empty (c) with adsorbed lipase (d) with encapsulated lipase, (C) ZIF-8: (a) simulated (b) empty (c) with adsorbed lipase (d) with XRD encapsulated lipase

4.1.3 Raman Spectroscopy

Figure 23 shows the high-resolution Raman spectrum of (a) HKUST-1, (b) ZIF-67 and (c) ZIF-8. The Raman results, which further supported the formation of metal organic frameworks, provided information on the compositions. The spectra of HKUST-1, in Figure 23(a), show the same spectroscopic characteristics with respect to those reported in literature [182]. Between 200 and 600 cm^{-1}, the peaks of vibrational modes involving Cu^{2+} ions are evident. More precisely, the doublet at 531-600 cm^{-1} is related to Cu-O stretching modes involving oxygen atoms of carboxylate bridges [183]. In the central region from 700 to 1200 cm^{-1}, it is possible to recognize the peaks related to the vibrational modes of the benzene rings. In particular, at 754 cm^{-1} and 834 cm^{-1}, the C-H out-of-plane bending modes of rings are observed, whereas at 1013 cm^{-1} the symmetric stretching mode of C=C is evident. In the region from 1400 to 1700 cm^{-1}, two vibrational modes of carboxylate bridges are present. The first, at 1470 cm^{-1}, corresponds to the symmetric stretching of O-C-O, and those functional groups support the formation of HKUST-1 [184]. In the spectra of ZIF-67, shown in Figure 23 (b), peaks at 230-555 cm^{-1} are attributed to the cobalt content, which are similar to what is reported in literature [185]. The signature of C–N, C-H and imidazole ring located at around 1115 cm^{-1}, 1450 cm^{-1} and 650 cm^{-1}, respectively, can all be identified in ZIF-67 crystals. In the Raman spectrum of hexahedral ZIF-8, shown in Figure 23(c), the major peaks are observed at 176 cm^{-1} of Zn–N, 680 cm^{-1} of HMeIm imidazole ring, 1155 cm^{-1} and 1175 cm^{-1} of C–N, 1472 cm^{-1} of C–H bending of methyl and 1500 cm^{-1} of C–C. These results agree well with reported results of ZIF-8 [186].

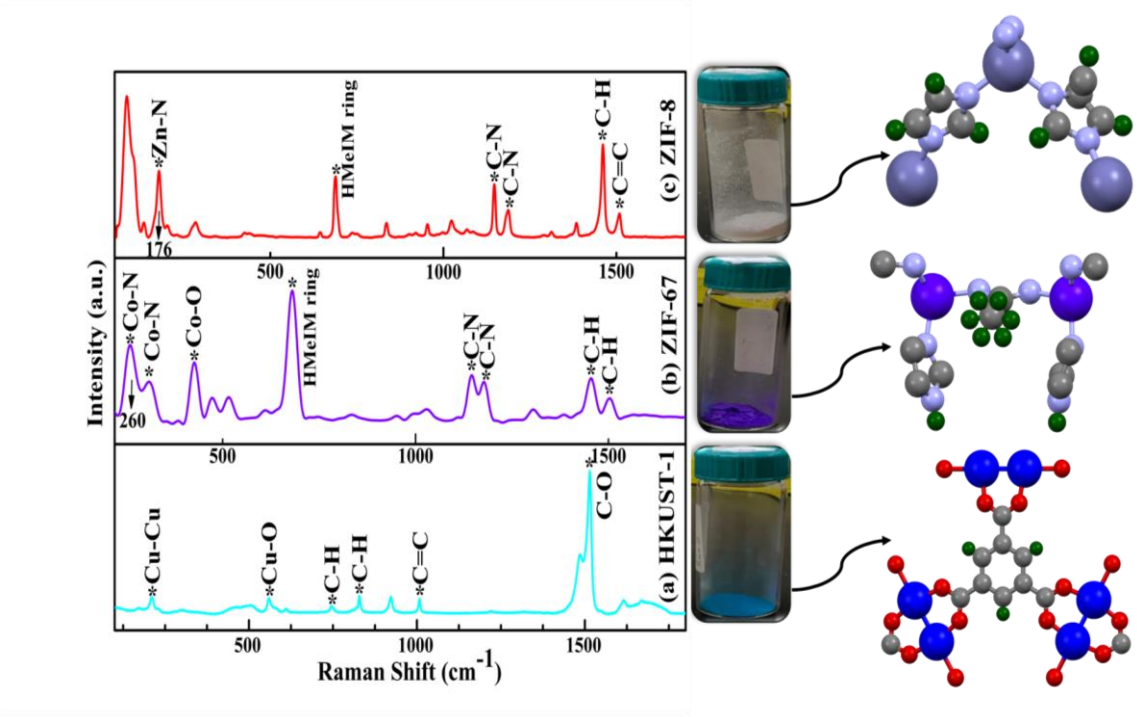

Figure 23: Raman spectra: of (a) HKUST-1 (b) ZIF-67 and (c) Hexahedral ZIF-8 pure crystals

4.1.4. Porosity and Surface Area

Figure 24 shows N_2 adsorption-desorption isotherms for (A) HKUST-1, (B) ZIF-67 and (C) hexahedral ZIF-8. The BET specific surface areas of empty HKUST-1, ZIF-67 and ZIF-8 were found to be 834.8 m^2/g, 1332.9 m^2/g and 281.6 m^2/g. The large area of ZIF-67 was a result of using diluted precursors solutions in this work, as it has been reported that a decrease reagents concentration, which slowdown the nucleation rate, resulting in bigger and more defined crystals [189]. A similar surface area of 1320 m^2/g was also reported for ZIF-67 prepared by hydrothermal synthesis [187]. According to BJH method, the average pore radius and volumes of HKUST-1, ZIF-67 and ZIF 8 were 2.002 nm and 0.84 cm^3/g, 1.14 nm and 0.74 cm^3/g, and 3.28 nm and 0.43 cm^3/g, respectively. Table 4 shows a summary of the surface properties. Although ZIF-67 showed the highest surface area, the average pore size was the

smallest. Whereas, ZIF-8, which showed the smallest surface area, had the largest average pore size. The N_2 adsorption isotherms of HKUST-1 and ZIF-8 followed the IUOPAC Type (IV) [162], which indicates mesoporous structure, Whereas, ZIF-67 showed Type (I) mode, associated with microporous pores. These observations agree with the respective pore sizes found for the three MOFs. These results indicated that the three MOFS are suitable immobilization surfaces, owing to their meso and micro-porous structures and high specific surface area.

There was no need to analyze the pore sizes of the MOFs with the adsorbed lipase, because the crystals were already pre-synthesized before the adsorption. However, the test was done on the lipase encapsulated ZIFs, as shown in Figures 24B and 24C. It was found that the encapsulation of lipase inside ZIF-67 and ZIF-8 had an effect on the adsorption isotherm, which changed from Type (I) to Type (IV) and from Type (IV) to Type (II), respectively. The pore size distribution was also affected by the lipase encapsulation, which changed from a unimodal to a bimodal distribution in ZIF-67 as shown in Figure 24B, whereas in ZIF-8 bimodal distribution disappeared, as shown in Figure 24C. This indicates that the encapsulated enzyme had resulted in a structural defect in the crystals. A similar change in the structure of ZIF-67 with lipase encapsulation was previously reported [176].

However, with enzyme encapsulation, a noticeable decrease in BET surface area and total pore volume was found for both ZIF-67 and ZIF-8 reaching on 533.5 $m^2 \cdot g^{-1}$ and 78.8 $m^2 \cdot g^{-1}$ and from 0.57 $cm^3 \cdot g^{-1}$ and 0.14 $cm^3 \cdot g^{-1}$, respectively. This drop was due to the partial occupation of the porous structure with enzyme molecules. However, the average pore radius of ZIF-67 and ZIF-8 increased after encapsulation to 2.15 nm and 3.69 nm, respectively. This is because the enzyme molecules occupy

the smaller pores, leaving the larger pores unfilled, rendering the average pore size after encapsulation larger. Similar results were also observed when *Candida rugose* lipase [176] and *Rhizomucor miehei* lipase [169] were encapsulated in ZIF-67 and ZIF-8, showing an increase in pore size after encapsulation.

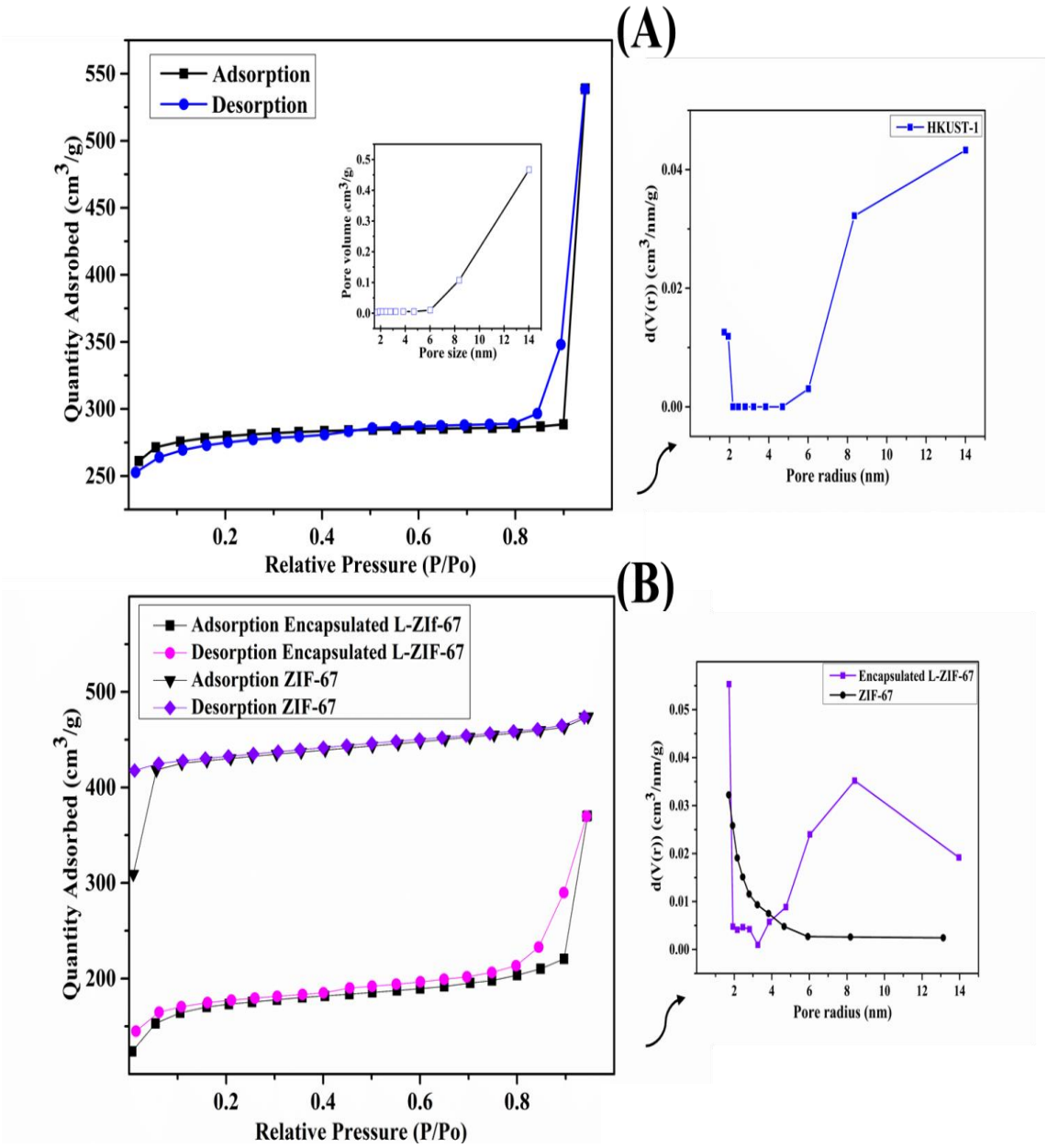

Figure 24: N_2 adsorption/desorption isotherms for and pore size distribution: of (a) HKUST-1 (b) ZIF-67 (empty and encapsulated with lipase) (c) ZIF-8 (empty and encapsulated with lipase)

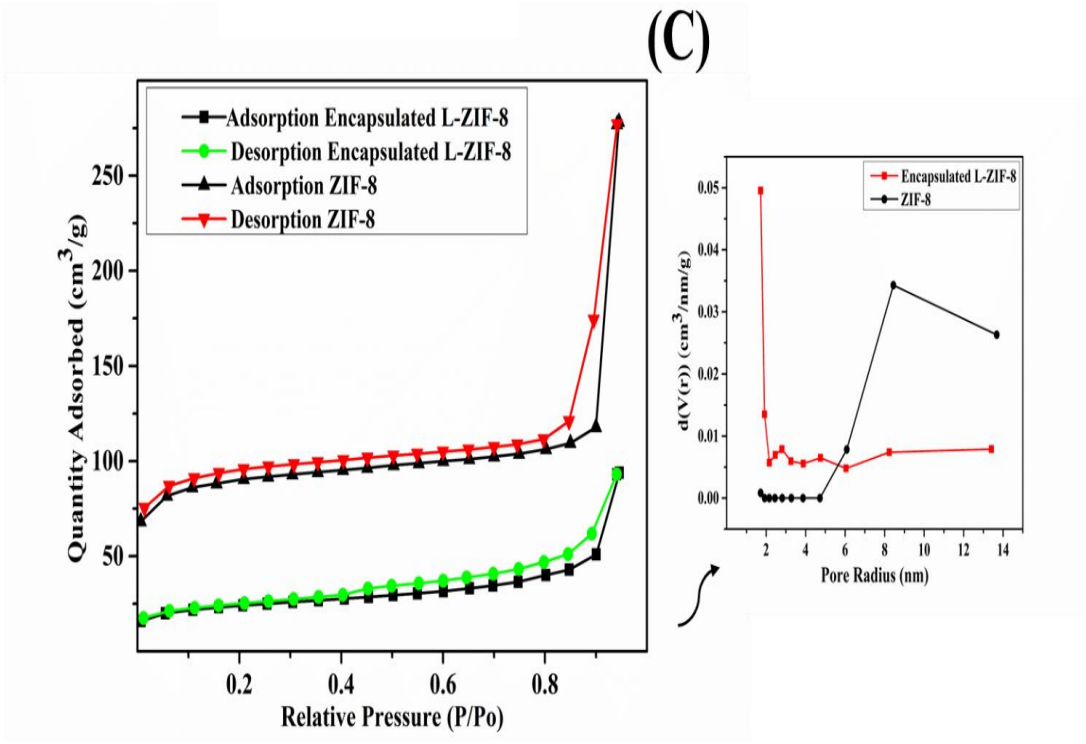

Figure 24: N_2 adsorption/desorption isotherms for and pore size distribution: of (a) HKUST-1 (b) ZIF-67 (empty and encapsulated with lipase) (c) ZIF-8 (empty and encapsulated with lipase) (continued)

Table 4: Surface Properties of HKUST-1 and ZIF's at 77 K

Sample	**Surface area (m^2g^{-1})**	**BJH pore volume (cm^3g^{-1})**	**Avg pore Radius (nm)**	**Adsorption Pore Radius (nm)**	**Desorption Pore Radius (nm)**
HKUST-1	834.84	0.84	2.00	14.44	14.01
ZIF-67	1332.93	0.74	1.14	1.722	1.71
ZIF-8	281.61	0.43	3.28	14.44	8.44
Encapsulated Lipase-ZIF-67	533.48	0.57	2.15	14.30	1.72
Encapsulated Lipase-ZIF-8	78.76	0.14	3.70	14.61	1.71

4.1.5. Surface Hydrophobicity

The static water angles on the three MOFs are shown in Figure 25. The contact angle of a water droplet on ZIF-8 at time zero, as shown in Figure 25a, was 49.6^{o}, and decreased to 0^{o} after 3s, as shown in Figure 25b. This indicates that the surface of ZIF-8 is hydrophilic. Similar results were observed with HKUST-1, shown in Figure 25e, with water drop being directly adsorbed, indicating that this surface was also hydrophilic. The contact angle of a water droplet on ZIF-67 however, was 120^{o}C, as shown in Figures 25c and 25d, indicating that the surface is hydrophobic. In biodiesel production process, hydrophobic surfaces are more favorable, as they favor the diffusion of the substrate. In addition, lipase, is characterized with significantly extended lipophilic regions that can interact effectively with hydrophobic supports, which enhances the support and reduces the leakage. However, most enzymes undergo conformational changes upon adsorption on hydrophobic surfaces, which can negatively affect their activity and stability [190].

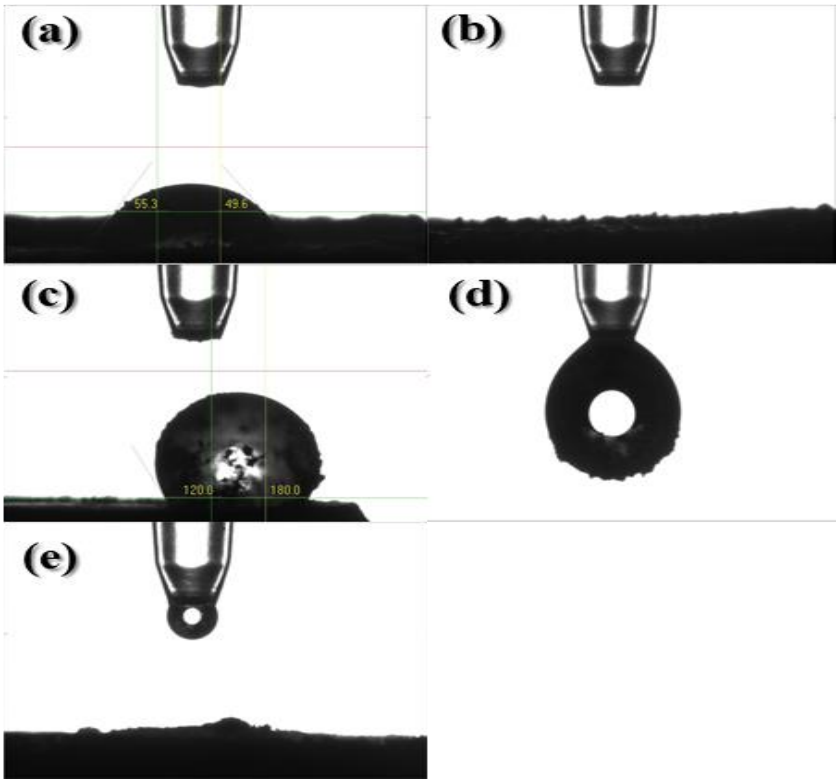

Figure 25: Static water angle: on (a) ZIF-8 at time zero (b) ZIF-8 after 3 s (c) ZIF-67 and (e) HKUST-1 (d) shows the ZIF-67 powder attached to pulled water droplet

4.1.6 Surface Morphology

The morphology of synthesized MOFs was characterized using Fe-SEM. Figures 26a and 26b show the images for HKUST-1, empty and with adsorbed lipase. Empty HKUST-1 (clearly exhibit well-defined octahedral shape with distinct edges and smooth surfaces with the particle size in the range of 0.5 –5.0 μm, which match reported results in literature [184]. With lipase adsorption, no significant changes were observed in the morphology of HKUST-1. However, the presence of the enzyme resulted in conglomeration of crystals, and that resulted in the drop in crystallinity observed in the previous XRD results as well (Figure 22a).

Figures 27a, 27b and 27c show the images for ZIF-67, empty, and with adsorbed lipase and encapsulated lipase, respectively. Empty ZIF-67 clearly showed

well defined dodecahedral shape and match what is reported in literature [188]. The particles sizes of ZIF-67 were non-uniform, which indicates a rapid nucleation of the crystals, resulting in different crystallinity shape [176, 189]. The average size however, was in the range of 1-4 nm. With lipase adsorption, ZIF-67 maintained is morphology and the attachment of the enzyme did not affect the crystal structures. However, the attached enzymes resulted in a slight conglomeration was observed. With lipase encapsulation, ZIF-67, preserved their dodecahedral shape. However, a drop in the size of the crystal was observed, which indicates that the presence of the enzyme molecule during the crystallization affected the process. A similar drop of mean average size was obtained with encapsulating *Rhizomucor miehei* lipase in microporous ZIF-8 [169]. The results also agree with previous XRD results presented earlier (Figure 22b). In a de novo approach, structural defects of crystals usually formed, due to the presence of protein in the crystallization process [190].

Figures 28a, 28b and 28c show the images for ZIF-8, empty, and with adsorbed lipase and encapsulated lipase, respectively. Empty ZIF-8 (exhibit well-defined hexahedral shape and match well what is reported in literature [162]. With lipase adsorption and encapsulation, no significant changes in the morphology of ZIF-8 was observed, and the crystals preserved their hexahedral shape. This result agrees with previous XRD results, presented earlier (Figure 22c). However, similar to ZIF-67, with encapsulation size of the crystals decreased. The decrease in the size of ZIF-8 crystals after lipase encapsulation was higher than that encountered by ZIF-67.

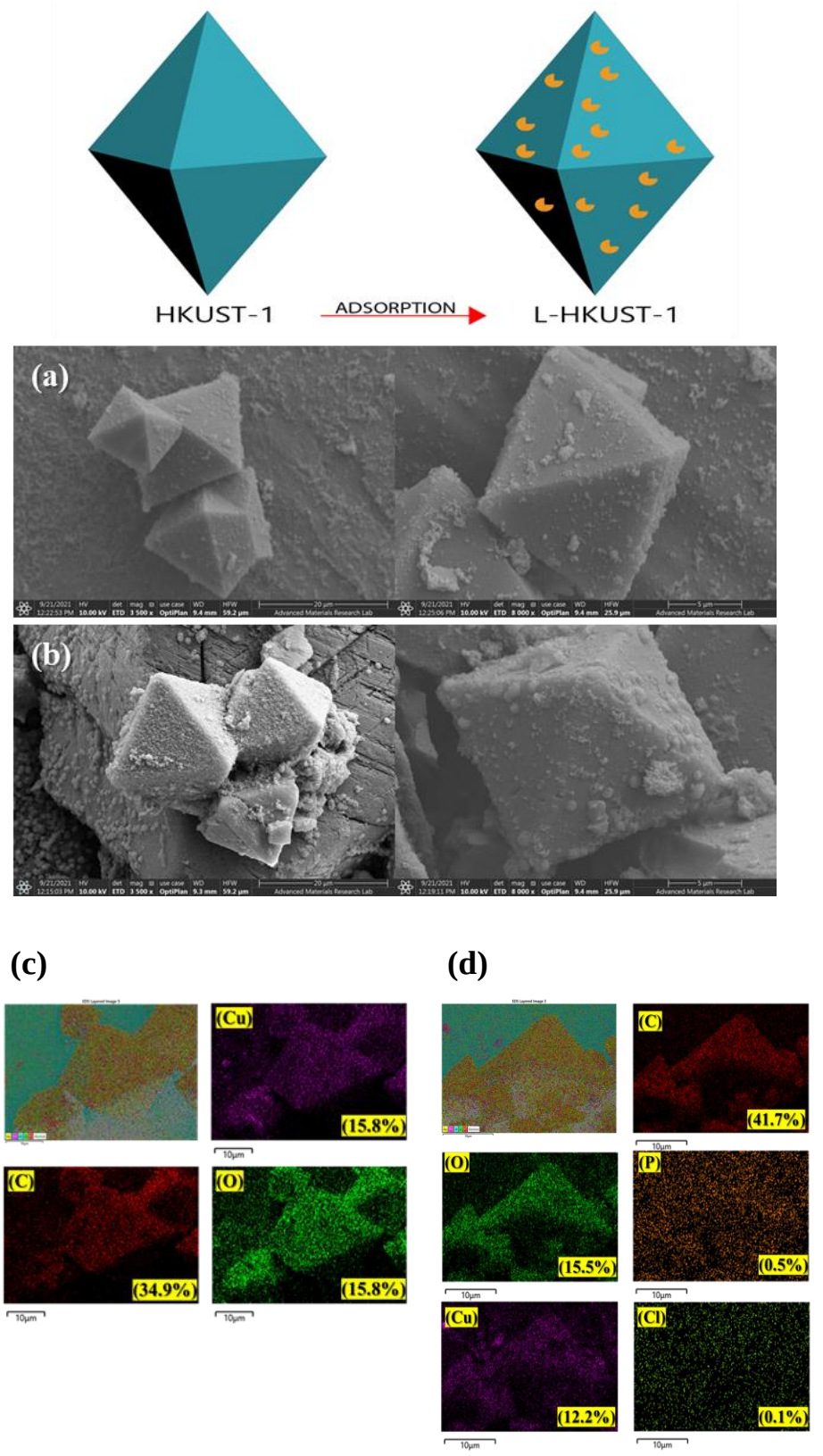

Figure 26: Fe-Scanning electron microscopy (Fe-SEM) images of HKUST-1: (a) pure (b) lipase adsorbed (c) EDS mapping of pure crystals (d) Adsorbed lipase

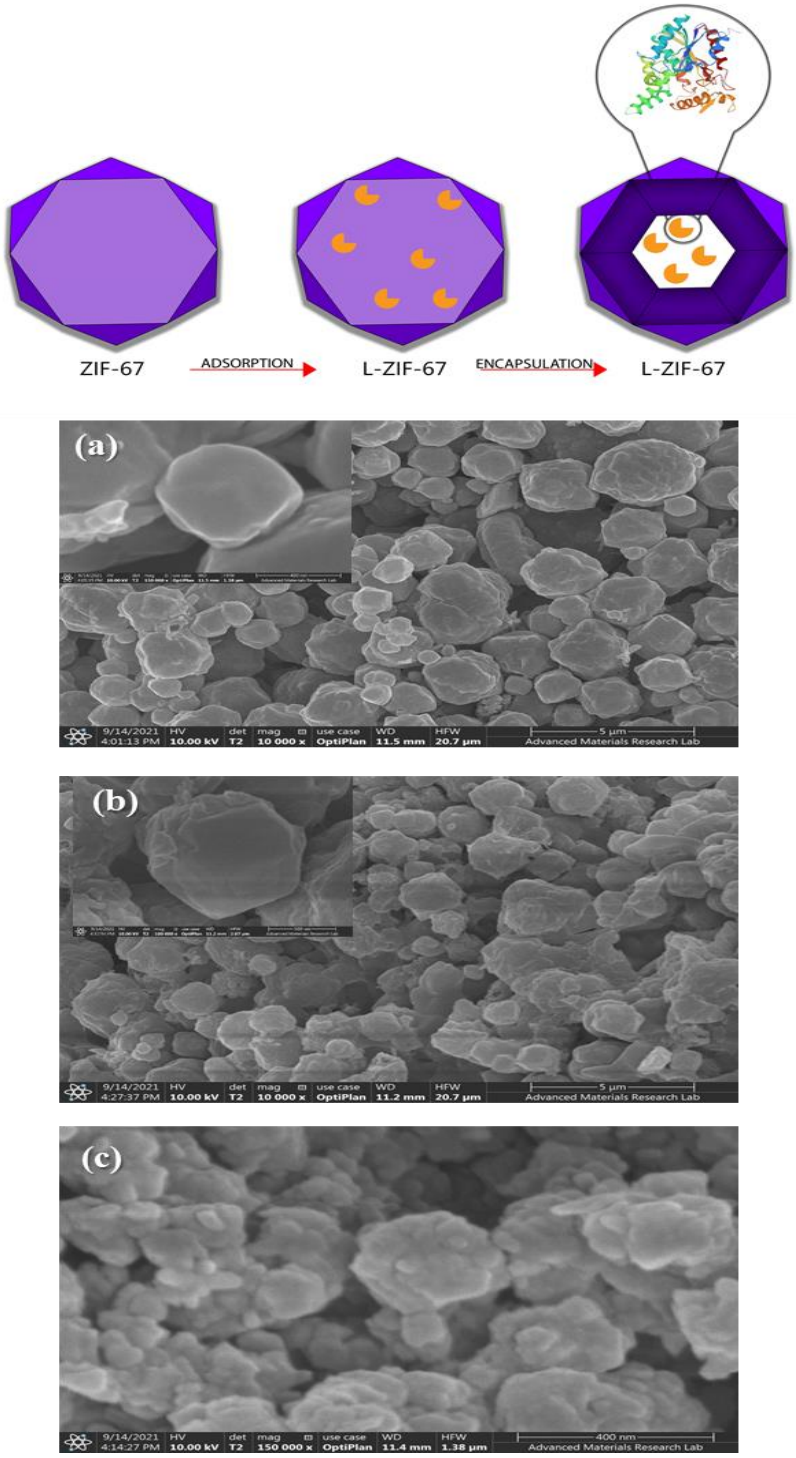

Figure 27: Fe-Scanning electron microscopy (Fe-SEM) images of ZIF-67: (a) empty (b) lipase adsorbed and (c) lipase encapsulated (d) EDS mapping of pure crystals (e) Adsorbed lipase and (f) encapsulated

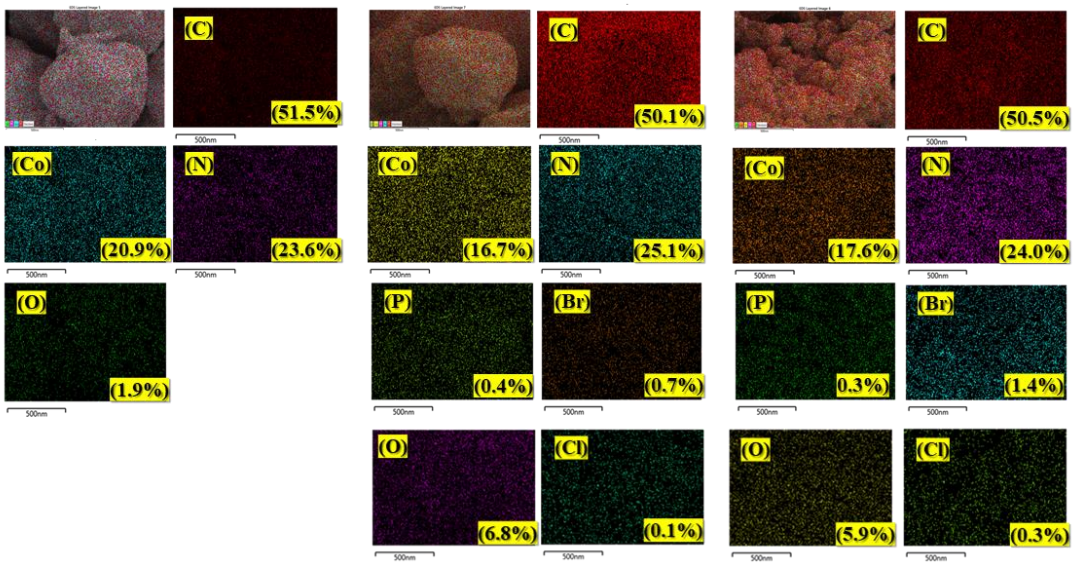

Figure 27: Fe-Scanning electron microscopy (Fe-SEM) images of ZIF-67: (a) empty (b) lipase adsorbed and (c) lipase encapsulated (d) EDS mapping of pure crystals (e) Adsorbed lipase and (f) encapsulated (continued)

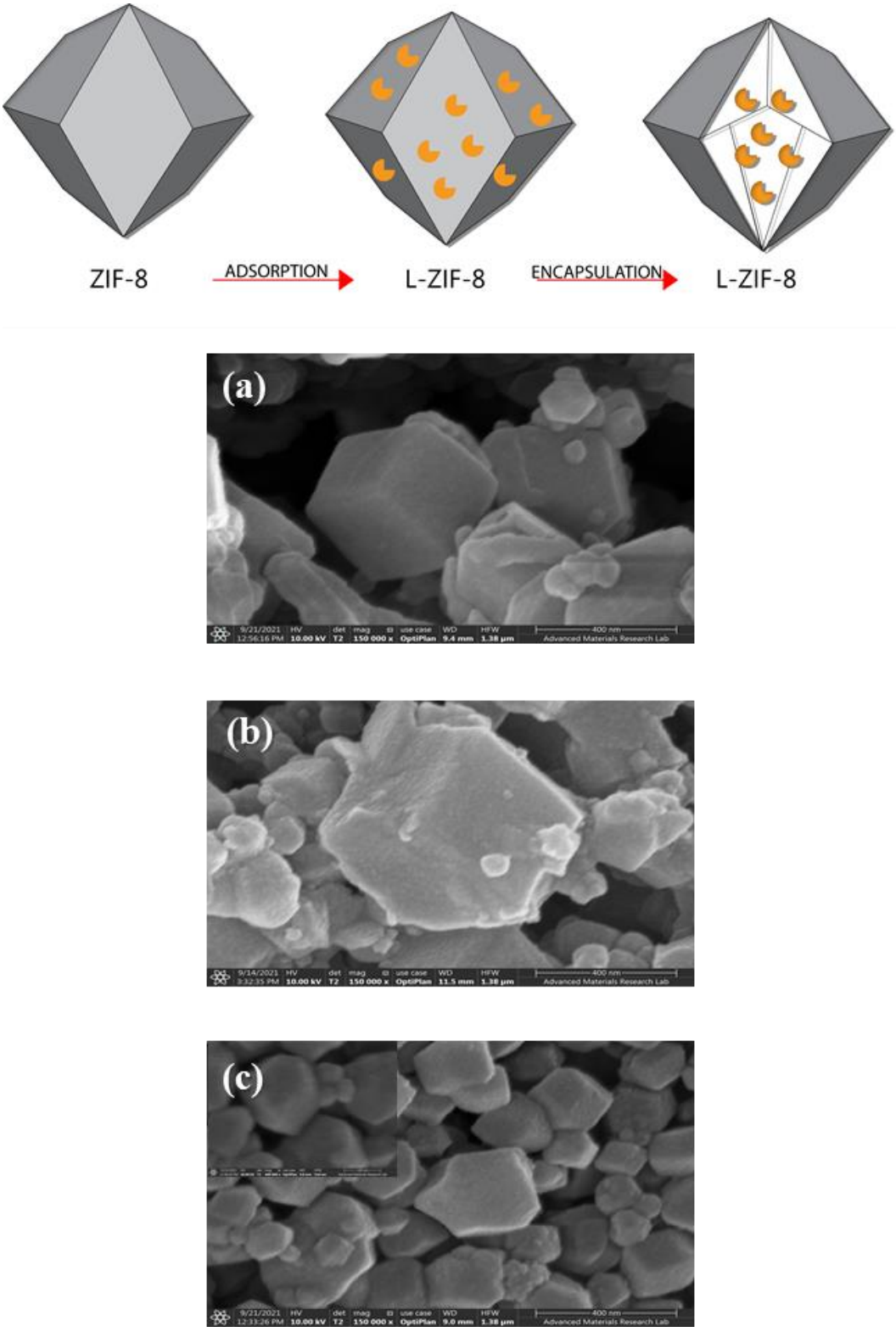

Figure 28: Fe-Scanning electron microscopy (Fe-SEM) images of ZIF-8: (a) empty (b) lipase adsorbed and (c) lipase encapsulated (d) EDS mapping of pure crystals (e) Adsorbed lipase and (f) encapsulate

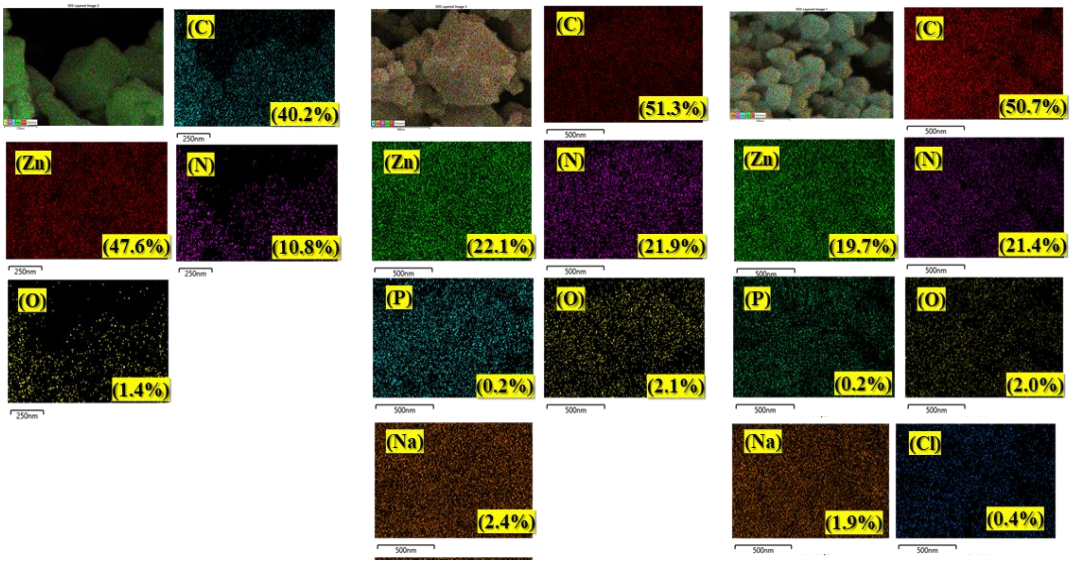

Figure 28: Fe-Scanning electron microscopy (Fe-SEM) images of ZIF-8: (a) empty (b) lipase adsorbed and (c) lipase encapsulated (d) EDS mapping of pure crystals (e) Adsorbed lipase and (f) encapsulate (continued)

4.2 Lipase adsorption isotherms

In order to evaluate lipase adsorption, the equilibrium adsorption isotherms were fitted to different models to identify the one that best correlate with experimental results. The experimental results of lipase equilibrium adsorption on ZIF-8, ZIF-67 and HKUST-1 at different temperatures as compared to Langmuir and Freundlich fitted models are shown in Figure 29. The parameters and the coefficient of determination for the two models are presented in Table 5 for the three tested MOFs. Generally, the Langmuir isotherm was found to provide a better fit than Freundlich for the three MOFs.

The Langmuir isotherm describes monolayer sorption, in which each lipase molecule is adsorbed on distinct localized sorption sites with no transmigration of the adsorbate in the plane of the surfaces giving uniform energies of monolayer sorption

onto the adsorbent surface [191]. From the Langmuir fitting, it was found that the maximum adsorption capacity of ZIF-8, ZIF-67 and HKUST-1 increased with temperature, which is typical for the adsorption of most protein [152].

Comparing the maximum capacity on the three MOFs showed that they all have similar values at their respective optimum temperatures. The value of *b*, which is an indication of adsorbate–adsorbent interaction [191] increased with temperature for ZIF-8 and HKUST-1 (i.e., endothermic process), but reduced for ZIF-67 (i.e., exothermic.

Table 5: Isotherm model parameters for lipase adsorption on ZIF-8, ZIF-67 and HKUST-1 at different temperature

ZIF-8			
Isotherm	**Parameter**	**35ºC**	**45ºC**
Langmuir	b(L/mg)	0.22	0.315
	q_m(mg/g)	33.06	102
	R^2	0.99	0.91
Freundlich	a_F	6.537	26.648
	b_F	1.031	1.067
	R^2	0.99	0.91
ZIF-67			
Isotherm	**Parameter**	**30ºC**	**45ºC**
Langmuir	b(L/mg)	6.76	0.84
	q_m(mg/g)	34.22	102
	R^2	0.873	0.96
Freundlich	a_F	3.5	102
	b_F	0.044	0.77
	R^2	0.69	1.00

HKUST-1				
Isotherm	**Parameter**	**35ºC**	**40ºC**	**45ºC**
Langmuir	b(L/mg)	4.12	5.5	6.84
	q_m(mg/g)	18.74	19.98	21.86
	R^2	1	1	1
Freundlich	a_F	18.98	19.1	20
	b_F	1.96	2.716	3.99
	R^2	0.98	1	1

The Gibbs free energy (ΔG^o), enthalpy (ΔH^o), and entropy (ΔS^o), which can be used to assess the spontaneity of the adsorption process, [192], were determined from the values of b at different temperatures, using Equation (3). As shown in Table 6, positive values of ΔG was obtained at all tested temperatures, except for ZIF-67 at the lowest tested temperature of 30^{o}C and HKUST-1 at the highest tested temperature of 45^{o}C. This indicates that the adsorption processes on ZIF-8 was generally non-spontaneous. Whereas for ZIF-67 and HKUST-1, the process becomes spontaneous at the low and high temperatures, respectively. The enthalpy of adsorption, ΔH_o (29.257 and 196.36 kJ/mol) for the two hydrophilic surfaces, ZIF-8 and HKUST-1 was found to be positive, which confirmed the endothermic nature of the process. Whereas for the hydrophobic surface, ZIF-67, the enthalpy of adsorption, ΔH_o, was negative. When ΔH is less than 40 kJ/mol, adsorption is considered to be physisorption [193], as in the case of ZIF-8, whereas the adsorption was chemisorption for HKUST-1. The positive value of ΔS For HKUST-1 and ZIF-8 indicates an increased randomness at the solid–solution interface during the adsorption process and a good affinity [194].

To explain these trends, the forces of attraction should be understood. The attachment of lipase on ZIF-8 and ZIF-67 is by physical adsorption, where it is by chemical adsorption for HKUST-1. In the former case, the forces of attraction are mainly the hydrophilic and Van der Waals forces, whereas in the latter MOF, it is chemical bonding. As temperature increases, the attachment of the hydrophilic proteins to the hydrophilic surface of ZIF-8 compensates the drop in the Van der Waals forces [156,195]. However, for HKUST-1 the extent of chemisorption increased with an increase in temperature, and the attachment of enzyme increased [161].

Table 6: Thermodynamic parameters of ZIF-8, ZIF-67 and HKUST-1

	Temperature (K)	**ΔG(KJ/mol)**	**ΔH (kJ/mol)**	**ΔS(kJ/mol.K)**
L-ZIF-8	308.15	3.879	29.257	0.0824
	318.15	3.055		
L-ZIF-67	303.15	-4.817	-111.48	-0.3518
	313.15	0.461		
L-HKUST-1	308.15	1.225	196.366	0.63107
	313.15	0.104		
	318.15	-5.085		

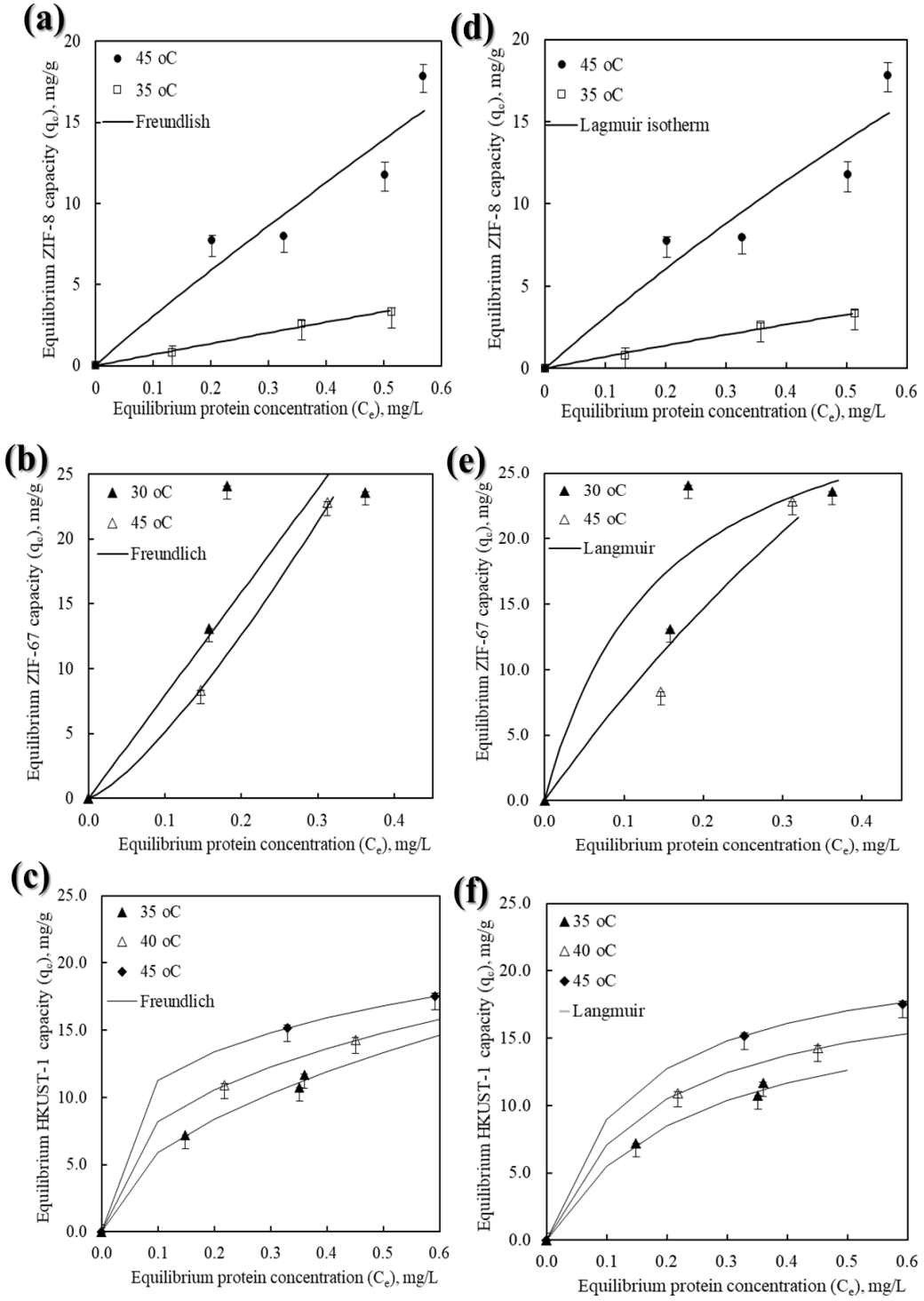

Figure 29: Freundlich model fitting of lipase adsorption isotherms at different temperatures: on (a) ZIF-8 (b) ZIF-67 and (c) HKUST-1 and Langmuir model fitting of lipase adsorption isotherms at different temperatures on (d) ZIF-8 (e) ZIF-67 and (f) HKUST-1

4.3 Adsorption kinetics

The Lipase adsorption kinetics profiles on ZIF-8, ZIF-67 and HKUST-1 at different initial concentrations and temperatures are shown in Figure 30. As shown in the kinetics profiles, there was generally an initial fast uptake of lipase from the solution in the first 60 min, before plateauing at 180 min of contact time. The faster initial uptake can be attributed to the presence of a large number of available empty adsorption sites [152]. As the lipase gets adsorbed, the number of these available sites decreases, and the slope flattens and the adsorption rate decreases [196]. For ZIF-8 (Figures 30a and 30b), at low protein concentration, the adsorption rate was found to increases with increasing the initial concentration. However, the significance of this effect diminished at higher concentration. This is mainly because the concentration gradient driving force becomes high enough that any increase in it did not result in a higher adoption. On the contrary, there was a slight decrease at the highest concentration, which is due to the faster filling of the outer pores, which then restricted the inner ones from being utilized. In addition, at high lipase concentration, agglomeration may take place , which negatively affects the diffusion rate and the ability to utilize the inner pores [152, 200]. On the other hand, the adsorption was found to reduce with temperature at low lipase concentration, and this effect also diminished at higher concentrations. The drop in adsorption rate with temperature was due to drop in the Van der Waals attractive forces, as explained in Section 3.2.

A similar trend was observed for ZIF-67, as shown in Figures 30c and 30d, wherein the adsorption rate increased with the increase in concentration. However, with ZIF-67, the adsorption rate consistently increased with temperature. A similar behavior was also observed for HKUST-1, with regards to concentration, where the

kinetics increase with the increase in concentration, but to a lesser extend compared to the other two supports. The effect of temperature, however, was opposite and a drop in kinetics was observed by increasing the temperature. However, the effect of temperature of HKUST-1 was similar to ZIF-8, wherein an increase in temperature resulted in an increase in adsorption rate, which the expected trend of a chemisorption process.

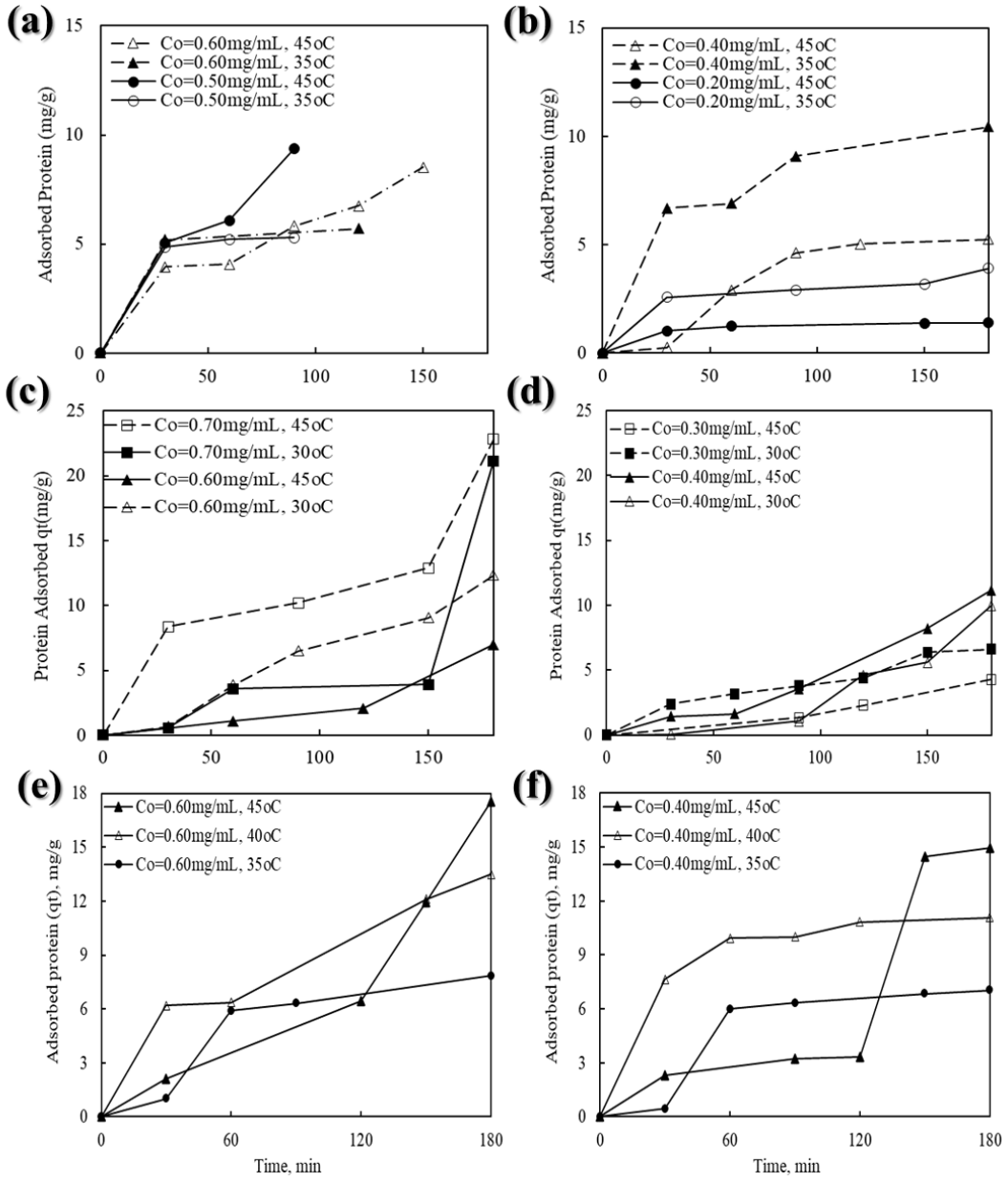

Figure 30: Lipase adsorption kinetics: on (a-b) ZIF-8, (c-d) ZIF-67 and (e-f) HKUST-1 at different temperatures and initial concentrations

Adsorption kinetics show large dependence on the physical and chemical characteristics of the adsorbent material, which also influence the adsorption mechanism that can either be film or pore diffusion or a combination of both, depending on the system hydrodynamics [199]. In order to express the kinetic characteristics of lipase adsorption on the support surface, non-linear pseudo-first order, pseudo-second-order and Elovich's models were fitted to the experimental data, and (Results are shown in the Appendix) the determined parameters and correlation coefficients (R^2) are listed in Table 7. The first order rate constant (k_1) was found to increase with the increase in temperature in Figure 31. Whereas, the second order rate constant (k_2) decreased Figure 33. This decrease in the second-order rate constant could be attributed to the propensity of adsorbate to migrate from the solid phase to the bulk phase with increasing temperature of the solution [174].

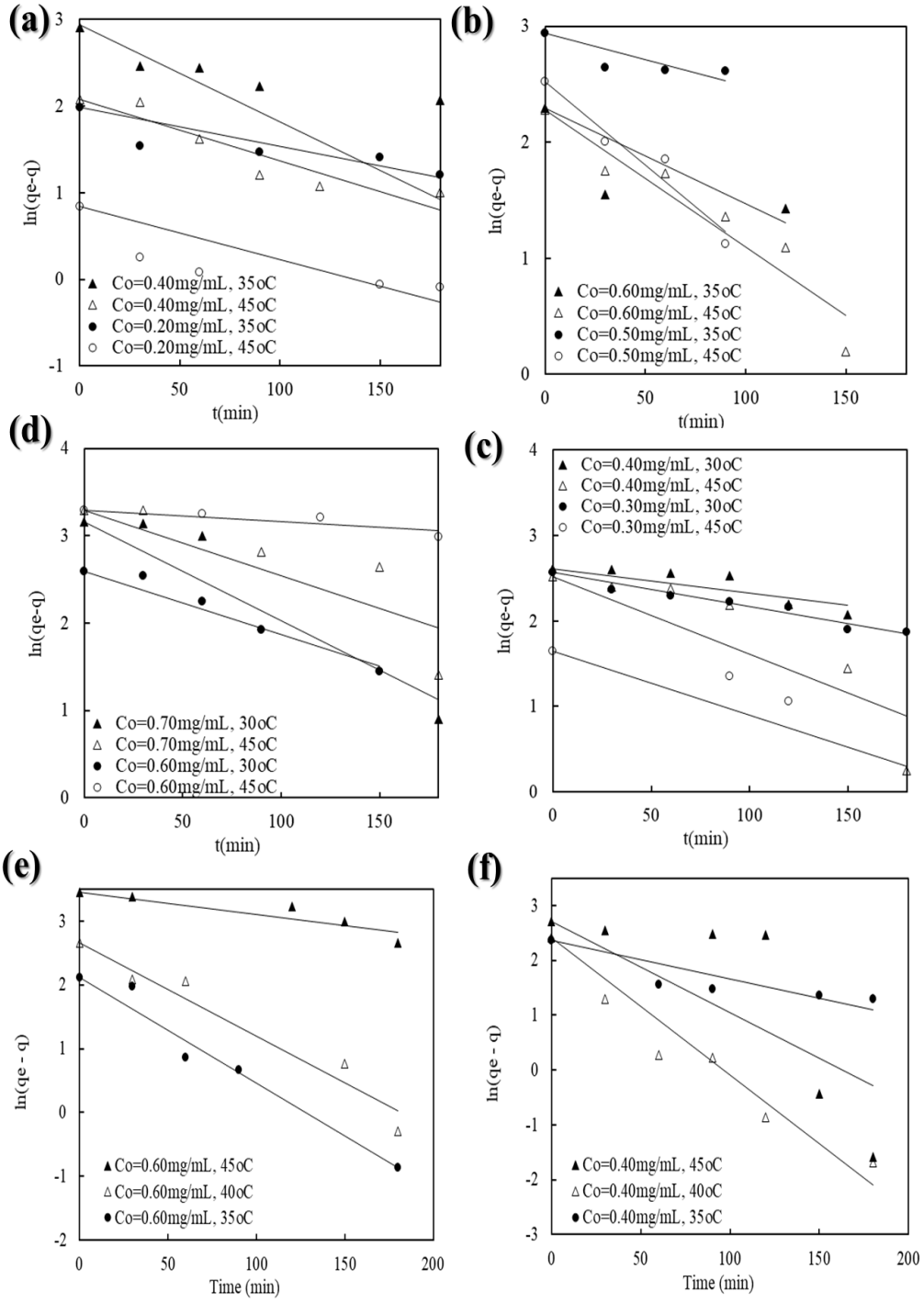

Figure 31: Pseudo first order model fitting of lipase adsorption kinetics data: on (a-b) ZIF-8 (c-d) ZIF -67 and (e-f) HKUST-1 at different temperatures and initial concentrations

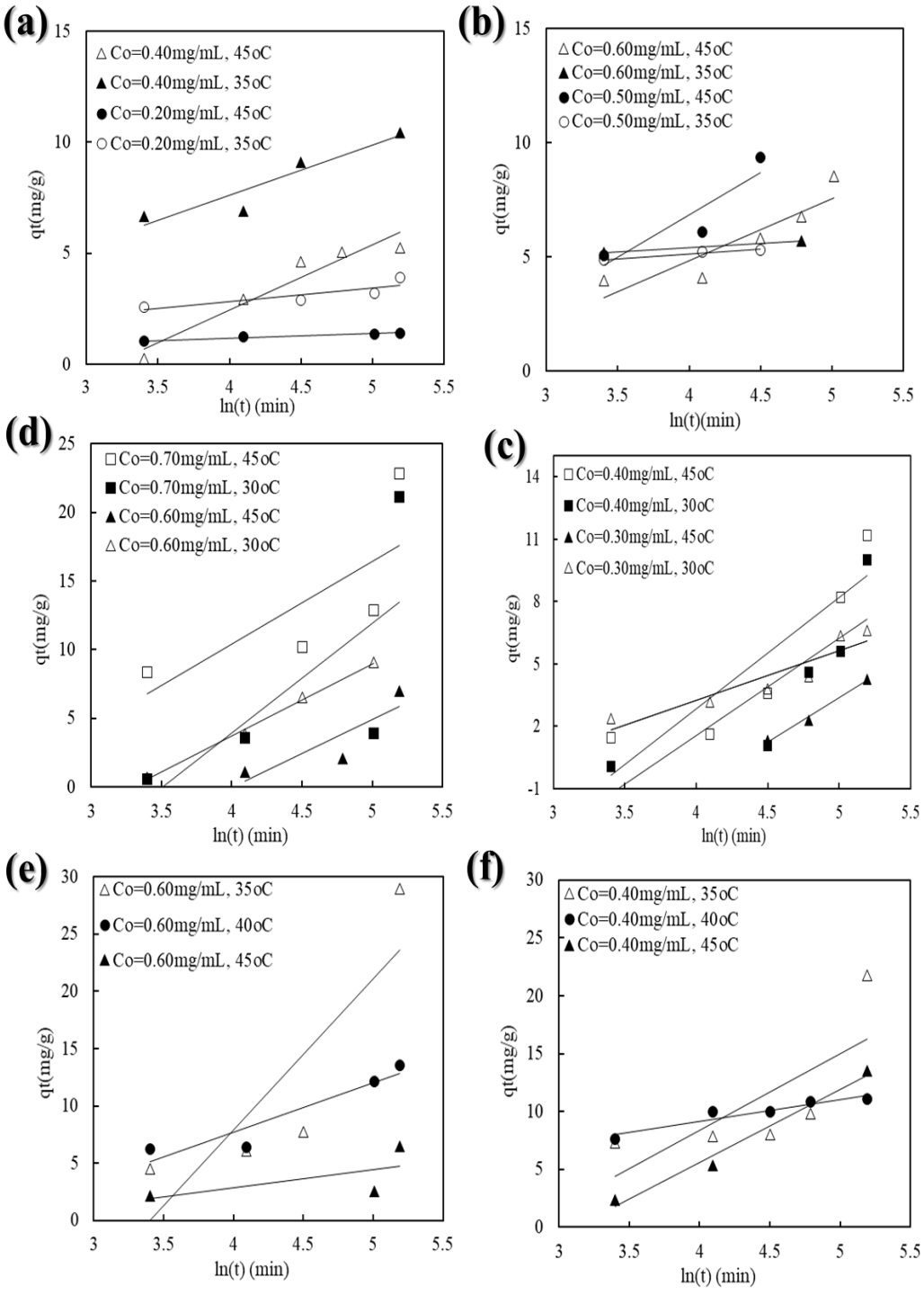

Figure 32: Elovish's model fitting of lipase adsorption kinetics data: on (a-b) ZIF-8 (c-d) ZIF -67 and (e-f) HKUST-1 at different temperatures and initial concentrations

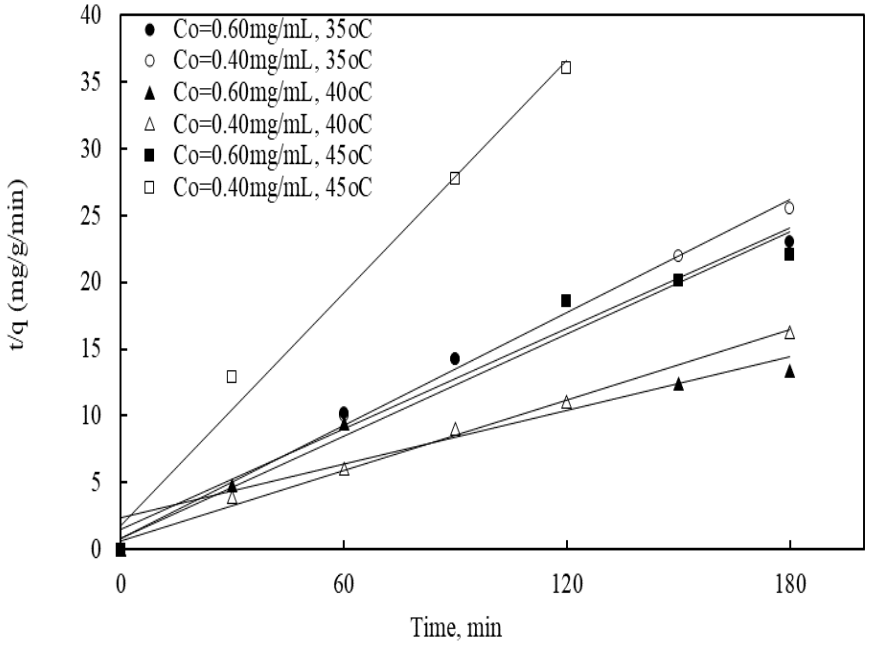

Figure 33: Pseudo second order model fitting of lipase adsorption: kinetics data on HKUST-1 at different temperatures and initial concentration

Generally, Elovish's model best presented the results of ZIF-8 and ZIF-67 shown in Figure 32. The Elovich's equation does not predict any definite mechanism, but it is useful in describing adsorption on highly heterogeneous adsorbents [172]. On the other hand, Pseudo Second order was the model that best described the results of HKUST-1. This may indicate that the adsorption of lipase takes place via surface exchange reactions until the surface functional sites are fully occupied; thereafter lipase molecules diffuse into the HKUST-1 network for further interactions (such as inclusion complex, hydrogen bonding, hydrogen phobic interactions) [174]. The pseudo-second-order model assumes that each lipase molecule is adsorbed onto two adsorption sites which allows a stable binuclear bond to form [174].

Table 7: Fitted kinetic parameters for the adsorption of Lipase onto ZIF-8, ZIF-67 and HKUST-1

T(°C)	C_o	q_e(mg/g)	Pseudo First order		Pseudo Second order		Elovish's model		
			k_1(min^{-1})	R^2	k_2(g/mg.min)	R^2	a(mg/gmin)	1/b(mg/g)	R^2
			L-ZIF-8						
35	0.6	9.88	0.0188	0.60	0.1234	1.0	1.48	1.26	0.96
	0.5	18.95	0.0105	0.70	0.0436	1.0	1.373	1.23	0.97
	0.4	18.35	0.0131	0.80	0.0057	0.96	1.84	1.96	0.97
	0.2	7.26	0.0271	0.80	0.0235	0.96	1.18	0.60	0.73
45	0.6	9.73	0.0278	0.91	0.0035	0.82	0.295	2.73	0.87
	0.5	12.47	0.0332	0.94	0.0082	0.84	0.433	3.66	0.90
	0.4	7.97	0.0163	0.87	0.0014	0.88	0.12	2.93	0.93
	0.2	2.31	0.0140	0.70	0.0479	1.0	1.18	0.20	0.97
			L-ZIF-67						
30	0.7	23.6	0.0306	0.94	0.00053	0.30	0.3518	11.89	0.94
	0.6	13.33	0.0165	0.96	0.00097	0.43	0.1943	5.28	1.0
	0.4	13.57	0.0644	0.82	0.00340	0.70	0.118	4.61	0.74
	0.3	4.26	0.0099	0.95	0.00073	0.79	0.17	2.39	0.85
45	0.7	23.5	0.0173	0.78	0.00032	0.51	0.615	6.05	0.57
	0.6	26.90	0.0029	0.81	0.00081	0.70	0.0897	4.94	0.75
	0.4	12.44	0.0209	0.82	0.00020	0.35	0.5	0.16	0.81
	0.3	5.96	0.0173	0.81	$8.2x10^{-6}$	0.91	2.497	0.063	1.0
			L-HKUST-1						
35	0.6	8.26	0.0382	0.97	0.01047	1	0.823	1.476	0.74
	0.4	10.73	0.0163	0.78	0.02318	1	1.443	1.377	1
40	0.6	14.25	0.0336	0.95	0.00187	0.88	0.472	4.31	0.90
	0.4	11.26	0.0578	0.95	0.01099	1	4.40	1.88	0.91
45	0.6	17.53	0.0081	0.85	0.01972	0.97	0.194	3.46	0.71
	0.4	15.15	0.0382	0.67	0.04743	0.98	0.274	6.10	1.0

Having said that, the kinetic adsorption models, described above, are not able to predict the mechanism and rate-controlling step in a solid-liquid adsorption process. This can be explained by the intraparticle diffusion model [156]. To better understand the lipase diffusion mechanism on the tested MOFs surfaces, the intraparticle diffusion model was applied, and the model fittings are shown in Figure 34, and the adsorption process was found to exhibit multi-linear plots. The early stage sharper portion is assumed to be due to the mass transfer external resistance; whereas the later linear portion is an indication of some intraparticle diffusion control [196]. In the high lipase concentration, range the intraparticle diffusion was found to start from time zero, which indicates that the adsorption of lipase at higher concentrations was completely controlled by intraparticle diffusion. Whereas, at lower concentration range, the

external mass transfer was observed [156]. This indicates that the intraparticle diffusion was not the only rate-limiting step, and film diffusion was also involved in the mechanism [174]. However, the intraparticle diffusion appeared to be slow, as reflected on the low intraparticle rate constants, as compared to that of the film diffusion [199]. The adsorption of lipase is expected to proceed through the following sequence of steps: (1) transport of lipase from the boundary film to the external surface of the adsorbent (film diffusion), (2) transfer of lipase molecule from the surface to the intra-particular active sites, and (3) uptake of lipase by the active sites of ZIF-67, ZIF-8 and HKUST-1 surface. In the initial stage of the adsorption process, the film diffusion is an important rate controlling step [156].

Intraparticle diffusion (D_P) in the three MOFs was obtained using Equation (8) at high and low concentration ranges shown in Figure 34 at 45^oC. For ZIF-8, D_p was 0.0085 nm^2/min in the high concentrations range of 0.5-0.6 mg/mL and increased to 0.0340 nm^2/min in the lower concentrations range of 0.2-0.4 mg/mL. A similar trend was also observed for ZIF-67, in which D_P was 0.001 nm^2/min in the high concentrations range of 0.6-0.7-0.6 mg/mL and increased 0.003 nm^2/min in the lower concentrations range of 0.3-0.4 mg/mL. For chemical adsorption on HKUST-1, a similar trend was observed, wherein D_p in the range of 0.60 mg/mL was 0.00316 nm^2/min whereas, which increased to 0.0034 nm^2/min at the lower concentration of 0.40 mg/mL.

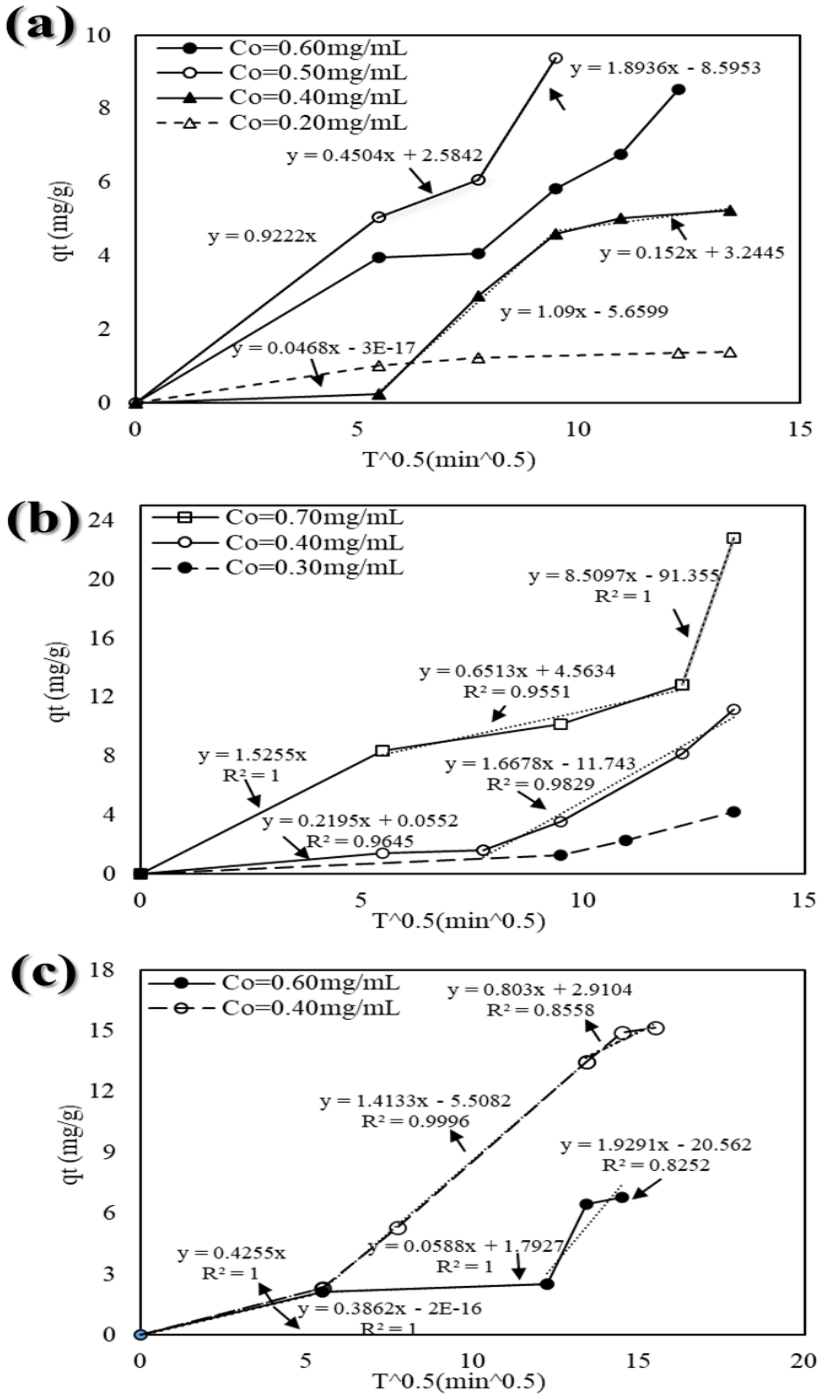

Figure 34: Intraparticle diffusion model for adsorption of lipase: on (a) ZIF-8 (b) ZIF-67 and (c) HKUST-1 at 45^{o}C and different initial protein loadings

The effect of isotherm shape can be used to predict whether an adsorption system is “favourable” or “unfavourable” both in fixed-bed systems as well as in batch processes[196]. According to Hall et al. [208] the essential features of the Langmuir isotherm can be expressed in terms of a dimensionless constant separation factor or equilibrium parameter K_R, which is defined by the following relationship in Equation(S1):

$$KR = \frac{1}{1 + bC_o} \quad \text{(S1)}$$

Where K_R is a dimensionless separation factor, C_0 is initial concentration (mg L^{-1}) and b is Langmuir constant (L mg^{-1}).

A figure with a relationship between K_R and C_0 was presented to show the essential features of the Langmuir isotherm [208] Figure 35 shows the values of K_R for Lipase at different temperatures.

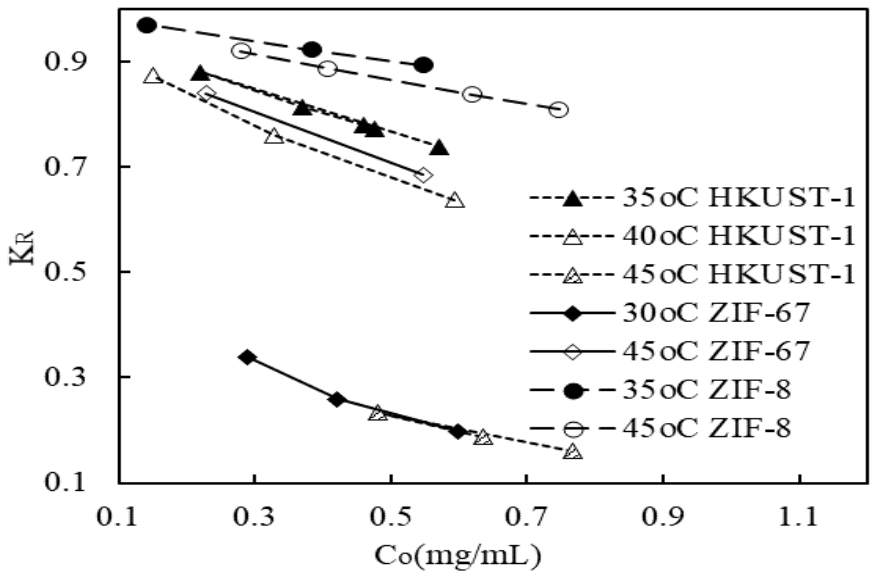

Figure 35: The values of K_R for Lipase into ZIF-8, ZIF-67 and HKUST-1 at different temperatures

The K_R values indicate that adsorption is more favorable at higher temperature than the lower one's for HKUST-1 and ZIF-8, while ZIF-67 is more favorable at lower temperature. However, The K_R value was less than 1 for all supports, indicating that the adsorption of Lipase onto the surface of the ZIF's and HKUST-1 particles was a favorable process.

4.4 Encapsulation of lipase on pre-synthesized ZIF-67 and ZIF-8

Effect of initial lipase concentration on encapsulation capacity in ZIF-8 and ZIF-67 is shown in Figures 36a and 36b, respectively. The highest lipase capacity of in ZIF-8 and ZIF-67 was found to 43 and 75mg/g, at initial loading of 0.46 mg/mL and 0.76 mg/mL, respectively.

It Cleary shown, if concentration of lipase increased, the loading capacity in the formed crystals increased, up to an optimum concentration, which was 0.46 mg/mL and 0.76 mg/mL for ZIF-8 and ZIF-67, respectively. This was expected, as more lipase molecules were available to be entrapped during the crystallization. However, beyond the optimum concentration, a drop in the capacity was observed, for both ZIF's. This may be attributed to negative effect of the large enzyme molecules at high concentrations on the crystallization.

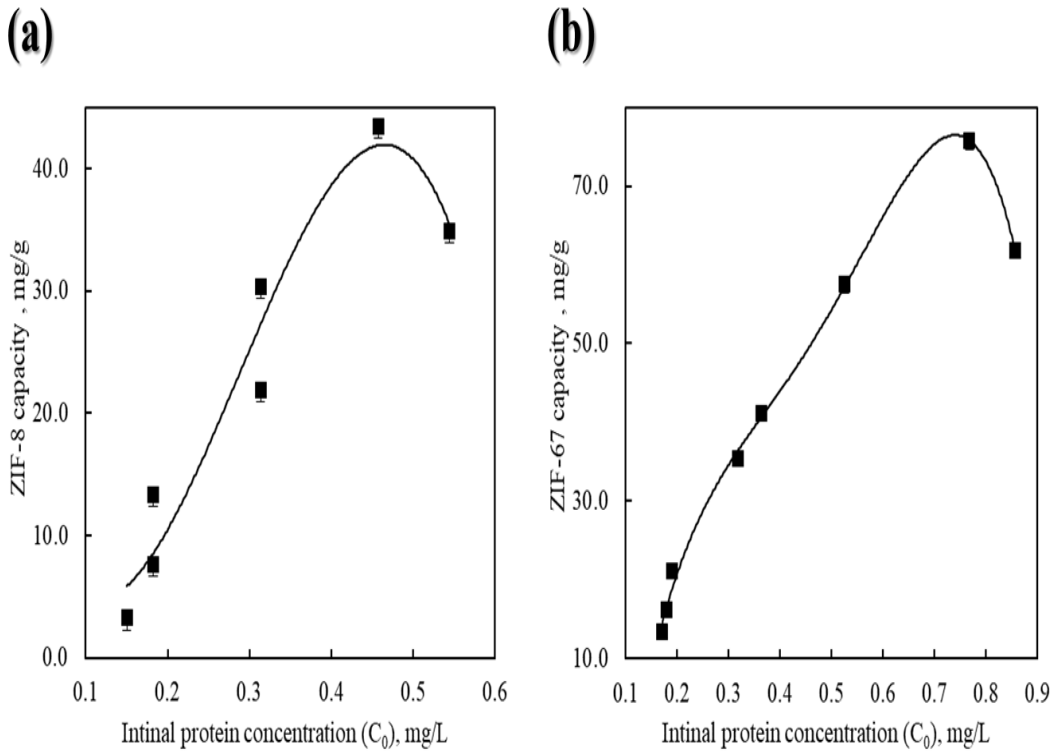

Figure 36: Effect of initial lipase concentration on encapsulation capacity: at 25^{o}C and 24 h in (a) ZIF-8 and (b) ZIF-67

The immobilization efficiency showed a constant increase whenever loading was raised for ZIF-67 and ZIF-8 in Fig 37b and 37d, respectively. The maximum immobilization efficiency 62% when initial loading of 0.40 mg/mL of enzyme for ZIF-67. While ZIF-8 the maximum efficiency is 78% of initial enzyme concentration 0.50 mg/mL. This is common due to the larger pore size obtained of ZIF-8 compared to ZIF-67. However, the increases in enzyme concentration decreases the crystallite rate of ZIF-67 and ZIF-8 crystal growth shown in Figures 37a and 37c, respectively. This is due the higher concentration of big molecules such as enzyme will reduce the nucleation process of crystals formation.

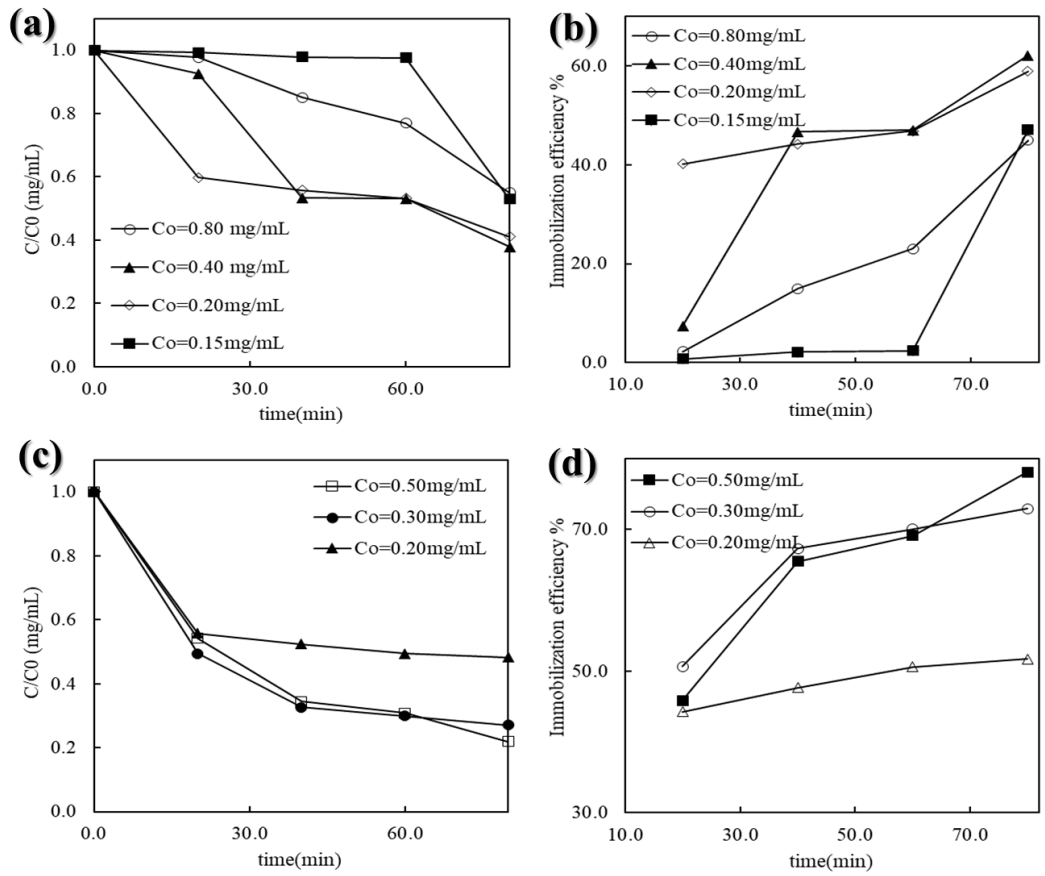

Figure 37: Encapsulation of lipase inside: (a-b) ZIF-67 and (c-d) ZIF-8 at 25^{o}C (a-c) drop in enzyme concentration with time, during the crystallization (b-d) immobilization efficiency with respect to the initial enzyme amount used

4.5 Transesterification reaction and operational stability

The ability of adsorbed lipase, at 45^{o}C, 0.60 mg/ml for ZIF-67 and HKUST-1 and at 35^{o}C, 0.50 mg/mL for ZIF-8 at 180 min, to catalyze the production of biodiesel via transesterification reaction from olive oil was evaluated. Figure 38 shows that under the same experimental conditions of 40^{o}C, 12:1 methanol to oil ratio, biodiesel yield after 4 h was 88.8%, 90.7% and 71.8% using catalyzed by adsorbed of lipase on ZIF-8, ZIF-67 and HKUST-1, respectively. Lipase adsorbed on L-ZIF-67 showed the highest yield. This proves the favorable effect of the hydrophobic interaction. The

higher yield was also due to the high higher surface area of ZIF-67, as compared to the other tested MOFs.

For industrial purposes, the stability and reusability of the biocatalyst is essential. The yield gradually decreased with reusing, due mainly to enzyme leaching from the surface. In terms of reusability, L-HKUST-1 showed the best performance, and maintained over 70% of the initial activity up to the third cycles. This is because of the adsorption on HKUST-1 was chemical, which is stronger than the physical adsorption on the other two ZIFs, which prevented leaching. However, despite its higher stability, lipase chemically adsorbed on HKUST-1 had the lowest activity, which is a common problem with chemical immobilization. Adsorbed lipase on ZIF-8 was the least stable, and the activity dropped to about 5% only in the fourth run 4 run.

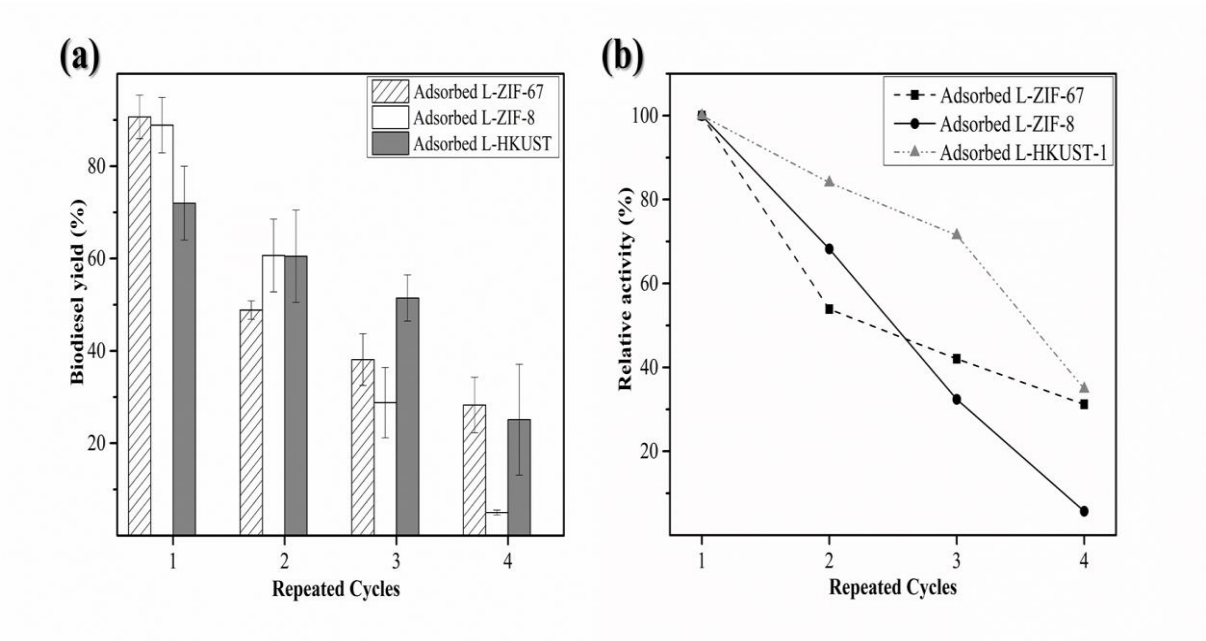

Figure 38: Biodiesel production: at 40^{o}C. 12:1 methanol: oil ratio and 4 h (a) biodiesel production yield % from Lipase Adsorbed on ZIF-67, ZIF-8 and HKUST-1 (b) relative activity of biodiesel production using adsorbed enzyme

Under the same conditions of 40^{o}C and 12:1 methanol to oil ratio, encapsulated lipase inside ZIF-67 and ZIF-8 was tested for biodiesel production. Figure 39 show the activity of encapsulated lipase inside ZIF-8 and ZIF-67. Opposite to absorbed case, the activity of encapsulated lipase in ZIF-67 was lower than that in ZIF-8, and lower than that of the adsorbed lipase on ZIF-67. As additional diffusion resistances are present in encapsulated enzyme [147]. This suggests that higher percentage of enzyme was encapsulated deeper inside the pores of the ZIF-67, owing to their larger crystals. Despite the higher stability of encapsulated lipase, as compared to adsorbed lipase, the continuous decreased in activity suggests that a high percentage of the lipase was actually attached to the outside surface due to large surface area of ZIF-67. The drop in the activity of encapsulated lipase in ZIF-8 was higher than that of encapsulated in ZIF-67, as shown in Figure 39c. This suggests that a higher percentage of the enzyme was attached to the outer surface of ZIF-8, as compared to ZIF-67, which was prone to leaching. This also explains the higher initial activity of encapsulated lipase in ZIF-8 as compared to ZIF-67. A similar drop in activity was also reported when *Aspergillus niger* lipase encapsulated inside ZIF-8 was used in the production of biodiesel [200].

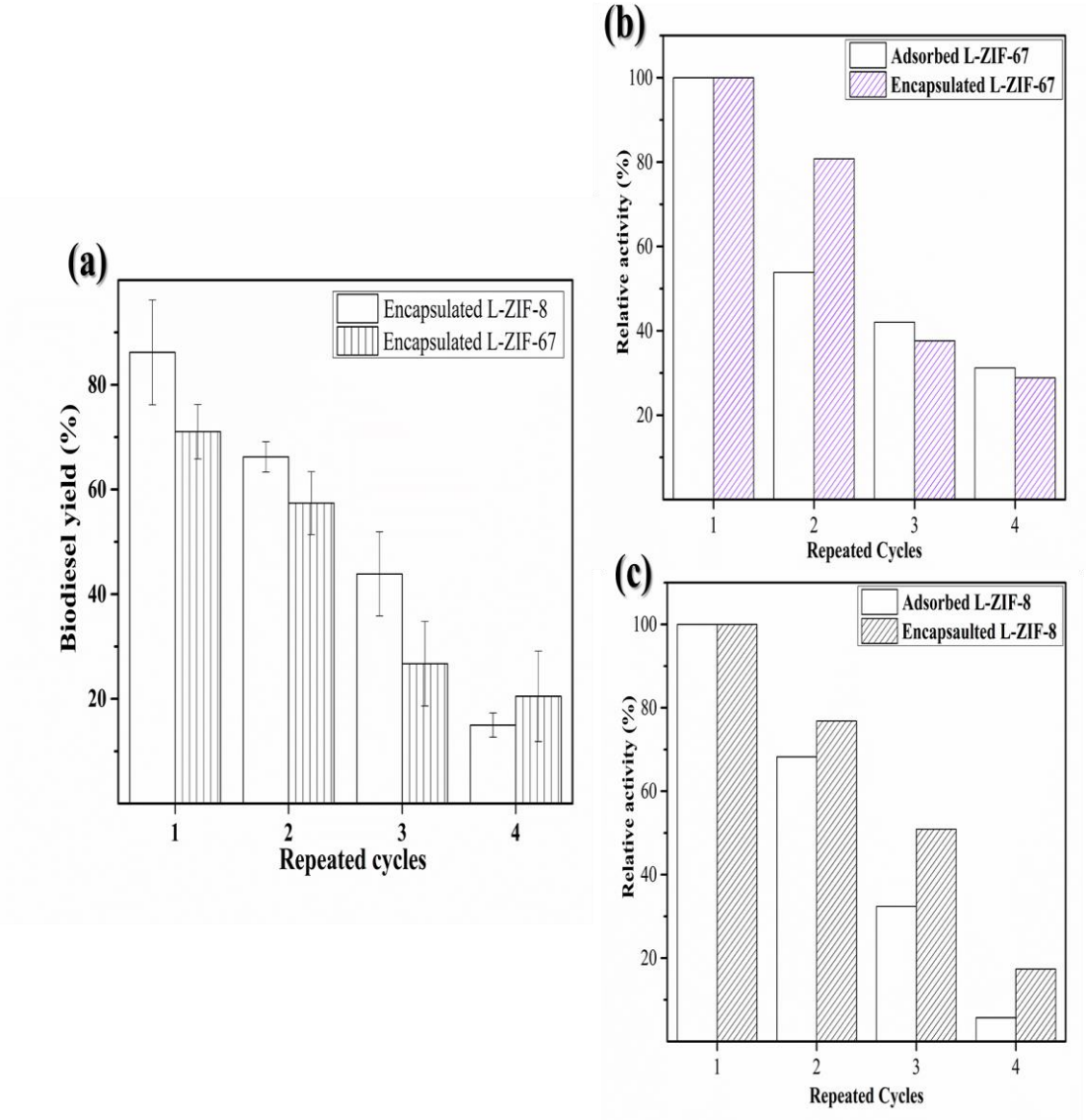

Figure 39: Biodiesel production of encapsulated Lipase at 40^{o}C. 12:1 methanol: oil ratio and 4 h (a) Biodiesel yield of encapsulated Lipase on ZIF-67 and ZIF-8, (b) Relative activity of Adsorbed vs Encapsulated L-ZIF-67 (c) Relative activity of Adsorbed vs Encapsulated L-ZIF-8

Table 8 shows a comparison of biodiesel yields using lipase immobilized on different supports as compared to the results presented in this work. The comparison shows that the yield obtained in this work was comparable those obtained by other studies. The reason for having a higher activity is attributed to the higher lipase dosage

used in this work as compared to those used in other studies, as shown in Table 8. In addition, in this work, n-hexane was used as a reaction medium, which has been proven to enhance enzymatic reaction rate [201]. The addition of solvent reduced the overall viscosity of the solution, which supported diffusion of the substrate to the active cites and the glycerol away from them. It has also been reported that the addition of *n*-hexane reduce the inhibition effect by methanol [202].

Despite the higher activity reported in this work, the reusability was lower than reported in previous studies. This could be due to the addition of all methanol at once in this study, whereas stepwise addition was adopted in other studies[162, 203]. In addition, in the other studies, the separated enzyme was washed between cycles with n-hexane and tert-butanol to remove deposited glycerol [176]. These measures were considered in this work, as it was assumed that *n*-hexane was sufficient to reduce methanol inhibition and glycerol deposition. Above that, the leaching from a high initial loading of enzyme showed a more evident drop in the activity, as compared to the case when a smaller amount of lipase is used, as in the other studies.

Table 8: Performance of lipase immobilized on different supports in biodiesel production

Enzyme	Support	Temp (ºC)	Time (h)	Methanol: Oil	Enzyme dosage wt%	yield %	Reusability, last relative activity%	Ref
Adsorbed								
Burkholderia cepacia	Mesoporous ZIF-8	40	12	6:1	6	93	71% after 8 cycles	[162]
Thermomyces Lanuginosus	Microporous ZIF-67	40	4	12:1	20	90	31% after 4 cycles,	This work
	Mesoporous ZIF-8	40	4	12:1	20	88	6% after 4 cycles	
Encapsulated								
Candida sp	ZIF-67	45	60	6:1	20	78	60% after 6 cycles	[135]
Rhizomucor miehei	X-shaped ZIF-8	45	24	4:1	8	92	86% after 10 cycles	[15]
Candida antarctica	MOF Bio-based	46	11.55	3.64:1	0.55	99	Not specified	[203]
Thermomyces Lanuginosus	Microporous ZIF-67	40	4	12:1	20	72	29% after 4 cycles	This work
	Mesoporous ZIF-8	40	4	12:1	20	86	17% after 4 cycles	

3.6 Diffusion-Reaction Model of ZIF-8

The reaction catalyzed by immobilized lipase is controlled simultaneously by diffusion of substrate to the surface of the immobilized support, followed by surface reaction with the attached enzyme. In order to better understand the reaction, an investigation of the diffusion-reaction system has been performed.

Assuming the reaction to be governed by Michaelis–Menten model [204], the kinetics parameters were initially estimated from the initial reaction rate determined from the FAMEs produces in the first 4 h. The initial reaction rate using the free and immobilized lipase, at the same protein amount is shown in Figures 40a and 40b. The results of the free enzyme were used to estimate the values of V_{max} and K_m, which were 24.1 mg/mL.h and 0.64 mg/mL, respectively, using Eadie-Hofstee linearized equation (Equation 12).

$$v = -k_m \frac{v}{[S_o]} + v_{max} \tag{12}$$

A comparison between the linear The effectiveness factor that compares the rate of reaction using the linear Eadie-Hofstee line of the free enzyme, and the curve of the immobilized enzyme clearly shows that the effectiveness, defined by Equation(13) [204] is less than 1.

$$\eta = \frac{v}{v_{free}} \tag{13}$$

Figure 40c shows the effect of substrate concentration on the effectiveness factor, using the experimental free enzyme results. It is clearly seen that increasing the initial substrate concentration results in increasing the effectiveness. This is because, as the initial substrate increases, the diffusion rate increases due to the increase in the driving force.

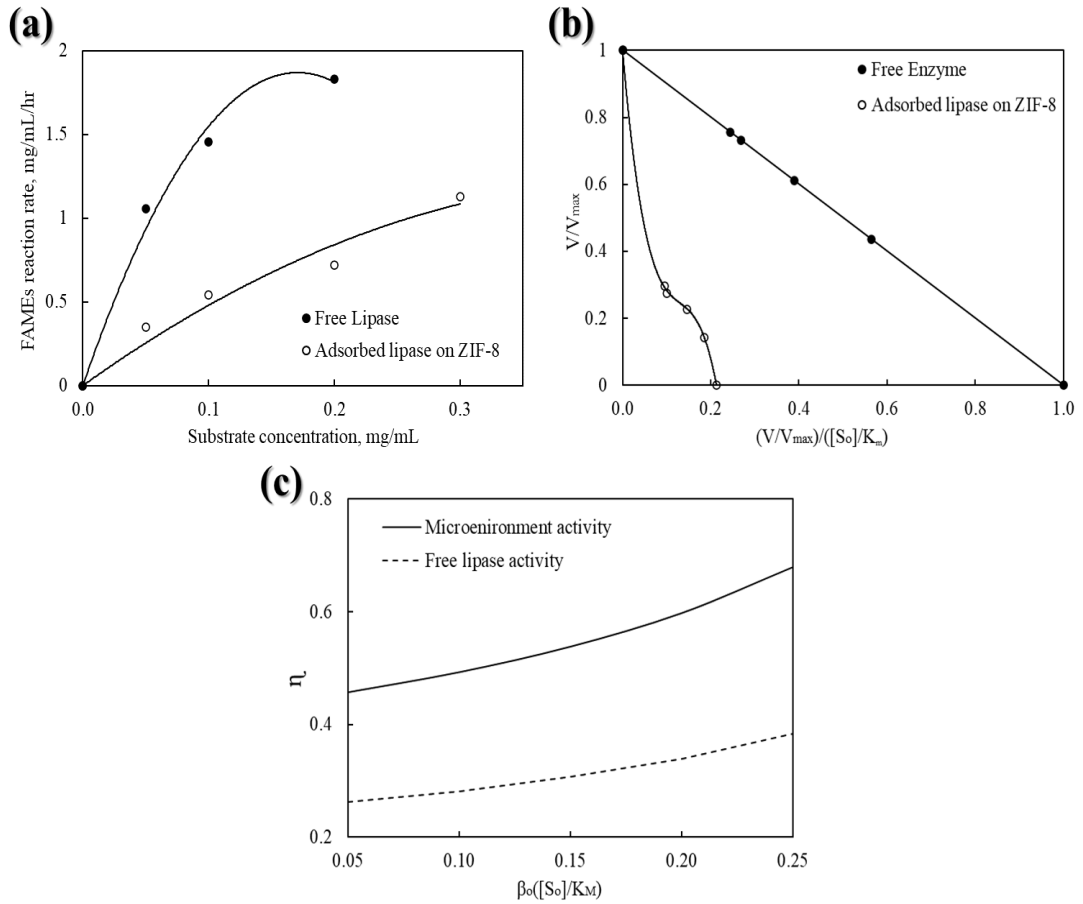

Figure 40: Effect of substrate concentration on FAME's reaction rate: using free and immobilized enzyme at 40°C and 12:1 methanol:oil ratio: (a) concentration vs. reaction rate, (b) Eadie-Hofstee relationship and (c) effect of substrate on the effectiveness using free enzyme data and predicted data based on microenvironment substrate concentration

With surface attachment on pre-synthesized ZIF-8, it was assumed that the lipase molecules accumulate mainly on the outside surface [205] Therefore, in this case, internal diffusion was neglected. Assuming that all of the surface is equally accessible, the rate of flow of substrate to the surface can be expressed by Equation (14) [204]:

$$\frac{V_{max}[s]}{K_m + [s]} = K_L A([S_o] - [S]) \qquad (14)$$

Where, $[S_o]$ and [S] are the substrate concentrations in the bulk of the solution and the microenvironment next to the surface, respectively, and K_{LA} is the mass transfer coefficient capacity coefficient, which was determined to be 0.203 (1/h) from the slope of the tangent of the activity of the immobilized enzyme, as shown in Figure 41a. The activity based on the microenvironmental substrate concentration was then determined graphically by the intercept of the negative slope and the activity at each tested point. Figure 41b shows a comparison between the activity of the free enzyme and the predicted activity of the immobilized enzyme based on the microenvironment substrate concentration. It can be seen that the model predicted was lower than the experimental data, which is an indication that internal diffusion effect was not completely insignificant.

Substrate modulus (μ), also known as the *Damköhler* number, was determined using Equation (15). This factor gives an indication on the significance of surface reaction resistance relative to external diffusion resistance. The higher the value of μ, the higher the diffusion resistance compared to surface reaction resistance. The large values of μ found in this work, which was 184.39, suggests the reaction was diffusion limited [206].

$$\mu = \frac{V_{max}}{K_L A \, K_M} \tag{15}$$

This conclusion was further confirmed in Figure 35c, which shows the effect of substrate concentration on the effectiveness factor based on reaction activity of free enzyme and predicted activity based on the microenvironment concentration. Similar to the free enzyme concentration results, increasing the initial substrate concentration

resulted in increasing the effectiveness. As mentioned earlier, this increase is due to the increase in diffusion driving force.

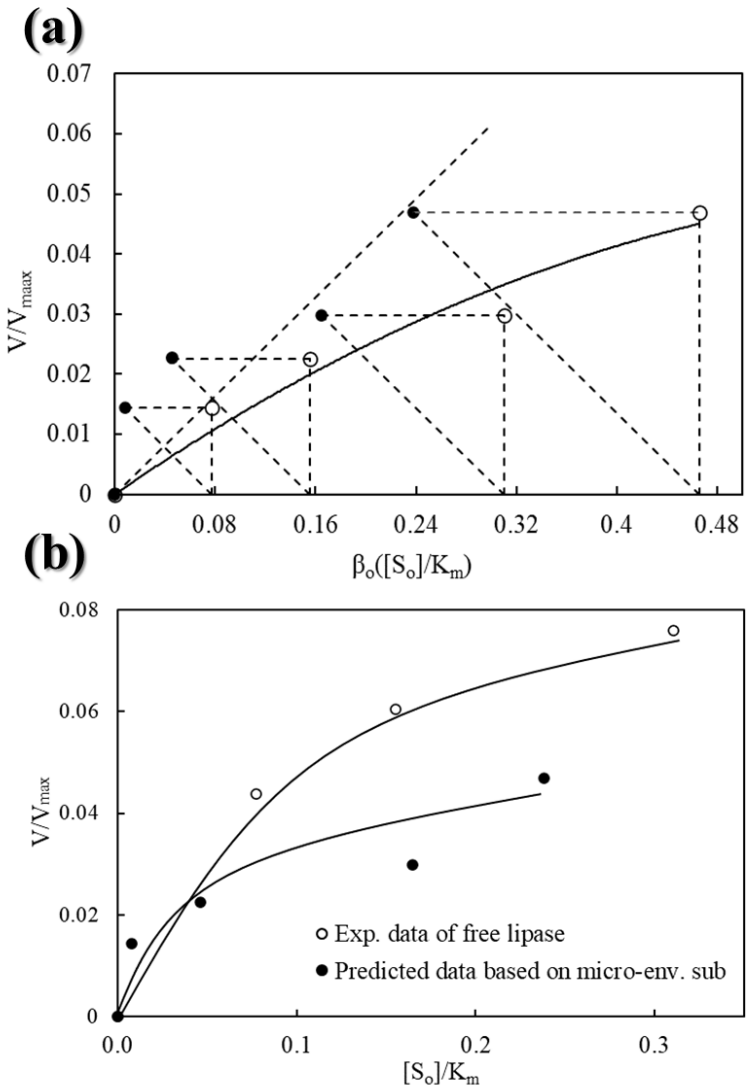

Figure 41: Predicted activity vs experimentally activity of free enzyme: (a) Graphical determination of the enzymatic activity based on microenvironmental substrate concentration and (b) Predicted activity based in the microenvironment substrate vs experimentally determined activity of free enzyme

4.6 Future work

The successful results of the biodiesel yield open a new horizon for easing and simplifying the process of immobilization of lipase into MOFs. However, there are still significant work must be done to enhance the biodiesel yield. An alternative of stepwise addition of alcohol should adopted to enhance the operational stability for industrial using similar to other studies. In addition, in the other studies, the separated enzyme was washed between cycles with n-hexane and tert-butanol to remove deposited glycerol must be investigated due to the many drawbacks on the enzyme activity. Furthermore, the effect of the lipase@MOF dosage wt% for on the FAME's yield could be investigated. Further studies could be carried out to examine and enhance the reusability of the Immobilized enzyme system.

According to the points discussed for enhancement of biodiesel yield, Lipase was tested in two different temperatures to prove the stability of the enzyme and enhance of this work. However, the optimum selection of temperature is to be between the high and low, this because the lipase will denature at a high temperature above 55^{o}C. And at a low temperature, the kinetic energy in the enzyme is relatively low, which affecting the chance of the collision of the enzyme and the substrate, which require a longer period of time for the lipase to break down lipids inside the oil in to glycerol and fatty acid [207]. From the Figure 42a results, at 45^{o}C, if has the fastest rate of breaking down the lipids into fatty acid, of equal of 89.5% of reaction of 4 hour. On the other hand, the different amount of lipase was tested as well shown in Figure 42b, the highest yield was 66% of using 2 ml of enzyme in the solution, whereas using of 0.3 ml of enzyme yield only 35%. This prove that the enzyme is active and showing

high conversion. Hence then, the enhancement of this study is by studying the thermal stability of enzyme in different temperatures.

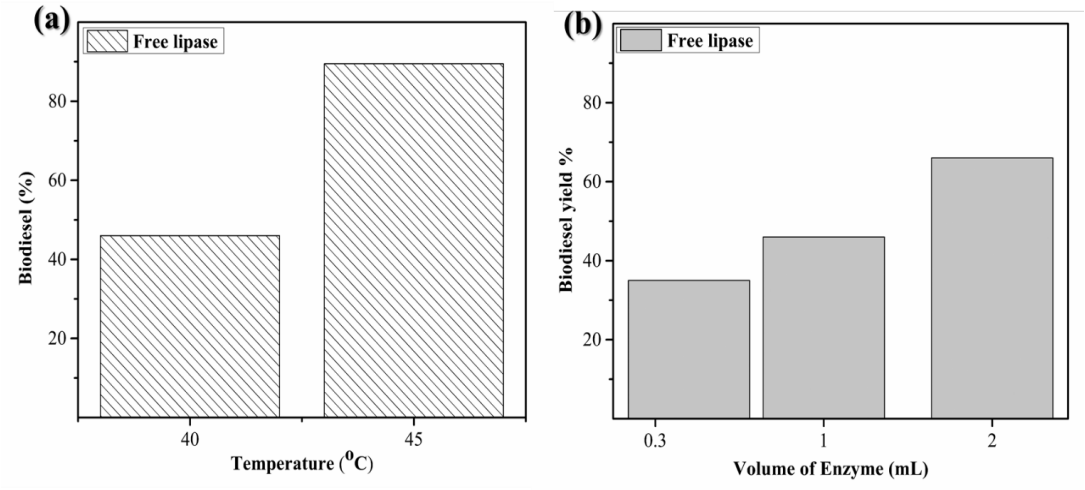

Figure 42: Enhanced future work: (a) different temperature used for biodiesel production at 40 and 45°C of 4 hr reaction (b) different amount of lipase used for the reaction 0.3,1,2 mL of 4 hr , 40°C of reaction

Chapter 5: Conclusion

The application of metal organic frameworks as support for enzyme immobilization is highly attractive due to its large surface area and porous size. Lipase was successfully adsorbed and encapsulated on ZIF-67, ZIF-8 and HKUST-1. The activity of the produced bio-catalytic composite on biodiesel production by solvent-free transesterification of olive-oil showed a good activity and stability up to 3 reuses cycles. The highest biodiesel yield of 90.5% using achieved using adsorbed lipase on ZIF-67, whereas lipase attached by chemical adsorption on HKUST-1 showed the best operational stability compared to other support studied. It was also shown that the adsorption equilibrium was better described by the Langmuir model, which was used to determine the thermodynamic properties. The kinetics was best described by Elovish's model for physical adsorption on ZIF-8 and ZIF-67, and by Pseudo Second order model for chemical adsorption on HKUST-1. The rate-limiting step of the adsorption process was found to be influenced by intraparticle diffusion for ZIF-8 and ZIF-67. The reusability of the immobilized lipase system was tested. In summary, the results of this work hold potential to significantly simplify the production of biodiesel from the metal organic frameworks, understand the mechanism of adsorption reaction, predict the diffusion-reaction system of ZIF-8.

References

1. Basha, S.A.; Gopal, K.R.; Jebaraj, S. A review on biodiesel production, combustion, emissions and performance. *Renew. Sustain. Energy Rev.* 2009, *13*, 1628–1634.
2. Casiello, M.; Catucci, L.; Fracassi, F.; Fusco, C.; Laurenza, A.G.; Di Bitonto, L.; Pastore, C.; D'Accolti, L.; Nacci, A. ZnO/Ionic Liquid Catalyzed Biodiesel Production from Renewable and Waste Lipids as Feedstocks. *Catalysts.* 2019, *9*, 71.
3. Pradhan, P.; Mahajani, S.M.; Arora, A. Production and utilization of fuel pellets from biomass: A review. *Fuel Process. Technol.* 2018, *181*, 215–232.
4. Ambat, I.; Srivastava, V.; Sillanpää, M. Recent advancement in biodiesel production methodologies using various feedstock: A review. *Renew. Sustain. Energy Rev.* 2018, *90*, 356–369.
5. Mishra, V.K.; Goswami, R. A review of production, properties and advantages of biodiesel. *Biofuels.* 2018, *9*, 273–289.
6. Masri, A.N.; Mutalib, M.A.; Aminuddin, N.F.; Lévêque, J. Novel SO_3H-functionalized dicationic ionic liquids—A comparative study for esterification reaction by ultrasound cavitation and mechanical stirring for biodiesel production. *Sep. Purif. Technol.* 2018, *196*, 106–114.
7. Srivastava, N.; Srivastava, M.; Gupta, V.K.; Manikanta, A.; Mishra, K.; Singh, S.; Singh, S.; Ramteke, P.W.; Mishra, P.K. Recent development on sustainable biodiesel production using sewage sludge. *3 Biotech.* 2018, *8*, 245.
8. Lam, H.L.; Varbanov, P.S.; Klemeš, J.J. Regional renewable energy and resource planning. *Appl. Energy.* 2011, *88*, 545–550.
9. Yun, H.; Wang, M.; Feng, W.; Tan, T. Process simulation and energy optimization of the enzyme-catalyzed biodiesel production. *Energy.* 2013, *54*, 84–96.
10. Alhassan, F.H.; Rashid, U.; Taufiq-Yap, Y. Synthesis of waste cooking oil-based biodiesel via effectual recyclable bi-functional $Fe_2O_3MnOSO_4^{2-}/ZrO_2$ nanoparticle solid catalyst. *Fuel* 2015, *142*, 38–45.
11. Yusuf, N.; Kamarudin, S.; Yaakub, Z. Overview on the current trends in biodiesel production. *Energy Convers. Manag.* 2011, *52*, 2741–2751.
12. Kim, D.-S.; Hanifzadeh, M.; Kumar, A. Trend of biodiesel feedstock and its impact on biodiesel emission characteristics. *Environ. Prog. Sustain. Energy.* 2018, *37*, 7–19.
13. Jeevahan, J.; Mageshwaran, G.; Joseph, G.B.; Raj, R.D.; Kannan, R.T. Various strategies for reducing No x emissions of biodiesel fuel used in conventional diesel engines: A review. *Chem. Eng. Commun.* 2017, *204*, 1202–1223.
14. Zhang, Q.; Liu, X.; Yang, T.; Yue, C.; Pu, Q.; Zhang, Y. Facile synthesis of polyoxometalates tethered to post Fe-BTC frameworks for esterification of free fatty acids to biodiesel. *RSC Adv.* 2019, *9*, 8113–8120.

15. Adnan, M.; Li, K.; Xu, L.; Yan, Y. X-shaped zif-8 for immobilization rhizomucor miehei lipase via encapsulation and its application toward biodiesel production. *Catalysts.* 2018, *8*, 96.
16. Šánek, L.; Pecha, J.; Kolomazník, K.; Bařinová, M. Pilot-scale production of biodiesel from waste fats and oils using tetramethylammonium hydroxide. *Waste Manag.* 2016, *48*, 630–637
17. Meng, X.; Yang, J.; Xu, X.; Zhang, L.; Nie, Q.; Xian, M. Biodiesel production from oleaginous microorganisms. *Renew. Energy.* 2009, *34*, 1–5.
18. Han, M.; Li, Y.; Gu, Z.; Shi, H.; Chen, C.; Wang, Q.; Wan, H.; Guan, G. Immobilization of thiol-functionalized ionic liquids onto the surface of MIL-101 (Cr) frameworks by SCr coordination bond for biodiesel production. *Colloids Surf. A Physicochem. Eng. Asp.* 2018, *553*, 593–600
19. Kulkarni, M.G.; Dalai, A.K. Waste Cooking OilAn Economical Source for Biodiesel: A Review. *Ind. Eng. Chem. Res.* 2006, *45*, 2901–2913.
20. Li, J.; Guo, Z. Structure Evolution of Synthetic Amino Acids-Derived Basic Ionic Liquids for Catalytic Production of Biodiesel. *ACS Sustain. Chem. Eng.* 2016, *5*, 1237–1247.
21. Anwar, M.; Rasul, M.G.; Ashwath, N. Production optimization and quality assessment of papaya (*Carica papaya*) biodiesel with response surface methodology. *Energy Convers. Manag.* 2018, *156*, 103–112.
22. Cho, H.U.; Park, J.M. Biodiesel production by various oleaginous microorganisms from organic wastes. *Bioresour. Technol.* 2018, *256*, 502–508.
23. Li, Y.; Hu, S.; Cheng, J.; Lou, W. Acidic ionic liquid-catalyzed esterification of oleic acid for biodiesel synthesis. *Chin. J. Catal.* 2014, *35*, 396–406.
24. Deshmane, C.A.; Wright, M.W.; Lachgar, A.; Rohlfing, M.; Liu, Z.; Le, J.; Hanson, B.E. A comparative study of solid carbon acid catalysts for the esterification of free fatty acids for biodiesel production. Evidence for the leaching of colloidal carbon. *Bioresour. Technol.* 2013, *147*, 597–604.
25. Lee, A.F.; Wilson, K. Recent developments in heterogeneous catalysis for the sustainable production of biodiesel. *Catal. Today.* 2015, *242*, 3–18.
26. Talebian-Kiakalaieh, A.; Amin, N.A.S.; Mazaheri, H. A review on novel processes of biodiesel production from waste cooking oil. *Appl. Energy.* 2013, *104*, 683–710.
27. Ma, F.; Hanna, M.A. Biodiesel production: A review. *Bioresour. Technol.* 1999, *70*, 1–15.
28. Neumann, K.; Werth, K.; Martín, A.; Górak, A. Biodiesel production from waste cooking oils through esterification: Catalyst screening, chemical equilibrium and reaction kinetics. *Chem. Eng. Res. Des.* 2016, *107*, 52–62.
29. Wu, S.; Song, L.; Sommerfeld, M.; Hu, Q.; Chen, W. Optimization of an effective method for the conversion of crude algal lipids into biodiesel. *Fuel.* 2017, *197*, 467–473.

30. Guldhe, A.; Singh, P.; Ansari, F.A.; Singh, B.; Bux, F. Biodiesel synthesis from microalgal lipids using tungstated zirconia as a heterogeneous acid catalyst and its comparison with homogeneous acid and enzyme catalysts. *Fuel.* 2017, *187*, 180–188.
31. Ramos, L.P.; da Silva, F.R.; Mangrich, A.S.; Cordeiro, C.S. Tecnologias de produção de biodiesel. *Rev. Virtual Química.* 2011, *3*, 385–405.
32. Demirbas, A. Importance of biodiesel as transportation fuel. *Energy Policy.* 2007, *35*, 4661–4670.
33. Sani, Y.M.; Aziz, A.R.A.; Daud, W.M.A.W. *Biodiesel Feedstock and Production Technologies: Successes, Challenges and Prospects*; INTECH Open Access Publisher: London, UK, 2012.
34. Tangy, A.; Pulidindi, I.N.; Gedanken, A. SiO2 Beads Decorated with SrO Nanoparticles for Biodiesel Production from Waste Cooking Oil Using Microwave Irradiation. *Energy Fuels.* 2016, *30*, 3151–3160.
35. Gamba, M.; Lapis, A.A.M.; Dupont, J. Supported Ionic Liquid Enzymatic Catalysis for the Production of Biodiesel. *Adv. Synth. Catal.* 2008, *350*, 160–164.
36. Zhang, Q.; Wei, F.; Ma, P.; Zheng, W.; Zhao, Y.; Chen, H. Biodiesel Production by Catalytic Esterification of Oleic Acid over Copper (II)–Alginate Complexes. *J. Oleo Sci.* 2017, *66*, 491–497.
37. Veljković, V.B.; Stamenković, O.S.; Tasić, M.B. The wastewater treatment in the biodiesel production with alkali-catalyzed transesterification. *Renew. Sustain. Energy Rev.* 2014, *32*, 40–60.
38. Xu, Y.; Hanna, M. Synthesis and characterization of hazelnut oil-based biodiesel. *Ind. Crops Prod.* 2009, *29*, 473–479.
39. Park, J.-Y.; Kim, D.-K.; Lee, J.-S. Esterification of free fatty acids using water-tolerable Amberlyst as a heterogeneous catalyst. *Bioresour. Technol.* 2010, *101*, S62–S65.
40. Thangaraj, B.; Solomon, P.R.; Muniyandi, B.; Ranganathan, S.; Lin, L. Catalysis in biodiesel production—A review. *Clean Energy.* 2019, *3*, 2–23.
41. Math, M.C.; Chandrashekhara, K.N. Optimization of Alkali Catalyzed Transesterification of Safflower Oil for Production of Biodiesel. *J. Eng.* 2016, *2016*, 1–7.
42. Hossain, A.S. Alkaline and Acid Catalyzed Transesterification Bioprocess in Biodiesel Preparation from Fresh Water Algae. *Asian J. Biochem.* 2015, *10*, 205–213
43. Zheng, Y.; Zhiming, P.; Xinchen, W. Advances in photocatalysis in China. *Chin. J. Catal.* 2013, *34*, 524–535.
44. Wan, H.; Chen, C.; Wu, Z.; Que, Y.; Feng, Y.; Wang, W.; Wang, L.; Guan, G.; Liu, X. Encapsulation of heteropolyanion-based ionic liquid within the metal–organic framework MIL-100 (Fe) for biodiesel production. *ChemCatChem.* 2015, *7*, 441–449.

45. Ishak, Z.I.; Sairi, N.A.; Alias, Y.; Aroua, M.K.T.; Yusoff, R. A review of ionic liquids as catalysts for transesterification reactions of biodiesel and glycerol carbonate production. *Catal. Rev.* 2017, *59*, 44–93.
46. Fan, P.; Xing, S.; Wang, J.; Fu, J.; Yang, L.; Yang, G.; Miao, C.; Lv, P. Sulfonated imidazolium ionic liquid-catalyzed transesterification for biodiesel synthesis. *Fuel.* 2017, *188*, 483–488.
47. Rafiee, E.; Mirnezami, F. Temperature regulated Brønsted acidic ionic liquid-catalyze esterification of oleic acid for biodiesel application. *J. Mol. Struct.* 2017, *1130*, 296–302.
48. Liu, X.; Liu, Z.; Wang, R. Functionalized Metal–organic Framework Catalysts for Sustainable Biomass Valorization. *Adv. Polym. Technol.* 2020, *2020*, 1–11.
49. Guldhe, A.; Singh, B.; Mutanda, T.; Permaul, K.; Bux, F. Advances in synthesis of biodiesel via enzyme catalysis: Novel and sustainable approaches. *Renew. Sustain. Energy Rev.* 2015, *41*, 1447–1464.
50. Poppe, J.K.; Garcia-Galan, C.; Matte, C.R.; Fernandez-Lafuente, R.; Rodrigues, R.C.; Ayub, M.A.Z. Optimization of synthesis of fatty acid methyl esters catalyzed by lipase B from Candida antarctica immobilized on hydrophobic supports. *J. Mol. Catal. B Enzym.* 2013, *94*, 51–56.
51. Rana, Q.u.a.; Rehman, M.L.U.; Irfan, M.; Ahmed, S.; Hasan, F.; Shah, A.A.; Khan, S.; Badshah, M. Lipolytic bacterial strains mediated transesterification of non-edible plant oils for generation of high quality biodiesel. *J. Biosci. Bioeng.* 2019, *127*, 609–617.
52. Guil-Laynez, J.L.; Guil-Guerrero, J.L.; Guil-Laynez, Á. Bioprospecting for seed oils in tropical areas for biodiesel production. *Ind. Crops Prod.* 2019, *128*, 504–511.
53. Sun, S.; Li, K. Biodiesel production from phoenix tree seed oil catalyzed by liquid lipozyme TL100L. *Renew. Energy.* 2020, *151*, 152–160.
54. Doğan, T.H. The testing of the effects of cooking conditions on the quality of biodiesel produced from waste cooking oils. *Renew. Energy.* 2016, *94*, 466–473.
55. Wang, X.; Qin, X.; Li, D.; Yang, B.; Wang, Y. One-step synthesis of high-yield biodiesel from waste cooking oils by a novel and highly methanol-tolerant immobilized lipase. *Bioresour. Technol.* 2017, *235*, 18–24.
56. Mannu, A.; Ferro, M.; Dugoni, G.C.; Panzeri, W.; Petretto, G.L.; Urgeghe, P.; Mele, A. Improving the recycling technology of waste cooking oils: Chemical fingerprint as tool for non-biodiesel application. *Waste Manag.* 2019, *96*, 1–8.
57. Pirouzmand, M.; Anakhatoon, M.M.; Ghasemi, Z. One-step biodiesel production from waste cooking oils over metal incorporated MCM-41; positive effect of template. *Fuel.* 2018, *216*, 296–300.
58. Gude, V.G.; Grant, G.E. Biodiesel from waste cooking oils via direct sonication. *Appl. Energy.* 2013, *109*, 135–144.
59. Eze, V.C.; Phan, A.N.; Harvey, A.P. Intensified one-step biodiesel production from high water and free fatty acid waste cooking oils. *Fuel.* 2018, *220*, 567–574.

60. Hariprasath, P.; Vijayakumar, V.; Selvamani, S.T.; Vigneshwar,M.; Palanikumar, K. Some Studies on Waste Animal Tallow Biodiesel Produced by Modified Transesterification Method Using Heterogeneous Catalyst. *Mater. Today Proc.* 2019, *16*, 1271–1278.
61. Öner, C.; Altun, Ş. Biodiesel production from inedible animal tallow and an experimental investigation of its use as alternative fuel in a direct injection diesel engine. *Appl. Energy.* 2009, *86*, 2114–2120.
62. Liu, S.; Wang, Y.; Oh, J.-H.; Herring, J.L. Fast biodiesel production from beef tallow with radio frequency heating. *Renew. Energy* 2011, *36*, 1003–1007.
63. da Cunha, M.E.; Krause, L.C.; Moraes, M.S.A.; Faccini, C.S.; Jacques, R.A.; Almeida, S.R.; Rodrigues, M.R.A.; Caramão, E.B. Beef tallow biodiesel produced in a pilot scale. *Fuel Process. Technol.* 2009, *90*, 570–575.]
64. Adewale, P.; Dumont, M.-J.; Ngadi, M. Enzyme-catalyzed synthesis and kinetics of ultrasonic-assisted biodiesel production from waste tallow. *Ultrason. Sonochem.* 2015, *27*, 1–9.
65. Chung, K.-H.; Kim, J.; Lee, K.-Y. Biodiesel production by transesterification of duck tallow with methanol on alkali catalysts. *Biomass Bioenergy.* 2009, *33*, 155–158.
66. Bhatti, H.; Hanif, M.; Qasim, M. Ataurrehman Biodiesel production from waste tallow. *Fuel.* 2008, *87*, 2961–2966.
67. Vicente, G.; Martinez, M.; Aracil, J. A Comparative Study of Vegetable Oils for Biodiesel Production in Spain. *Energy Fuels.* 2006, *20*, 394–398.
68. Watanabe, Y.; Shimada, Y.; Sugihara, A.; Tominaga, Y. Conversion of degummed soybean oil to biodiesel fuel with immobilized Candida antarctica lipase. *J. Mol. Catal. B Enzym.* 2002, *17*, 151–155.
69. Atadashi, I.M.; Aroua, M.K.; Abdul Aziz, A.R.; Sulaiman, N.M.N. The effects of water on biodiesel production and refining technologies: A review. *Renew. Sustain. Energy Rev.* 2012, *16*, 3456–3470
70. Khan, F.I.; Lan, D.; Durrani, R.; Huan, W.; Zhao, Z.; Wang, Y. The Lid Domain in Lipases: Structural and Functional Determinant of Enzymatic Properties. *Front. Bioeng. Biotechnol.* 2017, *5*, 16.
71. Lotti, M.; Pleiss, J.; Valero, F.; Ferrer, P. Effects of methanol on lipases: Molecular, kinetic and process issues in the production of biodiesel. *Biotechnol. J.* 2015, *10*, 22–30
72. Shimada, Y.; Watanabe, Y.; Sugihara, A.; Tominaga, Y. Enzymatic alcoholysis for biodiesel fuel production and application of the reaction to oil processing. *J. Mol. Catal. B Enzym.* 2002, *17*, 133–142.
73. Soumanou, M.M.; Bornscheuer, U.T. Improvement in lipase-catalyzed synthesis of fatty acid methyl esters from sunflower oil. *Enzym. Microb. Technol.* 2003, *33*, 97–103.
74. Chen, G.; Ying, M.; Li, W. Enzymatic conversion of waste cooking oils into alternative fuel—Biodiesel. *Appl. Biochem. Biotechnol.* 2006, *132*, 911–921.

75. Lu, J.; Nie, K.; Xie, F.; Wang, F.; Tan, T. Enzymatic synthesis of fatty acid methyl esters from lard with immobilized Candida sp. 99-125. *Process. Biochem.* 2007, *42*, 1367–1370.
76. Musa, I.A. The effects of alcohol to oil molar ratios and the type of alcohol on biodiesel production using transesterification process. *Egypt. J. Pet.* 2016, *25*, 21–31.
77. Batista, A.; Silva, T.; Vieira, A.; de Oliveira, M. Biotechnological Applications of Lipases in Biodiesel Production. *Fungal Enzymes.* 2013.
78. Mat Radzi, S.; Basri, M.; Bakar Salleh, A.; Ariff, A.; Mohammad, R.; Abdul Rahman, M.B.; Abdul Rahman, R.N.Z.R. High performance enzymatic synthesis of oleyl oleate using immobilised lipase from Candida antartica. *Electron. J. Biotechnol.* 2005, *8*, 291–298.
79. Klibanov, A.M. Improving enzymes by using them in organic solvents. *Nat. Cell Biol.* 2001, *409*, 241–246.
80. Verma, P.; Sharma, M.P. Comparative analysis of effect of methanol and ethanol on Karanja biodiesel production and its optimisation. *Fuel* 2016, *180*, 164–174.
81. Almeida, L.; Barbosa, A.S.; Fricks, A.T.; Freitas, L.; Lima, Á.S.; Soares, C.M. Use of conventional or non-conventional treatments of biochar for lipase immobilization. *Process. Biochem.* 2017, *61*, 124–129.
82. Ycel, S.; Terziolu, P.; zime, D. Lipase Applications in Biodiesel Production. In *Biodiesel–Feedstocks, Production and Applications*; INTECHOpen: London, UK, 2012.
83. Hanif, M.A.; Nisar, S.; Rashid, U. Supported solid and heteropoly acid catalysts for production of biodiesel. *Catal. Rev.* 2017, *59*, 165–188.
84. Corma, A.; García, H.; Llabrés i Xamena, F.X. Engineering Metal Organic Frameworks for Heterogeneous Catalysis. *Chem. Rev.* 2010, *110*, 4606–4655.
85. Howarth, A.J.; Peters, A.W.; Vermeulen, N.A.; Wang, T.C.; Hupp, J.T.; Farha, O.K. Best Practices for the Synthesis, Activation, and Characterization of Metal–Organic Frameworks. *Chem. Mater.* 2017, *29*, 26–39.
86. Bobbitt, N.S.; Mendonca, M.L.; Howarth, A.J.; Islamoglu, T.; Hupp, J.T.; Farha, O.K.; Snurr, R.Q. Metal–organic frameworks for the removal of toxic industrial chemicals and chemical warfare agents. *Chem. Soc. Rev.* 2017, *46*, 3357–3385.
87. Silva, P.; Vilela, S.M.F.; Tomé, J.P.C.; Paz, F.A.A. Multifunctional metal–organic frameworks: From academia to industrial applications. *Chem. Soc. Rev.* 2015, *44*, 6774–6803.
88. Van de Voorde, B.; Bueken, B.; Denayer, J.; De Vos, D. Adsorptive separation on metal–organic frameworks in the liquid phase. *Chem. Soc. Rev.* 2014, *43*, 5766–5788.
89. Giménez-Marqués, M.; Hidalgo, T.; Serre, C.; Horcajada, P. Nanostructured metal–organic frameworks and their bio-related applications. *Co-ord. Chem. Rev.* 2016, *307*, 342–360.
90. Zhu, L.; Liu, X.-Q.; Jiang, H.-L.; Sun, L.-B. Metal–Organic Frameworks for Heterogeneous Basic Catalysis. *Chem. Rev.* 2017, *117*, 8129–8176.

91. Adil, K.; Belmabkhout, Y.; Pillai, R.S.; Cadiau, A.; Bhatt, P.M.; Assen, A.H.; Maurin, G.; Eddaoudi, M. Gas/vapour separation using ultra-microporous metal–organic frameworks: Insights into the structure/separation relationship. *Chem. Soc. Rev.* 2017, *46*, 3402–3430.
92. Yamada, T.; Sadakiyo, M.; Shigematsu, A.; Kitagawa, H. Proton-conductive metal–organic frameworks. *Bull. Chem. Soc. Jpn.* 2015, *89*, 1–10.
93. Sun, Y.; Huang, H.; Vardhan, H.; Aguila, B.; Zhong, C.; Perman, J.A.; Al-Enizi, A.M.; Nafady, A.; Ma, S. Facile Approach to Graft Ionic Liquid into MOF for Improving the Efficiency of CO_2 Chemical Fixation. *ACS Appl. Mater. Interfaces* 2018, *10*, 27124–27130.
94. Cohen, S.M. Postsynthetic Methods for the Functionalization of Metal–Organic Frameworks. *Chem. Rev.* 2011, *112*, 970–1000.
95. Abd El Rahman, S.K.; Hassan, H.M.; El-Shall, M.S. Metal–organic frameworks with high tungstophosphoric acid loading as heterogeneous acid catalysts. *Appl. Catal. A Gen.* 2014, *487*, 110–118
96. Zhang, Y.-B.; Furukawa, H.; Ko, N.; Nie, W.; Park, H.J.; Okajima, S.; Cordova, K.E.; Deng, H.; Kim, J.; Yaghi, O. Introduction of Functionality, Selection of Topology, and Enhancement of Gas Adsorption in Multivariate Metal–Organic Framework-177. *J. Am. Chem. Soc.* 2015, *137*, 2641–2650
97. Kitagawa, S. Metal–organic frameworks (MOFs). *Chem. Soc. Rev.* 2014, *43*, 5415–5418]
98. Nozari, V.; Keskin, S.; Uzun, A. Toward Rational Design of Ionic Liquid/Metal–Organic Framework Composites: Effects of Interionic Interaction Energy. *ACS Omega* 2017, *2*, 6613–6618.
99. Xia, H.; Li, N.; Zhong, X.; Jiang, Y. Metal–organic Frameworks: A Potential Platform for Enzyme Immobilization and Related Applications. *Front. Bioeng. Biotechnol.* 2020, *8*, 695.
100. Pangestu, T.; Kurniawan, Y.; Soetaredjo, F.E.; Santoso, S.P.; Irawaty, W.; Yuliana, M.; Hartono, S.B.; Ismadji, S. The synthesis of biodiesel using copper based metal–organic framework as a catalyst. *J. Environ. Chem. Eng.* 2019, *7*, 103277
101. Khan, N.A.; Jhung, S.H. Synthesis of metal–organic frameworks (MOFs) with microwave or ultrasound: Rapid reaction, phase-selectivity, and size reduction. *Co-ord. Chem. Rev.* 2015, *285*, 11–23.
102. Zhang, Q.; Lei, D.; Luo, Q.; Wang, J.; Deng, T.; Zhang, Y.; Ma, P. Efficient biodiesel production from oleic acid using metal–organic framework encapsulated Zr-doped polyoxometalate nano-hybrids. *RSC Adv.* 2020, *10*, 8766–8772.
103. AbdelSalam, H.; El-Maghrabi, H.; Zahran, F.; Zaki, T. Microwave-assisted production of biodiesel using metal–organic framework $Mg_3(bdc)_3(H_2O)_2$. *Korean J. Chem. Eng.* 2020, *37*, 670–676.

104. Nikseresht, A.; Daniyali, A.; Ali-Mohammadi, M.; Afzalinia, A.; Mirzaie, A. Ultrasound-assisted biodiesel production by a novel composite of Fe(III)-based MOF and phosphotangestic acid as efficient and reusable catalyst. *Ultrason. Sonochem.* 2017, *37*, 203–207.
105. Lestari, W.W.; Nugraha, R.E.; Winarni, I.D.; Adreane, M.; Rahmawati, F. Optimization on electrochemical synthesis of HKUST-1 as candidate catalytic material for Green diesel production. *AIP Conf. Proc.* 2016, *1725*, 20038.
106. Lian, X.; Fang, Y.; Joseph, E.; Wang, Q.; Li, J.; Banerjee, S.; Lollar, C.; Wang, X.; Zhou, H.-C. Enzyme–MOF (metal–organic framework) composites. *Chem. Soc. Rev.* 2017, *46*, 3386–3401.
107. Vaitsis, C.; Sourkouni, G.; Argirusis, C. Metal Organic Frameworks (MOFs) and ultrasound: A review. *Ultrason. Sonochem.* 2019, *52*, 106–119.
108. Soni, S.; Bajpai, P.K.; Arora, C. A review on metal–organic framework: Synthesis, properties and application. *Charact. Appl. Nanomater.* 2018, *2*, 551.
109. Nadar, S.S.; Rathod, V.K. Encapsulation of lipase within metal–organic framework (MOF) with enhanced activity intensified under ultrasound. *Enzym. Microb. Technol.* 2018, *108*, 11–20.
110. Zhu, H.; Zhang, Q.; Li, B.-G.; Zhu, S. Engineering Elastic ZIF-8-Sponges for Oil-Water Separation. *Adv. Mater. Interfaces* 2017, *4*, 1700560.
111. Nadar, S.; Rathod, V.K. One pot synthesis of α-amylase metal organic framework (MOF)-sponge via dip-coating technique. *Int. J. Biol. Macromol.* 2019, *138*, 1035–1043.
112. Feng, Y.; Yao, J. Design of Melamine Sponge-Based Three-Dimensional Porous Materials toward Applications. *Ind. Eng. Chem. Res.* 2018, *57*, 7322–7330.
113. Valizadeh, B.; Nguyen, T.N.; Stylianou, K.C. Shape engineering of metal–organic frameworks. *Polyhedron* 2018, *145*, 1–15.
114. Sijbesma, R.P.; Nolte, R.J.M. A molecular clip with allosteric binding properties. *J. Am. Chem. Soc.* 1991, *113*, 6695–6696.
115. Wang, L.-B.; Wang, Y.-C.; He, R.; Zhuang, A.; Wang, X.; Zeng, J.; Hou, J.G. A New Nanobiocatalytic System Based on Allosteric Effect with Dramatically Enhanced Enzymatic Performance. *J. Am. Chem. Soc.* 2013, *135*, 1272–1275.
116. Tan, T.; Lu, J.; Nie, K.; Deng, L.; Wang, F. Biodiesel production with immobilized lipase: A review. *Biotechnol. Adv.* 2010, *28*, 628–634.
117. Qiu, L.-G.; Xu, T.; Li, Z.-Q.; Wang, W.; Wu, Y.; Jiang, X.; Tian, X.-Y.; Zhang, L.-D. Hierarchically Micro- and Mesoporous Metal–organic Frameworks with Tunable Porosity. *Angew. Chem. Int. Ed.* 2008, *47*, 9487–9491.
118. Li, P.; Modica, J.A.; Howarth, A.J.; Vargas, L.E.; Moghadam, P.Z.; Snurr, R.Q.; Mrksich, M.; Hupp, J.T.; Farha, O.K. Toward Design Rules for Enzyme Immobilization in Hierarchical Mesoporous Metal–organic Frameworks. *Chem* 2016, *1*, 154–169.
119. Jegannathan, K.R.; Abang, S.; Poncelet, D.; Chan, E.S.; Ravindra, P. Production of Biodiesel Using Immobilized Lipase—A Critical Review. *Crit. Rev. Biotechnol.* 2008, *28*, 253–264.

120. Jung, S.; Kim, Y.; Kim, S.-J.; Kwon, T.-H.; Huh, S.; Park, S. Bio-functionalization of metal–organic frameworks by covalent protein conjugation. *Chem. Commun.* 2011, *47*, 2904–2906.
121. Nguyen, H.H.; Kim, M. An Overview of Techniques in Enzyme Immobilization. *Appl. Sci. Converg. Technol.* 2017, *26*, 157–163.
122. Nobakht, N.; Faramarzi, M.A.; Shafiee, A.; Khoobi, M.; Rafiee, E. Polyoxometalate-metal organic framework-lipase: An efficient green catalyst for synthesis of benzyl cinnamate by enzymatic esterification of cinnamic acid. *Int. J. Biol. Macromol.* 2018, *113*, 8–19.
123. Andreani, L.; Rocha, J.D. Use of ionic liquids in biodiesel production: A review. *Braz. J. Chem. Eng.* 2012, *29*, 1–13.
124. Ratti, R. Ionic Liquids: Synthesis and Applications in Catalysis. *Adv. Chem.* 2014, *2014*, 729842.
125. Chen, S.-Y.; Lo, W.-S.; Huang, Y.-D.; Si, X.; Liao, F.-S.; Lin, S.-W.; Williams, B.P.; Sun, T.-Q.; Lin, H.-W.; An, Y.; et al. Probing Interactions between Metal–Organic Frameworks and Freestanding Enzymes in a Hollow Structure. *Nano Lett.* 2020, *20*, 6630–6635.
126. Shieh, F.-K.; Wang, S.-C.; Yen, C.-I.; Wu, C.-C.; Dutta, S.; Chou, L.-Y.; Morabito, J.V.; Hu, P.; Hsu, M.H.; Wu, K.C.-W.; et al. Imparting Functionality to Biocatalysts via Embedding Enzymes into Nanoporous Materials by ade NovoApproach: Size-Selective Sheltering of Catalase in Metal–Organic Framework Microcrystals. *J. Am. Chem. Soc.* 2015, *137*, 4276–4279.
127. Liao, F.-S.; Lo, W.-S.; Hsu, Y.-S.; Wu, C.-C.; Wang, S.-C.; Shieh, F.-K.; Morabito, J.V.; Chou, L.-Y.; Wu, K.C.-W.; Tsung, C.-K. Shielding against Unfolding by Embedding Enzymes in Metal–Organic Frameworks via a de Novo Approach. *J. Am. Chem. Soc.* 2017, *139*, 6530–6533.
128. Wei, T.-H.; Wu, S.-H.; Huang, Y.-D.; Lo, W.-S.; Williams, B.P.; Chen, S.-Y.; Yang, H.-C.; Hsu, Y.-S.; Lin, Z.-Y.; Chen, X.-H.; et al. Rapid mechanochemical encapsulation of biocatalysts into robust metal–organic frameworks. *Nat. Commun.* 2019, *10*, 1–8.
129. Zhong, L.; Feng, Y.; Wang, G.; Wang, Z.; Bilal, M.; Lv, H.; Jia, S.; Cui, J. Production and use of immobilized lipases in/on nanomaterials: A review from the waste to biodiesel production. *Int. J. Biol. Macromol.* 2020, *152*, 207–222
130. Yu, D.; Tian, L.; Wu, H.; Wang, S.; Wang, Y.; Ma, D.; Fang, X. Ultrasonic irradiation with vibration for biodiesel production from soybean oil by Novozym 435. *Process. Biochem.* 2010, *45*, 519–525
131. Maceiras, R.; Vega, M.; Costa, C.; Ramos, P.; Márquez, M. Effect of methanol content on enzymatic production of biodiesel from waste frying oil. *Fuel* 2009, *88*, 2130–2134.
132. Ha, S.H.; Lan, M.N.; Lee, S.H.; Hwang, S.M.; Koo, Y.-M. Lipase-catalyzed biodiesel production from soybean oil in ionic liquids. *Enzym. Microb. Technol.* 2007, *41*, 480–483.

133. De Diego, T.; Manjón, A.; Lozano, P.; Vaultier, M.; Iborra, J.L. An efficient activity ionic liquid-enzyme system for biodiesel production. *Green Chem.* 2011, *13*, 444.
134. Lai, J.-Q.; Hu, Z.-L.; Wang, P.-W.; Yang, Z. Enzymatic production of microalgal biodiesel in ionic liquid [BMIm][PF6]. *Fuel* 2012, *95*, 329–333.
135. Rafiei, S.; Tangestaninejad, S.; Horcajada, P.; Moghadam, M.; Mirkhani, V.; Mohammadpoor-Baltork, I.; Kardanpour, R.; Zadehahmadi, F. Efficient biodiesel production using a lipase@ZIF-67 nanobioreactor. *Chem. Eng. J.* 2018, *334*, 1233–1241.
136. Adnan, M.; Li, K.; Wang, J.; Xu, L.; Yan, Y. Hierarchical ZIF-8 toward Immobilizing Burkholderia cepacia Lipase for Application in Biodiesel Preparation. *Int. J. Mol. Sci.* 2018, *19*, 1424.
137. Corrêa, I.N.D.S.; De Souza, S.L.; Catran, M.; Bernardes, O.L.; Portilho, M.F.; Langone, M.A.P. Enzymatic Biodiesel Synthesis Using a Byproduct Obtained from Palm Oil Refining. *Enzym. Res.* 2011, *2011*, 814507.
138. Ruzich, N.I.; Bassi, A.S. Investigation of enzymatic biodiesel production using ionic liquid as a co-solvent. *Can. J. Chem. Eng.* 2010, *88*, 277–282.
139. Xie, W.; Huang, M. Enzymatic Production of Biodiesel Using Immobilized Lipase on Core-Shell Structured Fe_3O_4@MIL-100(Fe) Composites. *Catalysts* 2019, *9*, 850.
140. Liu, X.; Liu, P.; An, N.; Liu, C. Metal-organic Frameworks as a Robust Biocatalysis Platform for Enzymatic Production of Biodiesel. *E3S Web Conf.* 2021, *245*, 01023.
141. Sebastian, J.; Muraleedharan, C.; Santhiagu, A. A comparative study between chemical and enzymatic transesterification of high free fatty acid contained rubber seed oil for biodiesel production. *Cogent Eng.* 2016, *3*, 225–240.
142. Lv, L.; Dai, L.; Du, W.; Liu, D. Progress in Enzymatic Biodiesel Production and Commercialization. *Processes* 2021, *9*, 355
143. Stoytcheva, M.; Montero, G.; Toscano, L.; Gochev, V.; Valdez, B. The Immobilized Lipases in Biodiesel Production. *Biodiesel Feedstocks Process. Technol.* 2011.
144. Jegannathan, K.R.; Eng-Seng, C.; Ravindra, P. Economic assessment of biodiesel production: Comparison of alkali and biocatalyst processes. *Renew. Sustain. Energy Rev.* 2011, *15*, 745–751.
145. Plechkova, N.V.; Seddon, K.R. Applications of ionic liquids in the chemical industry. *Chem. Soc. Rev.* 2008, *37*, 123–150.
146. O'Connor, S.; Pillai, S.C.; Ehimen, E.; Bartlett, J. Production of Biodiesel Using Ionic Liquids. *In Nanotechnology-Based Industrial Applications of Ionic Liquids*; Springer International Publishing: Cham, Switzerland, 2020; pp. 245–269.
147. Liu, J.; Thallapally, P.K.; McGrail, B.P.; Brown, D.R.; Liu, J. Progress in adsorption-based CO_2 capture by metal–organic frameworks. *Chem Soc. Rev.* 2012, *41*, 2308–2322.

148. Shomal, R.; Ogubadejo, B.; Shittu, T.; Mahmoud, E.; Du, W.; Al-Zuhair, S. Advances in enzyme and Ionic liquid immobilization for enhanced in mofs for biodiesel production. *Molecules.* 2021, 26, 3512.
149. Lyu, F.; Zhang, Y.; Zare, R. N.; Ge, J.; Liu, Z. One-pot synthesis of protein-embedded metal–organic frameworks with enhanced biological activities. *Nano Letters.* 2014, 14, 5761–5765.
150. Thangaraj, B.; Solomon, P. R.; Muniyandi, B.; Ranganathan, S.; Lin, L. Catalysis in biodiesel production—A Review. *Clean Energy.* 2018, 3, 2–23.
151. Abdi, Y.; Shomal, R.; Taher, H.; Al-Zuhair, S. Improving the reusability of an immobilized lipase-ionic liquid system for biodiesel production. *Biofuels.* 2018, 10, 635–641.
152. Alves, M. D.; Aracri, F. M.; Cren, É. C.; Mendes, A. A. Isotherm, kinetic, mechanism and thermodynamic studies of adsorption of a microbial lipase on a mesoporous and hydrophobic resin. *Chemical Engineering Journal.* 2017, 311, 1–12.
153. Lykourinou, V.; Chen, Y.; Wang, X.-S.; Meng, L.; Hoang, T.; Ming, L.-J.; Musselman, R. L.; Ma, S. Immobilization of MP-11 into a mesoporous metal–organic framework, MP-11@mesoMOF: A new platform for enzymatic catalysis. *Journal of the American Chemical Society* 2011, 133, 10382–10385.
154. Hu, Y.; Dai, L.; Liu, D.; Du, W.; Wang, Y. Progress & prospect of metal-organic frameworks (mofs) for enzyme immobilization (enzyme/mofs). *Renewable and Sustainable Energy Reviews.* 2018, 91, 793–801.
155. Mohamad, N. R.; Marzuki, N. H.; Buang, N. A.; Huyop, F.; Wahab, R. A. An overview of technologies for immobilization of enzymes and surface analysis techniques for immobilized enzymes. *Biotechnology & Biotechnological Equipment*. 2015, 29, 205–220.
156. Lage, F. A. P.; Bassi, J. J.; Corradini, M. C. C.; Todero, L. M.; Luiz, J. H. H.; Mendes, A. A. Preparation of a biocatalyst via physical adsorption of lipase from thermomyces lanuginosus on hydrophobic support to catalyze biolubricant synthesis by esterification reaction in a solvent-free system. Enzyme and *Microbial Technology.* 2016, 84, 56–67.
157. Liang, K.; Ricco, R.; Doherty, C. M.; Styles, M. J.; Bell, S.; Kirby, N.; Mudie, S.; Haylock, D.; Hill, A. J.; Doonan, C. J.; Falcaro, P. Biomimetic mineralization of metal-organic frameworks as protective coatings for biomacromolecules. *Nature Communications.* 2015, 6.
158. Xia, H.; Li, N.; Zhong, X.; Jiang, Y. Metal-organic frameworks: A potential platform for enzyme immobilization and related applications. *Frontiers in Bioengineering and Biotechnology*. 2020, 8.
159. Liu, W.-L.; Lo, S.-H.; Singco, B.; Yang, C.-C.; Huang, H.-Y.; Lin, C.-H. Novel trypsin–FITC@MOF bioreactor efficiently catalyzes protein digestion. *Journal of Materials Chemistry B*. 2013, 1, 928.
160. Homaei, A. A.; Sariri, R.; Vianello, F.; Stevanato, R. Enzyme immobilization: An update. *Journal of Chemical Biology.* 2013, 6, 185–205.

161. Salis, A.; Casula, M. F.; Bhattacharyya, M. S.; Pinna, M.; Solinas, V.; Monduzzi, M. Physical and chemical lipase adsorption on SBA-15: Effect of different interactions on enzyme loading and catalytic performance. *ChemCatChem*. 2010, 2, 322–329.
162. Adnan, M.; Li, K.; Wang, J.; Xu, L.; Yan, Y. Hierarchical zif-8 toward immobilizing burkholderia cepacia lipase for application in biodiesel preparation. *International Journal of Molecular Sciences.* 2018, 19, 1424.
163. Gascón-Pérez, V.; Jiménez, M. B.; Molina, A.; Blanco, R. M.; Sánchez-Sánchez, M. Efficient one-step immobilization of CaLB lipase over MOF support NH2-mil-53(AL). *Catalysts*. 2020, 10, 918.
164. Homaei, A. A.; Sariri, R.; Vianello, F.; Stevanato, R. Enzyme immobilization: An update. *Journal of Chemical Biology.* 2013, 6, 185–205.
165. Fernandez-Lorente, G.; Rocha-Martín, J.; Guisan, J. M. Immobilization of lipases by adsorption on hydrophobic supports: Modulation of enzyme properties in biotransformations in anhydrous media. *Methods in Molecular Biology.* 2020, 143–158.
166. Nobakht, N.; Faramarzi, M. A.; Shafiee, A.; Khoobi, M.; Rafiee, E. Polyoxometalate-Metal Organic Framework-lipase: An efficient green catalyst for synthesis of benzyl cinnamate by enzymatic esterification of cinnamic acid. *International Journal of Biological Macromolecules*. 2018, 113, 8–19.
167. Xia, H.; Li, N.; Zhong, X.; Jiang, Y. Metal-organic frameworks: A potential platform for enzyme immobilization and related applications. *Frontiers in Bioengineering and Biotechnology.* 2020, *8*.
168. Huo, J.; Aguilera-Sigalat, J.; El-Hankari, S.; Bradshaw, D. Magnetic MOF microreactors for recyclable size-selective biocatalysis. *Chemical Science.* 2015, 6, 1938–1943.
169. Adnan, M.; Li, K.; Xu, L.; Yan, Y. X-shaped zif-8 for immobilization RHIZOMUCOR miehei lipase via encapsulation and its application toward biodiesel production. *Catalysts.* 2018, 8, 96.
170. Zhang, Q.; Lei, D.; Luo, Q.; Wang, J.; Deng, T.; Zhang, Y.; Ma, P. Efficient biodiesel production from oleic acid using metal–organic framework encapsulated ZR-doped polyoxometalate nano-hybrids. *RSC Advances.* 2020, *10*, 8766–8772.
171. Shen, B.; Wang, B.; Zhu, L.; Jiang, L. Properties of cobalt- and nickel-doped zif-8 framework materials and their application in heavy-metal removal from wastewater. *Nanomaterials.* 2020, *10*, 1636.
172. El-Naas, M. H.; Al-Zuhair, S.; Alhaija, M. A. Removal of phenol from petroleum refinery wastewater through adsorption on date-pit activated carbon. *Chemical Engineering Journal*. 2010, 162, 997–1005.
173. El-Naas, M. H.; Al-Zuhair, S.; Alhaija, M. A. Reduction of COD in refinery wastewater through adsorption on date-pit activated carbon. *Journal of Hazardous Materials.* 2010, 173, 750–757.

174. Ray, S. S.; Gusain, R.; Kumar, N. Adsorption equilibrium isotherms, kinetics and thermodynamics. *Carbon Nanomaterial-Based Adsorbents for Water Purification.* 2020, 101–118.
175. Rafiei, S.; Tangestaninejad, S.; Horcajada, P.; Moghadam, M.; Mirkhani, V.; Mohammadpoor-Baltork, I.; Kardanpour, R.; Zadehahmadi, F. Efficient biodiesel production using a lipase@zif-67 nanobioreactor. *Chemical Engineering Journal*. 2018, 334, 1233–1241.
176. Yang, A.; Li, P.; Zhong, J. Facile preparation of low-cost HKUST-1 with lattice vacancies and high-efficiency adsorption for uranium. *RSC Advances*. 2019, 9, 10320–10325.
177. Domán, A.; Madarász, J.; László, K. In Situ Evolved Gas Analysis assisted thermogravimetric (TG-FTIR and TG/DTA–MS) studies on non-activated copper benzene-1,3,5-tricarboxylate. *Thermochimica Acta.* 2017, 647, 62–69.
178. Gross, A. F.; Sherman, E.; Vajo, J. J. Aqueous room temperature synthesis of cobalt and zinc sodalite zeolitic imidizolate frameworks. *Dalton Transactions* 2012, 41, 5458.
179. Wang, M.; Liu, J.; Guo, C.; Gao, X.; Gong, C.; Wang, Y.; Liu, B.; Li, X.; Gurzadyan, G. G.; Sun, L. Metal–organic frameworks (ZIF-67) as efficient cocatalysts for photocatalytic reduction of CO2: The Role of the morphology effect. *Journal of Materials Chemistry A*. 2018, 6, 4768–4775.
180. Zou, Z.; Wang, S.; Jia, J.; Xu, F.; Long, Z.; Hou, X. Ultrasensitive determination of inorganic arsenic by hydride generation-atomic fluorescence spectrometry using Fe 3 O 4 @ZIF-8 nanoparticles for preconcentration. *Microchemical Journal*. 2016, 124, 578–583.
181. Todaro, M.; Alessi, A.; Sciortino, L.; Agnello, S.; Cannas, M.; Gelardi, F. M.; Buscarino, G. Investigation by Raman spectroscopy of the decomposition process of HKUST-1 upon exposure to air. *Journal of Spectroscopy*. 2016, 2016, 1–7.
182. Prestipino, C.; Regli, L.; Vitillo, J. G.; Bonino, F.; Damin, A.; Lamberti, C.; Zecchina, A.; Solari, P. L.; Kongshaug, K. O.; Bordiga, S. Local structure of framework cu(ii) in HKUST-1 Metallorganic framework: spectroscopic characterization upon activation and interaction with adsorbates. *Chemistry of Materials*. 2006, 18, 1337–1346.
183. Cortés-Súarez, J.; Celis-Arias, V.; Beltrán, H. I.; Tejeda-Cruz, A.; Ibarra, I. A.; Romero-Ibarra, J. E.; Sánchez-González, E.; Loera-Serna, S. Synthesis and characterization of an SWCNT@HKUST-1 composite: Enhancing the CO2 Adsorption Properties of HKUST-1. *ACS Omega*. 2019, 4, 5275–5282.
184. Andrew Lin, K.-Y.; Chen, B.-C. Efficient elimination of caffeine from water using oxone activated by a magnetic and recyclable cobalt/carbon nanocomposite derived from zif-67. *Dalton Transactions*. 2016, 45, 3541–3551.

185. Radhakrishnan, D.; Narayana, C. Guest dependent brillouin and Raman scattering studies of zeolitic imidazolate framework-8 (zif-8) under external pressure. *The Journal of Chemical Physics*. 2016, 144, 134704.
186. Shi, Q.; Chen, Z.; Song, Z.; Li, J.; Dong, J. Synthesis of zif-8 and Zif-67 by steam-assisted conversion and an investigation of their tribological behaviors. *Angewandte Chemie*. 2010, 123, 698–701
187. Hou, S.; Lian, Y.; Bai, Y.; Zhou, Q.; Ban, C.; Wang, Z.; Zhao, J.; Zhang, H. Hollow Dodecahedral Co3s4@nio derived from zif-67 for Supercapacitor. *Electrochimica Acta*. 2020, 341, 136053.
188. Qian, J.; Sun, F.; Qin, L. Hydrothermal synthesis of zeolitic imidazolate framework-67 (ZIF-67) nanocrystals. *Materials Letters*. 2012, 82, 220–223.
189. Dhanjal, J. K.; Malik, V.; Radhakrishnan, N.; Sigar, M.; Kumari, A.; Sundar, D. Computational protein engineering approaches for effective design of New Molecules. *Encyclopedia of Bioinformatics and Computational Biology*. 2019, 631–643.
190. Desta, M. B. Batch sorption experiments: Langmuir and freundlich isotherm studies for the adsorption of textile metal ions onto Teff Straw (eragrostis TEF) agricultural waste. *Journal of Thermodynamics*. 2013, 2013, 1–6.
191. Guo, Y.; Liu, Y. Adsorption properties of methylene blue from aqueous solution onto thermal modified rectorite. *Journal of Dispersion Science and Technology*. 2014, 35, 1351–1359.
192. Egbosiuba, T. C.; Abdulkareem, A. S.; Kovo, A. S.; Afolabi, E. A.; Tijani, J. O.; Auta, M.; Roos, W. D. Ultrasonic enhanced adsorption of methylene blue onto the optimized surface area of activated carbon: Adsorption isotherm, kinetics and thermodynamics. *Chemical Engineering Research and Design*. 2020, 153, 315–336.
193. Karam, E. A.; Abdel Wahab, W. A.; Saleh, S. A. A.; Hassan, M. E.; Kansoh, A. L.; Esawy, M. A. Production, immobilization and thermodynamic studies of free and immobilized aspergillus awamori amylase. *International Journal of Biological Macromolecules*. 2017, 102, 694–703.
194. Fu, Y.; Guan, E.; Liang, J.; Ren, G.; Chen, L. Probing the effect of ag2s quantum dots on human serum albumin using spectral techniques. *Journal of Nanomaterials*. 2017, 2017, 1–7.
195. Edet, U. A.; Ifelebuegu, A. O. Kinetics, isotherms, and thermodynamic modeling of the adsorption of phosphates from model wastewater using recycled brick waste. *Processes*. 2020, 8, 665.
196. Lan, D.; Hou, S.; Yang, N.; Whiteley, C.; Yang, B.; Wang, Y. Optimal production and biochemical properties of a lipase from candida albicans. *International Journal of Molecular Sciences.* 2011, 12, 7216–7237.
197. Ahmad, K.; Shah, H.-ur-R.; Ashfaq, M.; Shah, S. S.; Hussain, E.; Naseem, H. A.; Parveen, S.; Ayub, A. Effect of metal atom in zeolitic imidazolate frameworks (Zif-8 & 67) for removal of PB2+ & Hg2+ from water. *Food and Chemical Toxicology*. 2021, 149, 112008.

198. Pholosi, A.; Naidoo, E. B.; Ofomaja, A. E. Intraparticle diffusion of cr(vi) through biomass and magnetite coated biomass: A comparative kinetic and Diffusion Study. *South African Journal of Chemical Engineering*. 2020, 32, 39–55.
199. Hu, Y.; Zhou, H.; Dai, L.; Liu, D.; Al-Zuhair, S.; Du, W. Lipase immobilization on macroporous ZIF-8 for enhanced enzymatic biodiesel production. *ACS Omega*. 2021, 6, 2143–2148.
200. Langseter, A. M.; Dzurendova, S.; Shapaval, V.; Kohler, A.; Ekeberg, D.; Zimmermann, B. Evaluation and optimisation of direct transesterification methods for the assessment of lipid accumulation in oleaginous filamentous fungi. *Microbial Cell Factories*. 2021, 20.
201. Dianursanti; Religia, P.; Wijanarko, A. Utilization of n-hexane as co-solvent to increase biodiesel yield on direct transesterification reaction from marine microalgae. *Procedia Environmental Sciences.* 2015, 23, 412–420.
202. Li, Q.; Chen, Y.; Bai, S.; Shao, X.; Jiang, L.; Li, Q. Immobilized lipase in bio-based metal-organic frameworks constructed by biomimetic mineralization: A sustainable biocatalyst for biodiesel synthesis. *Colloids and Surfaces B: Biointerfaces*. 2020, 188, 110812.
203. M. F. Chaplin and C. Bucke, *Enzyme Technology*. CUP Archive, 1990.
204. Burhan, M.; Shahzad, M. W.; Ng, K. C. A universal theoretical framework in material characterization for tailored porous surface design. *Scientific Reports* 2019, 9.
205. Rehage, H.; Kind, M. The first Damköhler number and its importance for characterizing the influence of mixing on competitive chemical reactions. *Chemical Engineering Science*. 2021, 229, 116007.
206. Holm, H. C.; Nielsen, P. M.; Longin, F. Upscaling of enzymatic processes. *Lipid Modification by Enzymes and Engineered Microbes*. 2018, 343–373.
207. Hu, Y.; Dai, L.; Liu, D.; Du, W.; Wang, Y. Progress & prospect of metal-organic frameworks (mofs) for enzyme immobilization (enzyme/mofs). *Renewable and Sustainable Energy Reviews.* 2018, 91, 793–801.
208. Hall, K. R.; Eagleton, L. C.; Acrivos, A.; Vermeulen, T. Pore- and solid-diffusion kinetics in fixed-bed adsorption under constant-pattern conditions. *Industrial & Engineering Chemistry Fundamentals*. 1966, 5, 212–223.

List of Publications

1- Review Paper and Article of Immobilized Enzyme

Shomal, R.; Ogubadejo, B.; Shittu, T.; Mahmoud, E.; Du, W.; Al-Zuhair, S. Advances in enzyme and Ionic liquid immobilization for enhanced in mofs for biodiesel production. *Molecules* 2021, *26*, 3512.

Shomal, R.; Du, W.; Al-Zuhair, S. Immobilization of lipase on metal organic frameworks for biodiesel production. *SSRN Electronic Journal* 2021.